# Exhortations

Fourteen billion years ago, in the first fraction of a second of our universe's existence, the most extreme high-energy physics experiment took place. Our ability to use the cosmic microwave background (CMB) to investigate this fantastic event, at energy scales a trillion times higher than can be obtained at the CERN, is at the very core of our quest to understand the fundamental nature of space and time and the physics that drive the evolution of the universe.

The CMB allows direct tests of models of the quantum mechanical origin of all we see in the universe. Subtle correlations in its anisotropy imparted by the interplay of gravitational and quantum physics at high energies contain information on the unification of gravity and quantum physics. Separately, correlations induced on the background at later times encode details about the distribution of all the mass, ordinary and dark, in the universe, as well as the properties of the neutrinos, including the number of neutrino species and types, and their still unknown masses.

Here we describe the scientific case for the next generation ground-based cosmic microwave background experiment, CMB-S4, consisting of dedicated telescopes at the South Pole, the high Chilean Atacama plateau and possibly a northern hemisphere site, all equipped with new superconducting cameras that will provide a dramatic leap forward in cosmological studies, crossing critical thresholds in testing inflation, the number and masses of the neutrinos or the existence of other 'dark radiation', providing precise constraints on the nature of dark energy, and testing general relativity on large scales.

Through the efforts of the CMB experimental groups over the last decade, the technologies needed for CMB-S4 are now in place. There are, however, considerable technical challenges presented by the required scaling up of the instrumentation as well as by the scope and complexity of the data analysis and interpretation. CMB-S4 will require: scaled up superconducting detector arrays with well understood and robust material properties and processing techniques; high throughput mm-wave telescopes and optics with unprecedented precision and rejection of systematic contamination; full characterization of astronomical foreground emission; large cosmological simulations and theoretical modeling with accuracies yet to be achieved; and computational methods for extracting minute correlations in massive, multi-frequency data sets contaminated by noise and a host of known and unknown signals.

The purpose of this document is to set the scientific goals for CMB-S4 and the instrumental configuration required to achieve them. This is of course an iterative process, involving detailed simulations as well as cost considerations. In this chapter we set out the overarching goals for CMB-S4, which are then refined in later chapters. We start with a brief history and the current status of CMB measurements.

## 0.1   Brief History and Current Status of CMB measurements

From its discovery 50 years ago, measurements of the cosmic microwave background (CMB) have led to spectacular scientific insights into the fundamental workings of space and time, from the quantum mechanical origin of the Universe at extremely high energies in the first moments of the Universe, through the growth of structure and the emergence of the dark energy that now dominates the energy density of the Universe. Studies of the CMB connect physics at the smallest scales and highest energies with the largest scales in the

Universe, roughly 68 orders of magnitude in length scale. They connect physics at the earliest times to the structure that surrounds us now, over 52 magnitudes in time scale.

The deep connections of CMB studies and particle physics predate the discovery of the background, going back to the 1940s when Alpher and Gamow were considering a hot, dense, early Universe as a possible site for nucleosynthesis. To produce the amount of helium observed in the local Universe, they concluded there had to be about $10^{10}$ thermal photons for every nucleon and predicted that this background of photons would persist to the present day as a thermal bath at a few degrees Kelvin.

The continuing, remarkably successful, story of CMB studies is one driven by the close interplay of theory and phenomenology with increasingly sensitive and sophisticated experiments. The high degree of isotropy of the CMB across the sky, to a part of one in a hundred thousandth, led to the theory of inflation and cold dark matter in the 1980's. It was not until 1992 that COBE discovered the anisotropy, and pinned the level of anisotropy for the following higher angular resolution measurements to characterize. In 2006 the COBE measurements of the background anisotropy and its black-body spectrum were recognized with the second Nobel Prize in physics; the first was awarded in 1978 to Penzias and Wilson for the discovery of the CMB. In the decade after the COBE results, measurements with ground and balloon-based instruments revealed the acoustic peaks in the CMB angular power spectrum, which showed that the Universe was geometrically flat in accord with predictions of inflation and provided strong support for contemporary Type 1a SN based claims for an accelerating Universe, which were recognized with the 2011 Nobel Prize in physics. The early anisotropy measurements also provided an estimate of the universal baryon density and found it to be in excellent agreement with the level estimated at $t \sim 1$ second by BBN calculations constrained to match the observed elemental abundances, and clearly showed that dark matter was non-baryonic. The polarization anisotropy was discovered ten years after COBE at the level predicted from temperature anisotropy measurements. The now standard $\Lambda$CDM cosmological model was firmly established.

Two CMB satellites have mapped the entire sky over the last 15 years, first WMAP with moderate angular resolution up to 12 arcminutes, followed by Planck with resolution up to 5 arcminutes. Higher resolution maps of smaller regions of the sky have been provided by ground-based experiments, most notably by the 10m South Pole Telescope (SPT) and the 6m Actacama Cosmology Telescope. The primary CMB temperature anisotropy is now well characterized through the damping tail, i.e., to multipoles $\ell \sim 3000$. The $\Lambda$CDM model continues to hold up stunningly well, even as the precision of the CMB determined parameters has increased substantially. Inflationary constraints include limits on curvature constrained to be less than 3% of the energy density, non-Gaussian fluctuations limited to $f_{NL} < 10$, and the departure from pure scale invariance of the primordial fluctuations detected at 5 sigma confidence. Also of interest to particle physics, the effective number of light relativistic species (i.e., neutrinos and any yet identified "dark radiation") is shown to be within one sigma of $N_{\text{eff}} = 3.046$, the number predicted by BBN. The sum of the masses of the neutrinos is found to be less than 0.6 eV. Dark matter is shown to be non-baryonic matter at $> 40$ sigma. Early dark energy models are highly constrained as are models of decaying dark matter.

*** add r and IGW – BICEP etc.

There remains much science to extract from the CMB, including: 1) using CMB B-mode polarization to search for primordial gravitational waves to constrain the energy scale of inflation and to test alternative models, and to provide insights into quantum gravity; 2) obtaining sufficiently accurate and precise determinations of the effective number of light relativistic species (dark radiation) to allow independent and rigorous tests of BBN as well as our understanding of the evolution of the Universe at $t = 1$ sec; 3) a detection of the sum of the neutrino masses, even if at the minimum mass allowed by oscillation experiments and in the normal hierarchy; 4) using secondary CMB anisotropy measurements to provide precision tests of dark energy through its impact on the growth of structure; and 5) testing general relativity and constraining alternate theories of gravity on large scales.

Currently the best cosmological constraints come from analyzing the combination of primary and secondary CMB anisotropy measurements with other cosmological probes, such as baryon acoustic oscillations (BAO) and redshift distortions, weak lensing, galaxy and galaxy cluster surveys, Lyman-alpha forest, Hubble constant, Type 1a SN, and others. The CMB primary anisptropy measurements provide highly complementary data for the combined analysis, in particular by providing a precision measurement of the Universe at $z = 1100$, which will provide a precise prediction for measurements of the late time Universe for any cosmological model and set of parameters – the Hubble constant being an excellent example. Secondary CMB measurements, e.g., CMB lensing, the SZ effects and SZ cluster catalogs, also provide critical late time constraints for the standard cosmological models and extensions to it. The cosmological reach of future cosmological surveys will be greatly extended by **joint analyses** with secondary background measurements, in particular CMB lensing.

## 0.2 Science reach of CMB-S4

CMB-S4 should be the definitive ground-based CMB project. The key science it should cover, and cover well, are

1. Inflation: CMB-S4 should make the definitive B-mode measurements of the recombination bump at degree angular scales. This includes multiple bands to untangle the foregrounds and degree through arcminute angular scales to measure CMB lensing and E-mode for de-lensing. If it can be demonstrated that foregrounds and atmospheric noise can be mitigated at very low multipoles, CMB-S4 could also target the re-ionization bump. At the lowest multipoles, CMB-S4, balloon and satellite mission would be highly complementary.

   CMB-S4 should answer whether or not large scale slow-roll-single-field inflation models are viable ($r \gtrsim 0.01$) with high significance. If no detection at $r \sim 0.01$, then CMB-S4 should be able to test the currently popular Starobinski model and others by achieving $\sigma(r) < 10^{-4}$ with an ultra deep survey.

   If $r$ is detected before or by CMB-S4, then CMB-S4 should provide a robust cosmic variance limited measure of its value (requiring a large area survey), and set the best possible constraints on $n_t$ (requiring an ultra deep survey).

   CMB-S4 should provide the polarization data to test predictions of models that attempt to explain the low-ell TT power spectrum "anomalies", that may offer clues to inflation. It will be particularly important to achieve accurate $20 < \ell < 100$ EE measurements.

   CMB-S4 will also extend the leverage arm for $n_s$, particularly in the EE spectrum. It may be possible to extend the primary EE spectrum to multipoles exceeding 10,000 because of the very low level of polarized foregrounds at high $\ell$.

   The CMB-S4 data set should be the definitive data set with which any model for the origin of the primordial fluctuations, be it inflationary or an alternative theory, must be consistent with to be viable.

2. Neutrinos and light relativistic species:

   There are two primary areas in which CMB-S4 will provide interesting neutrino constraints.

   a) The first is the effective number of light relativistic species, $N_{\rm eff}$. This is uniquely probed by the CMB and provides a critical constraint on any model for the neutrinos and their interactions. It is a highly complementary probe to BBN and to sterile neutrino models. Finding consistency with $N_{\rm eff} = 3.046$ at a precision of 0.020 would be an exciting and fundamental achievement linking particle physics and our understanding of the evolution of the first seconds of the Universe. Finding a departure from 3.046 would be even more exciting.

b) The second is the constraint on the sum of the masses of the neutrinos, $\Sigma m_\nu$. Here CMB-S4 will achieve $\sigma(\Sigma m_\nu) = 16$ meV (with DESI BAO prior), with the CMB sensitivity coming primarily through CMB lensing. This will lead to a definite detection of neutrino mass, even at the minimum mass and the normal hierarchy. The sensitivity to the sum of the masses is unique and complementary to terrestrial neutrino experiments.

3. Dark Energy and Gravity:

The CMB can be used to investigate Dark Energy through growth of structure tests, i.e., CMB lensing and SZ clusters, and through testing Gravity on large scales, i.e., though exploiting the kinematic SZ effect to measure the momentum field and large scale flows. The power of these probes is amplified by combining CMB-S4 data with galaxy surveys and Lyman alpha surveys, such as DESI, LSST, Euclid and WFIRST.

a) CMB lensing maps from CMB-S4 will provide hi-fidelity projected mass maps that will be cross-correlated with optical survey maps. This will increase the reach and precision of the dark energy constraints, as well as provide independent checks. Papers in the literature have quantified the DE FOM improvement of various projects with the addition of CMB lensing. Simulations need to be done to quantify the projected improvements with CMB-S4.

b) The DE task force pointed out that galaxy cluster evolution had the highest sensitivity of the DE probes considered. However, it also had the largest systematic. The issue is the uncertainty in understanding the mass scaling of the cluster observable. The thermal SZ effect has now been demonstrated to be a low scatter observable with the extraordinary feature of its brightness being redshift independent; an SZ survey probes all redshifts to a limiting mass. However, there still remain large uncertainties in the SZ observable mass scaling. CMB-S4 will be revolutionary in that it is expected to be able to calibrate the mass scaling to better than 1% through CMB lensing. This coupled with a low mass threshold will enable CMB-S4 to identify of order 100,000 clusters, probe the growth of structure to redshifts beyond $z \sim 2.5$, and will allow CMB-S4 to realize the full potential of galaxy clusters as a probe of dark energy. In combination with other Stage-IV baryon acoustic oscillation, supernova, and weak lensing surveys, a Stage-IV cluster survey similar to CMB-S4 would improve the overall dark energy figure of merit to approximately 1250, nearly a factor of two improvement than achieved without clusters.

c) Testing GR on large scales is important for our understanding of dark energy and the underlying workings of space and matter in general. The kinematic SZ effect allows measurement on the peculiar velocity (departure from Hubble flow) of structures. By measuring the differences in kSZ between pairs of clusters with known redshifts (a synergy of CMB-S4 and optical surveys), gravity can be tested on scales of 100 Mpc and larger. In this way, CMB-S4 paired with a Stage-IV spectroscopic survey would improve constraints on the growth rate predicted by general relativity by a factor of two.

Lastly it would be an oversight not to point out the obvious: there is only one CMB sky. It holds a wealth of information on fundamental physics and the origin and evolution of the Universe. While we have learned a great deal from CMB measurements, including discoveries that have pointed the way to new physics, we have only begun to tap the information contained in CMB polarization, CMB lensing and secondary effects. CMB-S4 should be designed to maximize discovery space by producing high fidelity maps.
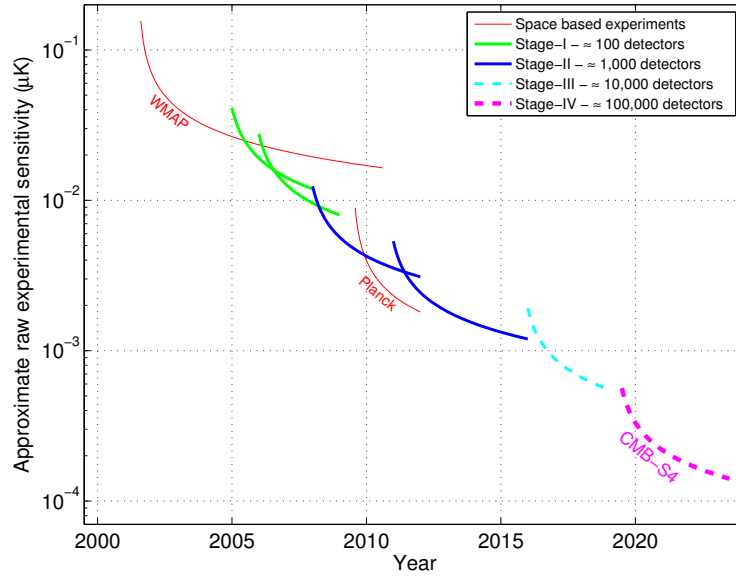
**Figure 1.** *Plot illustrating the evolution of the raw sensitivity of CMB experiments, which scales as the total number of bolometers. Ground-based CMB experiments are classified into Stages with Stage II experiments having O(1000) detectors, Stage III experiments having O(10,000) detectors, and a Stage IV experiment (such as CMB-S4) having O(100,000) detectors. Figure from Snowmass CF5 Neutrino planning document.*

## 0.3 From science goals to CMB-S4 design

### 0.3.1 Conceptual design of CMB-S4

The science goals discussed above leads to a rough conceptual design of CMB-S4.

#### 0.3.1.1 Sensitivity and detector count

The sensitivity of CMB measurements has increased enormously since Penzias and Wilson's discovery in 1965, following a Moore's Law like scaling, doubling every roughly 2.3 years. Fig. 6 shows the sensitivity of recent experiments as well as expectations for upcoming Stage 3 experiments, characterized by order 10,000 detectors on the sky, as well as the projection for a Stage 4 experiment with order 100,000 detectors. To obtain many of the CMB-S4 science goals requires of order 1 $\mu$K arcminute sensitivity over roughy 70% of the sky, which for a four year survey requires of order 500,000 CMB-sensitive detectors.

To maintain the Moore's Law-like scaling requires a major leap forward, it requires a phase change in the mode of operation of the ground based CMB program. Two constraints drive the change: 1) CMB detectors are background limited, so more pixels are needed on the sky to increase sensitivity; and 2) the pixel count for CMB cameras are nearing saturation. Even using multichroic pixels and wide field of view optics, CMB telescopes are able to field only tens of thousands of polarization detectors, far fewer than needed to meet the CMB-S4 science goals.

CMB-S4 thus requires multiple telescopes, each with a maximally outfitted focal plane of pixels utilizing superconducting, background limited, CMB detectors. To achieve the large sky coverage and to take advantage of the best atmospheric conditions, the South Pole and the Chilean Atacama sites are baselined, with the possibility of adding a new northern site to increase sky coverage to 100%.

### 0.3.1.2 Inflationary B-modes: low $\ell$ sensitivity, foregrounds and atmospheric noise mitigation

At the largest angular scales (low $\ell$), the angular scales that must be measured well to pursue inflationary B-modes (as well as critical tests of the E-mode polarization), the CMB polarization anisotropy is highly contaminated by foregrounds. Galactic synchrotron dominates at low frequencies and galactic dust at high frequencies, as recently shown by the Planck and Planck/BICEP/KECK polarization results. Multi-band polarization measurements are required to distinguish the primordial polarized signals from the foregrounds.

Adding to the complexity of low multipole CMB observations is the need to reject the considerable atmospheric noise contributions over the large scans needed to extract the low $\ell$ polarization. While the spatial and temporal fluctuations of the atmosphere are not expected to be polarized, any mismatches in the polarized beams or detector gains will lead to T-P leakage. These issues can be mitigated by including additional modulations into the instrument design, such as bore-sight rotation or modulation of the entire optics with a polarization modulation scheme in front of the telescope. Implementing such modulations is easier for small telescopes, although they could in principle be implemented on large telescopes as well. The cost of a small aperture telescope is dominated by the detector array, making it feasible to deploy multiple telescopes each optimized for a single band, or perhaps multiple bands within the relatively narrow atmosphere windows.

It is therefore an attractive option for CMB-S4 to include dedicated small aperture telescopes for pursuing low-$\ell$ polarization. The default plan for CMB-S4 is to target the recombination bump, with E-mode and B-mode polarization down to $\ell \sim 20$. If Stage 3 experiments demonstrate that it is feasible to target the reionization bump from the ground, those techniques may be incorporated into CMB-S4. More likely, however, this is the $\ell$ range for which CMB-S4 will be designed to be complementary to balloon-based and satellite based measurements.

### 0.3.1.3 Neutrinos and dark energy: high $\ell$ sensitivity

At the highest angular resolution (high $\ell$), the angular scales needed for de-lensing the inflationary B-modes, constraining $N_{\text{eff}}$ and $\Sigma m_\nu$, investigating dark energy and performing gravity tests with secondary CMB anisotropy, the CMB polarization anisotropy is much less affected by both foregrounds and atmospheric noise. In fact, it should be possible to measure the primary CMB anisotropy in E-mode polarization to multipoles a factor of a few times higher than possible in TT, thereby extending the lever arm to measure the spectral index and running of the primordial scalar (density) fluctuations. CMB-lensing benefits from $\ell_{max}$ of order 5000 and secondary CMB measurements are greatly improved with $\ell_{max}$ of order 10,000 and higher, requiring large aperture telescopes with diameters of several meters. Owing to the steep scaling of telescope cost with aperture diameter, it is likely not cost-effective to consider separate large aperture telescopes each optimized for a single frequency band.

CMB-S4 is therefore envisioned to include dedicated large aperture, wide field of view telescopes equipped with multi-chroic detector arrays.

### 0.3.2 Refining the CMB-S4 science case and key performance parameters

The rough conceptual design outlined above clearly needs to be refined. The first priorities are to determine the instrumental specifications to meet each of the science goals. We need to determine: the required resolution and sensitivity; the number of bands to mitigate foreground contamination, which is likely to be function of angular scale; the required sky coverage; the beam specifications (can we tolerate segmented primary reflectors?); the scanning strategy and instrument stability; etc.

Determining these specifications requires simulations, informed by the best available data and phenomenological models. Only when we have these specifications in hand can we design the instrument and answer such basic questions as the number and sizes of the telescopes.

## 0.4 The Road from Stage 3 to Stage 4

The Stage 2 and 3 experiments are logical technical and scientific stepping stones to CMB-S4. Fig. 7 shows the timeline of the CMB sensitivity and the expected improvement in a few of the key cosmological parameters. The enormous jump in sensitivity with the corresponding improvement in science reach is clear.

Finally, in Fig. 3 we show how the scientific findings (yellow), the technical advances (blue) and satellite selections (green) would effect the science goals, survey strategy and possibly the design of CMB-S4. THIS NEEDS TO BE CLEANED UP
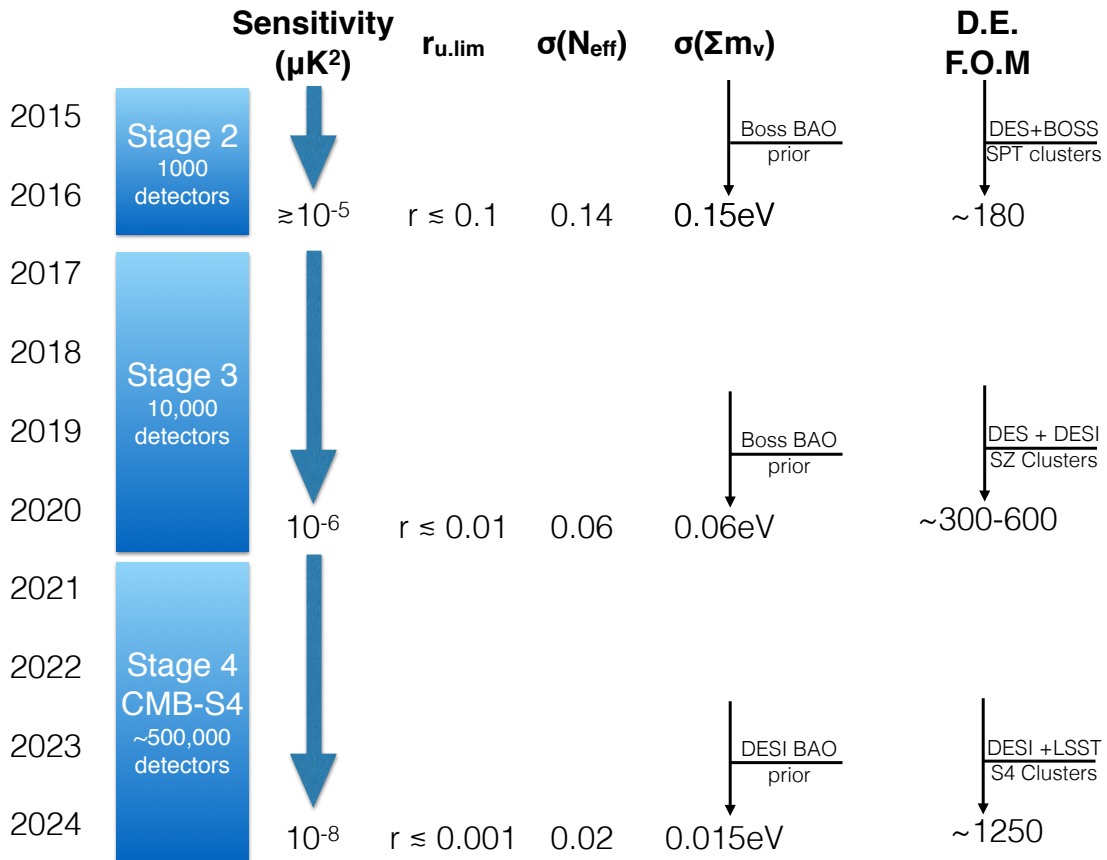
**Figure 2.** *Schematic timeline of evolution of Stage 3 and CMB-S4 sensitivity in $\mu K^2$ and the expected improvement in a few of the key cosmological parameters.*
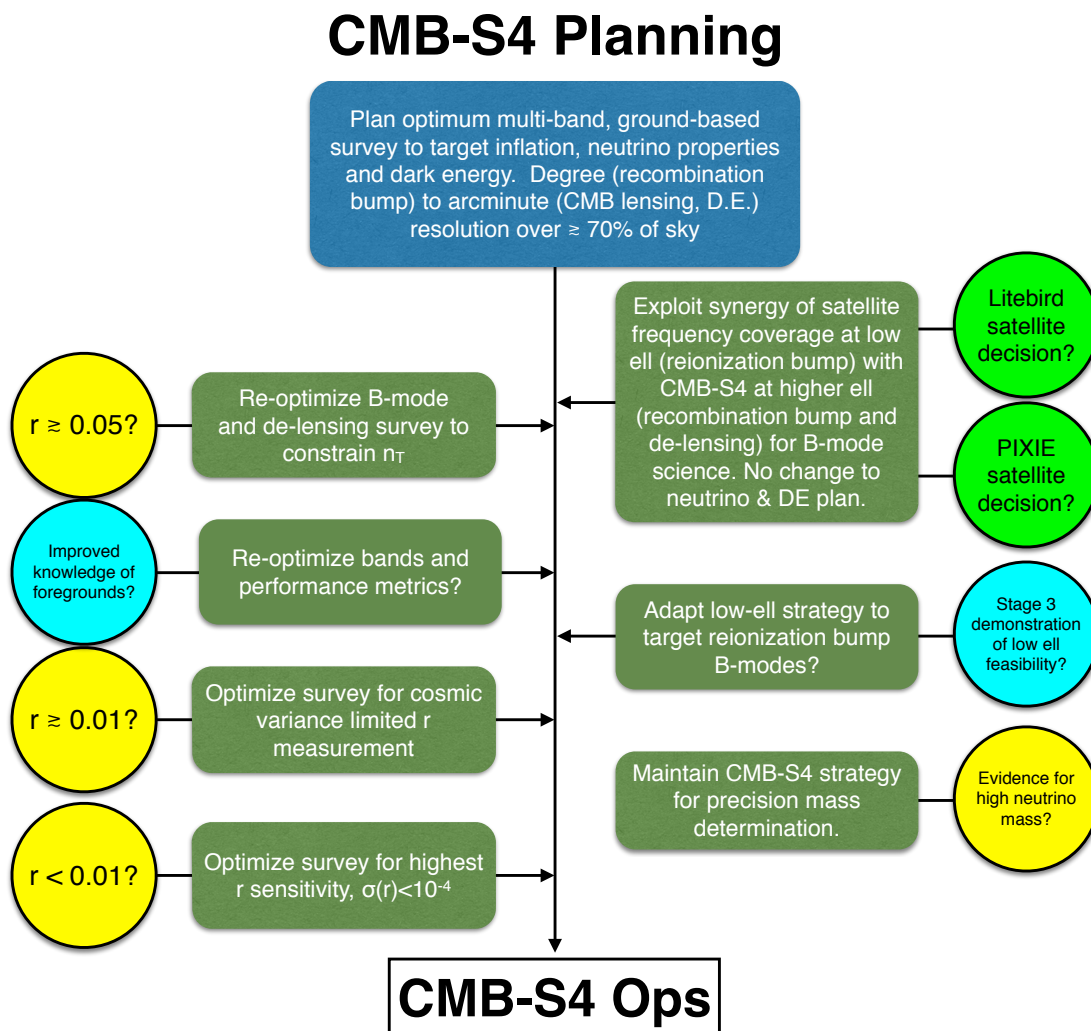
# CMB-S4 Planning



**Figure 3.** *Schematic flow chart showing how the scientific findings (yellow), the technical advances (blue) and satellite selections (green) would effect the science goals, survey strategy and possibly the design of CMB-S4 (green boxes).*

# Inflation Physics from the Cosmic Microwave Background

## 1 Introduction

The small anisotropies in the cosmic microwave background radiation contain invaluable information about the primordial universe. On the one hand, they encode the properties of the primordial scalar (or density) perturbations and hence the matter sector of the primordial universe. CMB-S4 will significantly improve current constraints on primordial observables in the scalar sector, typically by a factor of at least five. On the other hand, on degree scales a polarization pattern known as B-mode polarization would reveal the existence of primordial tensor modes or gravitational waves. In the tensor sector, CMB-S4 will improve current constraints by almost two orders of magnitude. This is especially interesting because it allows this next generation instrument to reach theoretically well-motivated thresholds for the tensor-to-scalar ratio (the ratio of power in tensor modes to power in scalar modes), which consequently serves as the primary inflationary science driver for the design. A detection of primordial gravitational waves in the range accessible to this instrument would:

- Reveal a new scale of particle physics far above those accessible with terrestrial particle colliders.

- Rule out the only currently developed competitor to inflation (ekpyrotic scenario)

If, in addition, we can conclusively determine that any detected signal is dominated by vacuum fluctuations then a detection would also

- Identify the energy scale of inflation.

- Provide strong evidence that the complete theory of quantum gravity must accommodate a Planckian field range for the inflaton.

- Provide strong evidence that gravity is quantized, at least at the linear level.

- Constrain the mass of the graviton

In the absence of a detection CMB-S4 will rule out large classes of inflation models.

In Section 2 we review in detail what a detection of primordial gravitational waves would mean and what follow-up measurements should or could be done to further characterize any signal. Section 3 explains the implications of a robust upper limit of $r < 0.001$. Section 4 lays out what is required to achieve that goal. The final two sections describe the significant gains CMB-S4 will allow in constraining other aspects of the primordial universe, both standard and more speculative. These include characterizing the scalar power spectrum, constraining curvature, non-Gaussianity, isocurvature modes, further probes of CMB 'anomalies' and test/constraints of cosmic strings.

# 2   Implications of a detection of primordial gravitational waves with CMB-S4

The overall evolution of the universe is well modeled by a Friedmann-Lemaître-Robertson-Walker line element

$$ds^2 = -dt^2 + a^2(t)\left[\frac{dr^2}{1-kr^2} + r^2 d\Omega^2\right], \tag{1.1}$$

where $k = \pm 1$ allows for spatial curvature and the time evolution is specified by the scale factor, $a(t)$. The Hubble parameter, $H = \dot{a}/a$, gives the rate of expansion of the universe.

The existence of primordial Helium and the cosmic microwave background radiation provide strong evidence for a hot big bang, a period during which the universe was dominated by radiation before it became dominated by matter and eventually dark energy. In the context of general relativity, observations of the cosmic microwave background furthermore provide strong evidence for a period preceding the hot big bang during which the co-moving Hubble radius, $(a|H|)^{-1}$, was decreasing with time: the measured average CMB temperature and the statistics of the measured anisotropies are the same over regions that otherwise share no causal history.

In an expanding universe a decreasing co-moving Hubble radius requires an era of accelerated expansion, $\ddot{a} > 0$, cosmic inflation. Such a period will drive the spatial curvature close to zero, in good agreement with current observations. Thus, we will assume spatial flatness and set $k = 0$ for most of the discussion, but will return to constraints on the curvature in Section 6. Since the period of cosmic inflation must end, there must exist a clock, or scalar degree of freedom. According to the uncertainty principle this clock must fluctuate, generating density perturbations that are adiabatic. In the most economic scenarios, these density perturbations are the seeds that grow into the anisotropies observed in the cosmic microwave background radiation and the stars and galaxies around us. Other degrees of freedom could, of course, also be present during this phase and might even be responsible for the generation of density perturbations we observe. **(Mention isocurvature modes here?)**

Alternatively, the phase of decreasing co-moving Hubble radius could have occurred during a period of decelerating contraction which must then be followed by a bounce as in the ekpyrotic or matter bounce scenarios.

For these early times, the ADM formalism provides a convenient parametrization of the line element

$$
\begin{aligned}
ds^2 &= -N^2 dt^2 + h_{ij}(dx^i + N^i dt)(dx^j + N^j dt) \\
h_{ij} &= a^2(t)[e^{2\zeta}\delta_{ij} + \gamma_{ij}].
\end{aligned}
\tag{1.2}
$$

The equations of motion for $N$ (the lapse) and $N^i$ (the shift) are the Hamiltonian and momentum constraints, while $\zeta$ ($= -\mathcal{R}$ of *Planck*) and $\gamma_{ij}$ contain the dynamical scalar and tensor degrees of freedom. In scenarios with matter sources other than a scalar field there may also be vector perturbations. These rapidly decay and can be neglected unless they are actively sourced in the post-inflationary universe, e.g. by cosmic strings.

Because the equations of motion are invariant under translations and the perturbations are linear or nearly so, it is convenient to work with the Fourier transforms

$$\zeta(t,\vec{x}) = \int \frac{d^3k}{(2\pi^3)}\zeta(t,\vec{k})e^{i\vec{k}\cdot\vec{x}} + h.c. \quad \text{and} \quad \gamma_{ij}(t,\vec{x}) = \sum_s \int \frac{d^3k}{(2\pi^3)}\gamma_s(t,\vec{k})e_{ij}(\vec{k},s)e^{i\vec{k}\cdot\vec{x}} + h.c., \tag{1.3}$$

where $e_{ij}(\vec{k}, s)$ is the transverse traceless polarization tensor for the graviton. The solutions oscillate when the modes are deep inside the horizon, $k \gg aH$. By definition, the modes exit the horizon when $k = aH$ and in single-field models approach a constant outside the horizon when $k \ll aH$.

The statistical properties of the scalar and tensor fluctuations, $\zeta$ and $\gamma_s$, at times sufficiently late so that they have frozen out provide the link between the primordial era and the CMB as well as other probes of the structure of the late universe. For a universe that is statistically homogeneous and isotropic and in which the primordial fluctuations are Gaussian, the information about the statistical properties is contained in the two-point correlation functions

$$\langle \zeta(\vec{k}) \zeta(\vec{k}') \rangle = (2\pi)^3 \delta^3(\vec{k} + \vec{k}') \frac{2\pi^2}{k^3} \mathcal{P}_\zeta(k)$$

$$\langle \gamma_s(\vec{k}) \gamma_{s'}(\vec{k}') \rangle = (2\pi)^3 \delta_{ss'} \delta^3(\vec{k} + \vec{k}') \frac{2\pi^2}{k^3} \frac{1}{2} \mathcal{P}_t(k)$$

$$(1.4)$$

where the factor of $1/2$ in the second to last line accounts for the fact that the measured power includes contributions from each of the two graviton polarizations. In single field slow-roll inflation, the gauge invariant combination of metric and scalar field fluctuations that is conserved outside the horizon has the power spectrum

$$\mathcal{P}_\zeta(k) = \frac{1}{2\epsilon M_p^2} \left( \frac{H}{2\pi} \right)^2 \Bigg|_{k=aH} \tag{1.5}$$

where $\epsilon = -\dot{H}/H^2$ is the first slow-roll parameter, and $M_p = 1/\sqrt{8\pi G}$ is the reduced Planck mass. As indicated, the Hubble parameter and $\epsilon$ are to be evaluated at horizon exit when the wavenumber $k$ is equal to the inverse comoving Hubble radius. In the absence of additional sources, the tensor power spectrum generated by inflation is

$$\mathcal{P}_t(k) = \frac{8}{M_p^2} \left( \frac{H}{2\pi} \right)^2 \Bigg|_{k=aH} \tag{1.6}$$

It is convenient to introduce the logarithmic derivatives of these power spectra

$$n_s(k) - 1 \equiv \frac{d \ln \mathcal{P}_\zeta}{d \ln k} \qquad \text{and} \qquad n_t(k) \equiv \frac{d \ln \mathcal{P}_t}{d \ln k} \, . \tag{1.7}$$

If the Hubble rate and slow-roll parameter only weakly depend on time as in slow-roll inflation, these will be $n_s(k) \approx 1$ and $n_t(k) \approx 0$ and can be expanded around a pivot scale $k_\star$ accessible by the CMB

$$n_s(k) - 1 = n_s - 1 + \frac{dn_s(k)}{d \ln k} \bigg|_{k_\star} \ln(k/k_\star) + \dots \qquad \text{and} \qquad n_t(k) = n_t + \frac{dn_t(k)}{d \ln k} \bigg|_{k_\star} \ln(k/k_\star) + \dots \tag{1.8}$$

In this approximation, the power spectra are

$$\mathcal{P}_\zeta(k) = A_s \left( \frac{k}{k_\star} \right)^{n_s - 1 + \frac{1}{2} \frac{dn_s}{d \ln k} \big|_{k=k_\star} \ln(k/k_\star) + \dots} \, ,$$

$$\mathcal{P}_t(k) = A_t \left( \frac{k}{k_\star} \right)^{n_t + \frac{1}{2} \frac{dn_t}{d \ln k} \big|_{k=k_\star} \ln(k/k_\star) + \dots} \, , \tag{1.9}$$

where $A_s$, $A_t$ are the scalar and tensor amplitudes, and $n_s$ and $n_t$, are the scalar and tensor spectral index, respectively, both at the pivot scale. The tensor-to-scalar ratio, $r$, is the relative power in the two types of fluctuations at a chosen pivot scale $k_\star$ accessible by the CMB

$$r = \frac{A_t}{A_s} \tag{1.10}$$

The power spectra of $\zeta$ and $\gamma_s$ are time-independent as long as the modes are outside the horizon, and only begin to evolve once the modes of interest re-enter the horizon at late times. In particular, they set the initial conditions for the system of equations governing the time evolution of the universe from around $10^9$ K when electrons and positrons have annihilated to the present. To exhibit the link between the primordial perturbations and late time observables explicitly, note that in a spatially flat universe, the contributions of primordial scalar perturbations to the angular power spectra of temperature or E-mode anisotropies are given by

$$C_{XX,\ell}^{(S)} = \int \frac{dk}{k} \mathcal{P}_\zeta(k) \left| \int_0^{\tau_0} d\tau S_X^{(S)}(k,\tau) j_\ell(k(\tau_0 - \tau)) \right|^2 , \tag{1.11}$$

where $S_X^{(S)}(k,\tau)$ with $X = T, E$ are source functions that encode the physics of recombination and $j_\ell$ is a spherical Bessel function that encodes the (spatially flat) geometry of the universe. At linear order, scalar perturbations only contribute to angular power spectra of temperature and E-mode polarization and the cross-spectrum of temperature and E-mode polarization, while the tensor perturbations in addition generate B-mode polarization. The primordial contribution of the tensor perturbations to the angular power spectrum of B-modes is

$$C_{BB,\ell} = \int \frac{dk}{k} \mathcal{P}_t(k) \left| \int_0^{\tau_0} d\tau S_B^{(T)}(k,\tau) j_\ell(k(\tau_0 - \tau)) \right|^2 . \tag{1.12}$$

where $S_B^{(T)}(k,\tau)$ is the appropriate source function.

At present, bounds on the tensor contribution to the temperature and E-mode anisotropies are comparable to constraints on the tensor-to-scalar ratio from B-mode observations. The former constraints are now cosmic variance limited. There is no limit on the latter from cosmic variance, and improvements and a potential detection with CMB-S4 will rely on measurements of B-mode polarization on degree scales.

Constraints on the amplitude of primordial tensor modes already strongly disfavor once popular inflationary models like minimally coupled chaotic inflation with a quadratic potential. We will discuss in detail what a detection of primordial gravitational waves would imply for inflation in the next several sections, but it is also important to note that a detection would rule out contracting universe scenarios. A contracting universe can also put large scales in causal contact if the scale factor $a$ is nearly constant while the magnitude of the Hubble parameter increases. This means the spectrum of gravitational wave fluctuations will be very blue [188]. In addition the Hubble parameter at the end of the contracting phase can be approximately bounded (minimally, $H < M_p$, or $H \sim T_{\text{reheat}}$) and so the value of $H$ that sets the amplitude of tensor fluctuations on scales accessible through the CMB must be exponentially smaller. The vacuum fluctuations in a contracting universe are then far too small to be detected [68].

## 2.1   The energy scale of inflation

According to the inflationary prediction for the amplitude of primordial gravitational waves, Eq. (1.6), a detection provides a direct measurement of the Hubble scale during inflation. In single field slow-roll models,

Eq. (1.5), the value of the amplitude of the power spectrum of scalar fluctuations measured by the *Planck* satellite together with the Friedmann equation $3H^2 M_p^2 \approx V$ determine the energy scale of inflation in terms of $r$ (all at the pivot scale $k_\star = 0.05$ Mpc$^{-1}$)

$$V^{1/4} = 1.04 \times 10^{16} \text{GeV} \left( \frac{r_\star}{0.01} \right)^{1/4} , \tag{1.13}$$

so that a detection of primordial gravitational waves determines the energy scale of inflation to within a few per cent.

In more general models of inflation the relation can be modified by changing the power in the scalar sector so that a detection only determines the order of magnitude of the new energy scale. Familiar examples are models in which the speed of sound of the inflaton quanta differs from unity or multi-field models. The extent to which the relation can be modified is bounded by constraints on non-Gaussianity. **be more specific** In other examples string or particle production events source gravitational waves [93, 269]. To maximize the production of gravitational waves, the field $\chi$ creating and annihilating the quanta should be massless, since massive particles contribute a smaller quadrupole moment and are a weaker source of gravitational waves [42]. Furthermore, $\chi$ should be a stronger source of tensor than of scalar modes, because the properties of the latter are tightly constrained by current bounds on the bispectrum [43], and in some models by constraints on the running of $n_s$ [225]. Current bounds on an equilateral bispectrum imply that scenarios in which the inflaton is directly coupled to the additional field sourcing gravitational waves cannot lead to a signal that is parameterically larger than the vacuum signal [42, 132, 229, 303]. So in this case, a detection remains a good indicator of the scale of inflation. Improved constraints on non-Gaussianity (see Section [**?**]) will further restrict these scenarios. A bound $f_{\text{NL}}^{\text{equil}} <?$ achievable with CMB-S4 would constrain these scenarios to contribute at most xx% of any gravitational wave signal.

To evade constraints from scalar non-Gaussianity, the dynamics generating $\chi$ should be decoupled from the inflaton sector [42] (that is, only gravitationally coupled). Together with the considerations above, this suggests a scenario in which $\chi$ is a gauge field whose quanta are created by a parity violating interaction with a spectator field [93, 42], so that only modes with a definite handedness are produced [25]. The gauge fields in turn source gravity waves and scalar perturbations. Helicity conservation implies that gravitons of that same handedness are produced in much larger amount than gravitons of the opposite handedness [275], and than scalar modes [42]. In such a scenario current constraints on non-Gaussian correlations in the temperature anisotropies can be evaded if the production of $\chi$ quanta occurs only around the time the modes contributing to the multipoles relevant for the B-mode search leave the horizon [234] because constraints on non-Gaussianities are dominated by smaller scales. Reference [234] provides a model in which gravitational waves from gauge field production could be measured at a level of $r = 10^{-1}$ with a vacuum contribution of only $r = 10^{-4}$. While in that case the determination of the scale of inflation is affected by less than one order of magnitude, adjusting the parameters of the scenario, it may allow for more dramatic modifications of Eq. (1.13). However, in a regime in which the relation is strongly modified the B-mode anisotropies would be highly non-Gaussian. So in the case of a detection even the B-mode bispectrum would become observable with CMB-S4. In addition, since the signal would be parity violating, the angular bispectrum of B-modes would be dominated by $\ell_1 + \ell_2 + \ell_3 =$even, which would vanish in any theory that respects parity. Such a signal would not be confused with the vacuum fluctuations of the spacetime metric arising in single field slow-roll inflation. We return to this point in more detail in Section 2.4 below.

Finally, note that these secondary production mechanisms cannot be used to obtain a signal from a contracting primordial era... **does anyone know if this is true?**

**Should we address these papers at all: 1410.8845, rebutted in 1508.01527, re-rebutted in 1510.06759, (different author) 1510.07956?**

## 2.2  Planckian field ranges and symmetries

The spectrum of tensor fluctuations depends only on the Hubble parameter $H$ during inflation, while the scalar power depends on both $H$ and the evolution of the homogeneous field sourcing inflation. As a consequence, the tensor-to-scalar ratio $r$ determines the inflaton field range in Planck units [208]

$$\frac{\Delta\phi}{M_p} = \int_0^{\mathcal{N}_\star} d\mathcal{N} \left(\frac{r}{8}\right)^{1/2} , \tag{1.14}$$

where $\mathcal{N}_\star$ is the number of e-folds between the end of inflation and the moment when the mode with $k_\star = 0.05\,\mathrm{Mpc}^{-1}$ corresponding to the CMB pivot scale exits the horizon. In many common inflationary models $r$ is a monotonic function of $\mathcal{N}$ so that

$$\frac{\Delta\phi}{M_p} \gtrsim \left(\frac{r_\star}{8}\right)^{1/2} \mathcal{N}_\star \gtrsim \left(\frac{r}{0.01}\right)^{1/2} . \tag{1.15}$$

The value of $\mathcal{N}_\star$ is not well constrained and depends on unknown details of reheating, but $\mathcal{N}_\star \gtrsim 30$ provides a conservative lower limit, justifying the second inequality in equation (1.15). Thus, a tensor-to-scalar ratio $r > 10^{-2}$ typically corresponds to a trans-Planckian excursion in field space between the end of inflation and the epoch when the modes we observe in the CMB exit the horizon.

Unless we work in a UV complete theory such as string theory, we rely on an effective field theory description of the inflationary epoch. General relativity viewed as an effective field theory breaks down as energies approach the Planck scale because interactions between gravitons become strongly coupled. The same is true for matter coupled to general relativity, so that the effective field theory governing the inflationary period will generically have a sub-Planckian cut-off $\Lambda_{\mathrm{UV}} < M_p$. In fact, in any weakly coupled UV completion of general relativity the new degrees of freedom must enter well below the Planck scale to ensure weak coupling so that $\Lambda_{\mathrm{UV}} \ll M_p$.

According to the bound (1.15), a tensor-to-scalar ratio $r > 10^{-2}$ then requires a displacement in field space that is larger than the cut-off of the effective field theory. While this does not invalidate an effective field theory description, it has important consequences. The effective field theory was obtained by integrating out all modes parametrically heavier than the cut-off $\Lambda_{\mathrm{UV}}$ of the single-field model. In the absence of symmetries, we expect the inflaton $\phi$ to couple to heavy degrees of freedom $\chi$, schematically

$$S = \int d^4x \sqrt{-g} \left[ -\frac{1}{2} g^{\mu\nu} \partial_\mu\phi\partial_\nu\phi - \frac{1}{2} g^{\mu\nu} \partial_\mu\chi\partial_\nu\chi - \frac{1}{2} m^2\phi^2 - \frac{1}{2} M^2\chi^2 - \frac{1}{2}\mu\phi\chi^2 + \ldots \right] . \tag{1.16}$$

By assumption, the mass of the heavy degrees of freedom to be integrated out is $M \gtrsim \Lambda_{\mathrm{UV}}$, and the dots represent various other interaction terms. Generically the dimensionful coupling $\mu$ is also expected to be of order the cut-off, $\mu \sim \Lambda_{UV}$. From the last two terms in equation (1.16), we see that displacements of $\phi$ by a distance comparable to the cut-off may lead to cancellations in the effective mass of the heavy degrees of freedom, and heavy states, in this case $\chi$, may become light if $\phi$ is displaced by a distance large compared to the cut-off. In particular, since $\Lambda_{\mathrm{UV}} < M_p$ we should not expect potentials that are smooth over super-Planckian distances in a generic low energy effective field theory with cut-off $\Lambda_{\mathrm{UV}} < M_p$.

We can only expect potentials suitable for large-field inflation if some mass scales, in the example $m$ and $\mu$ are well below the cut-off, or if dimensionless couplings are small. This occurs naturally if the UV theory respects a weakly broken shift symmetry $\phi \to \phi + c$ that ensures that quantum corrections from the inflaton and graviton will not introduce large corrections to the inflationary Lagrangian [204, 178, 98, 183, 84]. At the level of an effective field theory we can simply postulate such an approximate shift symmetry, but one should keep in mind that we ultimately require the existence of such a symmetry in quantum gravity.

As the best developed theory of quantum gravity, string theory is a useful framework for exploring mechanisms that allow large-field inflation to be realized even in the presence of heavy degrees of freedom. Axions provide natural candidates for the inflaton [139, 9]. They are ubiquitous in string theory and enjoy a shift symmetry that is weakly broken by instanton effects as well as the presence of branes or fluxes [296]. Instanton effects generate periodic contributions to the potential. While the periodicities in string theory are expected to be sub-Planckian [41, 30], constraints on the scalar spectral index require super-Planckian axion decay constants so that a UV completion of these models does not currently exist. The claimed detection of primordial $B$-modes by Bicep2 has led to renewed interest in models in which the inflaton is an axion with a potential that is entirely due to instanton effects, and has intensified the discussion to what extent some means to achieve large field inflation via multiple axions may be incompatible with basic principles of quantum gravity [189, 263, 109, 262, 72, 38, 73, 159, 158, 194].

In addition to the familiar non-perturbative contributions that break the continuous shift symmetry to a discrete one, the presence of fluxes and branes lead to contributions to the axion potentials that break the discrete shift-symmetry as well. As the axion is displaced by one period, one unit of charge is induced, so that the axion field space becomes non-compact, and super-Planckian decay constants are not required for super-Planckian excursions. A number of constructions based on this mechanism, known as monodromy, have been studied [272, 220, 179, 54, 242, 221, 217, 60, 157].

In writing (1.15), we have assumed that $r$ is monotonic, or at least of the same order of magnitude throughout the inflationary period. One can easily construct models in which $r$ is non-monotonic to weaken the bound [52, 167, 83]. In the case of a detection with CMB-S4 of a spectrum that is at least approximately scale-invariant, we can write the weaker bound

$$\frac{\Delta\phi}{M_p} \gtrsim \left(\frac{r}{0.3}\right)^{1/2} , \qquad (1.17)$$

which bounds the distance in field space traveled during the time the modes we observe in the CMB exited the horizon. This inequality implies that even if the distance in field space traveled during this period is sub-Planckian, it is not parameterically smaller than $M_p$. Because general relativity is not UV complete and becomes strongly coupled at $M_p$, any weakly coupled UV completion will come with a scale of new physics $M$, e.g. the string scale, that must be parameterically smaller than the Planck scale to ensure weak coupling. This implies that we cannot avoid the question of the embedding of the inflation model into quantum gravity for $r = 0.01$ or even for $r = 0.005$ unless we assume the UV completion of general relativity is strongly coupled.

In deriving the primordial power spectra and equation (1.14), we have assumed the Bunch-Davies state. The relation between $r$ and the scale of inflation is modified if we assume that the tensor modes (and the scalar modes) either do not start in the Bunch-Davies state [34, 90], or that the evolution during inflation will lead to departures from it. The first option generically introduces a stronger scale-dependence into the tensor spectrum [26, ?] (and additional non-Gaussianity). In addition, this way of achieving observable primordial $B$-modes from a low-scale model has a similar feature to large-field models: one should show that the initial state is not only acceptable from the point of view of low energy considerations, but can be generated by pre-inflationary physics. The second option, discussed in section 2.1, leads to non-trivial higher $n$-point functions that are in principle measurable.

In summary, a conclusive detection of primordial $B$-modes with CMB-S4 would provide evidence that the theory of quantum gravity must accommodate a Planckian field range for the inflaton. Conversely, the absence of a detection of B-modes with CMB-S4 will mean that a large field range is not required.

*A detection of $r$, together with high confidence that the gravitational waves are predominantly due to vacuum fluctuations, would provide the only data point for the foreseeable future that weighs in on quantum gravity.*

## 2.3   Constraints on the graviton mass

Theories of massive gravity come in many flavors (see e.g. [117, 162]), and their predictions in the scalar sector differ significantly. However, by definition, the dispersion relation for the graviton in all of them is

$$\omega^2 = p^2 + m_g^2 \,, \tag{1.18}$$

where $p$ is the physical momentum and $m_g$ the possibly time-dependent graviton mass. As a consequence, gravitational waves necessarily have frequencies $\omega > m_g$. A detection of primordial $B$-mode polarization on angular degree scales may be considered as a detection of gravitational waves with frequencies $\omega \sim H_{\rm rec}$ through the quadrupole they produce in the primordial plasma, where $H_{\rm rec} \approx 3 \times 10^{-29}$ eV is the Hubble parameter at recombination. A detection then implies a model-independent bound $m_g < H_{\rm rec}$ or

$$m_g < 3 \times 10^{-29} \text{ eV} \,. \tag{1.19}$$

If the graviton mass is time-dependent, this should be interpreted as a constraint on the graviton mass around the time of recombination.

Because the perturbations in the primordial plasma before and around recombination are linear, the effect of the graviton mass is straightforward to incorporate by a simple modification of the field equation for tensor metric perturbations so that the above argument can be made more quantitative. The equation of motion for the transverse traceless metric perturbation $\gamma$ takes the same form as for a minimally coupled massive scalar field,

$$\ddot{\gamma}_k(\tau) + 2\frac{\dot{a}}{a}\dot{\gamma}_k(\tau) + (k^2 + m_g^2 a^2)\gamma_k(\tau) = 0 \,. \tag{1.20}$$

Here $k$ is the comoving momentum of the metric perturbation, and we work in the conformal coordinates so that the background cosmological metric is

$$ds^2 = a^2(\tau)(d\tau^2 - d\mathbf{x}^2) \,. \tag{1.21}$$

The consequences of this modification are discussed in detail in [118]. The most important consequence is that superhorizon modes start to oscillate around the time $\tau_m$ when $H(\tau_m) = m_g$, and their amplitude subsequently redshifts as $a^{-3/2}$. In contrast, in the massless case all modes remain frozen until they enter the horizon. This results in a suppression of the amplitude primordial $B$-mode for $m_g \gg H_{\rm rec}$, and a detection of $B$-modes would rule out this possibility. For masses around $H_{\rm rec}$, there is no suppression, but the angular power spectra are modified by the presence of a graviton mass, and a detection of primordial $B$-mode polarization would allow to measure the graviton mass. A detection of primordial gravitational waves with angular $B$-mode power spectrum consistent with that expected in general relativity would imply $m_g < 3 \times 10^{-29}$ eV.

For comparison, the current model-independent bounds on the graviton mass arise from the indirect detection of $\sim 3 \times 10^{-5}$ Hz gravitational waves through the timing of the Hulse-Taylor binary pulsar [134], and the bound on the difference in arrival times for gravitational waves with different frequencies in the recent direct detection of astrophysical gravitational waves with LIGO [6]. The resulting bounds are $m_g \lesssim 10^{-19}$ eV and $m_g \lesssim 10^{-22}$ eV, respectively.

*A detection of B-mode polarization on angular degree scales consistent with the expectation in the context of general relativity would improve current bounds on the mass of the graviton by nearly seven orders of magnitude.*

Measurements of $B$-mode polarization on the largest angular scales, possible only with a satellite, would further strengthen the bound.

## 2.4   Following up on a detection

Once a detection has been made, it becomes necessary to understand the source of the signal. In slow-roll inflation, we expect a nearly scale invariant power spectrum and a nearly Gaussian signal so that the spectral index and the bispectrum provide observables that can strengthen the interpretation of the signal. More generally, the scale-dependence of the B-mode spectrum and higher order correlations probe the contributions of sources other than vacuum fluctuations, and possible physics beyond Einstein gravity and/or minimal coupling of the inflationary matter fields to gravity. Although we do not find that these considerations affect the optimal design of CMB-S4, they are be important in order to distinguish vacuum fluctuations from secondary sources of B-modes, and because of the complementarity with other future direct detection instruments.

### 2.4.1   Distinguishing vacuum fluctuations from other particle physics sources of B-modes

As mentioned in section 2.1, string of particle production may generate gravitational waves that can compete with the vacuum fluctuations in the spacetime metric. In a regime in which the relation between the amplitude of tensor modes and the scale of inflation is strongly modified the B-mode anisotropies are generally highly non-Gaussian and in some cases parity violating. Such a signal is distinguishable from vacuum fluctuations with CMB-S4 provided... **Can we add a figure/some numbers?**

Scenarios in which non-Abelian gauge fields play a significant role in the inflationary dynamic are closely related. In chromo-natural inflation and gauge-flation scenarios [214, 19, 20, 17, 18, 114, 115], the central piece is a homogeneous and isotropic, flavor-space locked gauge field that helps slow the roll of the inflaton or else is the inflaton itself. For a non-Abelian field with SU(2) symmetry, this means the three flavor gauge vector potentials are mutually orthogonal in space. The stress-energy of this configuration could leave a unique imprint on a spectrum of primordial gravitational waves, which would be transferred to the B-mode spectrum in the CMB. The non-Abelian nature of the field introduces a preferred handedness onto this medium leading to an enhancement of left (or right) circularly polarized gravitational waves. Again this would lead to parity-violating EB and TB correlations [**?**, 146] or parity violating higher $n$-pt functions. If this process takes place in the post-inflationary environment, the gauge field could further impress a periodic modulation on the gravitational wave spectrum [58, 59]. Although the basic chromo-natural and gauge-flation models have been ruled out [233], these unique features are expected to be generic to any viable variations on these scenarios.

Multi-field inflationary scenarios that end with phase transitions [160, 291, 192, 286, 172, 173, 260] and models of brane-inflation in string theory [264, 174, 95] generically predict some level of vector and tensor modes actively sourced by topological defects. In particular, either a breaking of a $U(1)$ symmetry or the production of fundamental strings at the end of inflation can lead to "cosmic strings" whose B-mode spectrum is primarily generated by vector modes and peaks on small scales ($\ell \sim 600 - 1000$) and is more similar in shape to the E to B lensing signal than to the vacuum spectrum. CMB-S4 should be able to distinguish even a small contribution from such sources [289], but the precise bounds from non-detection are related to the precision with which the lensing signal can be removed. Estimates made in reference [268, 37] indicate that CMB-S4 should be able to improve the limit on cosmic string tension by at least an order of magnitude beyond the current bounds from the CMB ($G\mu \sim 10^{-7}$ [14, 12]) and may be competitive with direct detection limits from the stochastic gravitational wave background ($G\mu \sim 10^{-11}$ or $10^{-8}$ depending on the model assumed for string loops [33]). In addition, the spectra of different types of defects have different shapes, and should be distinguishable [288, 37]. Measuring the location of the main peak would provide

valuable insights into fundamental physics. For example, in the case of cosmic superstrings the position of the peak of the B-mode spectrum constrains the value of the fundamental string coupling $g_s$ in string theory [37].

Post-inflationary phase transitions themselves have also been proposed as a source of nearly scale-invariant gravitational waves detectable through CMB polarization (and direct detection) [196, 175]. Even for a spectrum that matches the inflationary result on small scales, any such signal can in principle be distinguished from the inflationary signal by the presence of super-horizon correlations at the time of recombination. A framework to extract specifically this bit of the signal was proposed in [50] and could be applied to robustly extract the part of any signal that must come from physics outside of the hot big bang paradigm. (**Can this be achieved with CMB-S4?**)

### 2.4.2   Probing matter and gravitational interactions at the inflationary scale

*The tensor amplitude and field content that modifies the scalar power:* Since non-minimal inflation models with multiple fields or a small sound speed for a single degree of freedom predict a tensor to scalar ratio that is suppressed, a detection of gravitational waves of can be used to constrain the physics that produces the suppression in these scenarios. For single clock scenarios, this link is relatively straightforward [48] and a detection of $r$ can provide an upper limit on the speed of sound (and so a limit on non-Gaussianities). For multi-field scenarios many more details of the model must be specified [259], but $r$ together with bounds on isocurvature and local type non-Gaussianities may aid in model discrimination.

*The tensor tilt as a probe of the potential and non-minimal coupling:* If the amplitude of primordial B-modes is large enough to be measured, we can begin to constrain the shape of the spectrum. The simplest inflation scenarios all predict a red spectrum for gravitational waves, and the canonical single field consistency relation fixes $n_t = -r/8$. For a single field with a sound speed less than one, or multiple fields, $n_t/r < -1/8$ instead [255]. However, allowing the inflaton to couple to higher curvature terms can produce a blue tilt [49]. A detection of primordial gravitational waves on CMB scales would allow precise predictions, especially relevant for a blue index, for the amplitude expected on the much smaller scales accessible to direct detection. The recent detection of gravitational waves by LIGO, as well as the beginning of operation of the LISA pathfinder instrument, open an exciting new era of gravitational wave science. If CMB-S4 also sees a signal, LIGO and future instruments may be particle physics detectors as well as astrophysical observatories. A recent analysis in [197] shows the complementarity between observations over a wide range of scales in constraining the spectrum (although one must assume a constant tilt $n_T$ over many orders of magnitude).

*Other signatures of a modified gravitational sector:* Coupling the inflaton to higher curvature terms can also introduce parity violation in the spectrum of primordial gravitational waves [207, 22, 92, 282]. Reference [282] contains some example amplitudes of the coupling that would be detectable for a detection of $r = 0.05$; reference [144] discusses distinguishability of chiral gravity waves from other possible sources of parity violation, such as uniform cosmic birefringence. In addition, the momentum structure of the three-point function of gravitational waves would also be a sensitive probe of possible extensions of Einstein gravity [212]. However, the amplitude of the three point correlations between tensors alone in both standard inflation and extensions is small, at most $f_{\rm NL}^{\rm tensor} \lesssim 1$ [213, 212]. So while any constraint on the gravitational three-point function would be a useful data point for secondary sources, it is unlikely to be significant for vacuum fluctuations. Finally, it is worth noting that, if primordial gravitational waves were indeed chiral, they may present themselves first through a non-vanishing cross-correlation of B-modes with temperature, as demonstrated in Ref. [92].

# 3    Lessons from upper limits

A detection of primordial gravitational waves has profound implications. Even excluding the presence of gravitational waves at a level observable by CMB-S4 has important consequences for the theory of inflation. Current constraints already strongly disfavor models that were plausible candidates such as chaotic inflation with a quadratic potential [57]. Upper limits from CMB-S4 would rule out entire classes of inflationary models.

We first present a version of an argument developed in [232, 261, 96] that does not rely on microscopic details of inflationary models. In the limit $\epsilon \ll 1$, equations (1.5) and (1.7) lead to a differential equation

$$\frac{d\ln\epsilon}{d\mathcal{N}} - (n_s(\mathcal{N}) - 1) - 2\epsilon = 0 \,, \tag{1.22}$$

where $\mathcal{N}$ is the number of e-folds until the end of inflation, and $n_s(\mathcal{N}) - 1$ denotes the spectral index evaluated for the mode which exits the horizon $\mathcal{N}$ e-folds before the end of inflation. Note that $\epsilon$ is small (but positive) during inflation and $\epsilon \sim 1$ when inflation ends. If $\epsilon$ is a monotonic function of $\mathcal{N}$ this implies $n_s(\mathcal{N}) - 1 \leq 0$ in agreement with observations.

Denoting the number of e-folds before the end of inflation at which the CMB pivot scale exits the horizon as $\mathcal{N}_\star$, the departure from a scale invariant spectrum observed by the *Planck* satellite is $\mathcal{O}(1/\mathcal{N}_\star)$. While this could be a coincidence, it would find a natural explanation if

$$n_s(\mathcal{N}) - 1 = -\frac{p+1}{\mathcal{N}} \,, \tag{1.23}$$

up to subleading corrections in an expansion in large $\mathcal{N}$ for some real $p$. Under this assumption, the general solution to equation (1.22) is

$$\epsilon(\mathcal{N}) = \frac{p}{2\mathcal{N}} \frac{1}{1 \pm (\mathcal{N}/\mathcal{N}_{\mathrm{eq}})^p} \,, \tag{1.24}$$

where we have chosen to parameterize the integration constant by $\mathcal{N}_{\mathrm{eq}}$ so that the magnitudes of the first and second term in the denominator become equal when $\mathcal{N} = \mathcal{N}_{\mathrm{eq}}$. We take $\mathcal{N}_{\mathrm{eq}} > 0$ and indicate the choice of sign for the integration constant by '$\pm$'.

Assuming the epoch during which the modes we observe in the CMB exit is not special so that $\mathcal{N}_\star \gg \mathcal{N}_{\mathrm{eq}}$ or $\mathcal{N}_\star \ll \mathcal{N}_{\mathrm{eq}}$, equation (1.22) leads to four classes of solutions

$$\text{I.} \quad \epsilon(\mathcal{N}) = \frac{p}{2\mathcal{N}} \,, \tag{1.25}$$

$$\text{II.} \quad \epsilon(\mathcal{N}) = \frac{p}{2\mathcal{N}} \left(\frac{\mathcal{N}_{\mathrm{eq}}}{\mathcal{N}}\right)^p \qquad \text{with} \qquad p > 0 \qquad \text{and} \qquad \mathcal{N}_{\mathrm{eq}} \ll \mathcal{N}_\star \,, \tag{1.26}$$

$$\text{III.} \quad \epsilon(\mathcal{N}) = \frac{|p|}{2\mathcal{N}} \left(\frac{\mathcal{N}}{\mathcal{N}_{\mathrm{eq}}}\right)^{|p|} \qquad \text{with} \qquad p < 0 \qquad \text{and} \qquad \mathcal{N}_{\mathrm{eq}} \gg \mathcal{N}_\star \,, \tag{1.27}$$

$$\text{IV.} \quad \epsilon(\mathcal{N}) = \frac{1}{2\mathcal{N}\ln\mathcal{N}_{\mathrm{eq}}/\mathcal{N}} + \frac{p}{4\mathcal{N}} + \dots \qquad \text{with} \qquad |p| \ll \frac{1}{\ln\mathcal{N}_{\mathrm{eq}}/\mathcal{N}_\star} \qquad \text{and} \qquad \mathcal{N}_{\mathrm{eq}} \gg \mathcal{N}_\star \,. \tag{1.28}$$

As we explain in what follows, if CMB-S4 does not detect primordial $B$-modes, only class II with $\mathcal{N}_{\mathrm{eq}} \lesssim 1$ will remain viable, the rest will be disfavored or excluded.

The value of $\mathcal{N}_\star$ depends on the post-inflationary history of the universe. Equation (1.23) implies that a measurement of the spectral index and its running would determine $p$ and hence $\mathcal{N}_\star$, but unfortunately a

measurement of the running at a level of $(n_s - 1)^2$ is out of reach for CMB-S4. A given reheating scenario predicts $\mathcal{N}_\star$, but the space of reheating scenarios is large. Instantaneous reheating leads to $\mathcal{N}_\star \approx 57$ for $k_\star = 0.05 \mathrm{Mpc}^{-1}$, smaller values correspond to less efficient reheating. We will assume $47 < \mathcal{N}_\star < 57$ for the following discussion.

Current constraints on $n_s$ and $r$ from [57] disfavor class III at just over $2\sigma$ relative to class II. Furthermore, the best-fit of class III occurs for $p \approx 0$ where classes I, II, and III degenerate so that class III need not be discussed seperately. Class IV is disfavored at $2 - 3\sigma$ relative to class II. As a consequence we focus on classes I and II in what follows.

For class I, constraints from the *Planck* satellite and the BICEP2 and *Keck Array* experiments [57] translate into $p = 0.32 \pm 0.16$ at $1\,\sigma$, and favor models with inefficient reheating. At the best-fit point in this class, $r = 0.044$ and $n_s = 0.973$, which is currently disfavored relative to class II at $1 - 2\,\sigma$. Upper limits on $r$ directly translate into constraints on $p$. A $1\,\sigma$ upper limit on the amount of primordial gravitational waves from CMB-S4 at a level of $r < 0.001$ would imply $p < 0.013$ and effectively rule out this class as it degenerates into class II in this limit.

For class II the tensor-to-scalar ratio is naturally smaller than in class I as long as $p$ is of order unity because $\mathcal{N}_\star \gg \mathcal{N}_{\mathrm{eq}}$. Under the additional assumption that the scaling (1.26) should be valid until the end of inflation we have $\mathcal{N}_{\mathrm{eq}} \simeq 1$. In this case, current data from [57] imply $p = 0.67 \pm 0.24$ after marginalization over $\mathcal{N}_\star$. The best-fit occurs for $p = 0.83$ and for instantaneous reheating so that in this class the data favors models with efficient reheating. At the best-fit point, $r = 0.004$ and $n_s = 0.968$. An upper limit of $r < 0.001$ would disfavor this scenario relative to scenarios with $\mathcal{N}_{\mathrm{eq}} \ll 1$ at approximately $2\,\sigma$. The precise significance depends slightly on the true value of the spectral index. Similarly, for an upper limit of $r < 0.001$, the regime with $p \ll 1$ and equivalently class I would be disfavored relative to class II with $\mathcal{N}_{\mathrm{eq}} \ll 1$ at $3\,\sigma$. To disfavor the scenario with $\mathcal{N}_{\mathrm{eq}} \simeq 1$ at approximately $3\,\sigma$ relative to $\mathcal{N}_{\mathrm{eq}} \ll 1$ would require an upper limit of $r \lesssim 5 \times 10^{-4}$.

In summary, in the absence of a detection of primordial gravitational waves, CMB-S4 would place constraints on $n_s$ and $r$ that are strong enough to rule out or disfavor all models that naturally explain the observed value of the scalar spectral index in the sense that $n_s(\mathcal{N}) - 1 \propto 1/\mathcal{N}$ and in which the behavior (1.25)-(1.28) provides a good approximation until the end of inflation.

To understand the implications better, let us discuss the models that underlie the classes favored by current data, classes I and II. The potentials can be obtained from

$$\frac{d\phi}{d\mathcal{N}} = M_p^2 \frac{V'}{V} \qquad \text{and} \qquad \left(\frac{d\phi}{d\mathcal{N}}\right)^2 = 2\epsilon M_p^2 \,, \tag{1.29}$$

where $M_p$ is the reduced Planck mass.

Class I corresponds to models of chaotic inflation with monomial potentials $V(\phi) = \mu^{4-2p}\phi^{2p}$ already considered in [203]. The most commonly studied examples were $p = 1, 2$, both of which are now ruled out or strongly constrained [57]. Models with fractional powers $1/3 < p < 1$ that are still viable candidates have naturally appeared in in the study of large-field models of inflation in string theory [272, 220, 136]. If gravitational waves are not observed with CMB-S4, these would be ruled out.

Provided $p \neq 1$, class II corresponds to potentials of the form

$$V(\phi) = V_0 \exp\left[-\left(\frac{\phi}{M}\right)^{\frac{2p}{p-1}}\right] \,, \tag{1.30}$$

with $M = \sqrt{\alpha(p)\mathcal{N}_{\mathrm{eq}}}M_p$ where $\alpha(p)$ is of order unity for the range of $p$ of interest. For $p > 1$ inflation occurs when $\phi \ll M$. In this regime, the potential behaves like a hilltop model $V(\phi) \approx V_0(1 - (\phi/M)^n)$ with $n = 2p/(p-1)$. For $0 < p < 1$ inflation occurs for $\phi \gg M$ and $V(\phi) \approx V_0(1 - (M/\phi)^n)$ with $n = 2p/(1-p)$. In the limit $p \to 0$ in which classes I, II, III become degenerate, the $\phi$-dependence becomes logarithmic.

For the special case $p = 1$ the dependence on the inflaton in (1.30) becomes exponential and in the inflationary regime the potential is well approximated by $V(\phi) \approx V_0\left(1 - \exp\left(-\phi/M\right)\right)$ with $M = \sqrt{\mathcal{N}_{\mathrm{eq}}}M_p$. There are many examples of models with a potential with this asymptotic behavior for $\phi \gg M$. Some of them are the Starobinsky model [276], Higgs inflation [**?**, **?**], an early example of chaotic inflation [149], and the T-model [177].

If only the asymptotic forms of the potentials agree with (1.30), equation (1.23) will not be exact and the departures from (1.30) will be encoded in the subleading terms that vanish more rapidly than $1/\mathcal{N}$ in the limit $\mathcal{N} \to \infty$. Unfortunately, just like the running of the scalar spectral index, the subleading contributions are typically too small to be detected.

Note that $\mathcal{N}_{\mathrm{eq}}$ sets the characteristic scale in field space. For $\mathcal{N}_{\mathrm{eq}}$ of order unity, the variation of the inflaton is naturally given in units of the reduced Planck mass while for $\mathcal{N}_{\mathrm{eq}} \ll 1$ the characteristic scale in field space is sub-Planckian.

This allows us to rephrase the lesson we can draw from an upper limit on $r$ from CMB-S4.

*In the absence of a detection, CMB-S4 would rule out or disfavor all models that naturally explain the observed value of the scalar spectral index and in which the characteristic scale in field space equals or exceeds the Planck scale.*

Unfortunately, because of the scaling $M \propto \sqrt{\mathcal{N}_{\mathrm{eq}}}$ it will only be possible to obtain constraints $M \lesssim M_p$ but not $M \ll M_p$. It should also be kept in mind that a natural explanation of the value of the scalar spectral index is not guaranteed and its value could be an accident. That a natural explanation is possible is, however, encouraging.

# 4 CMB data products and simulations required to achieve goals for PGW

# 5 Improved constraints on primordial density perturbations

All current data are consistent with primordial density perturbations that are adiabatic, Gaussian, and nearly scale invariant. Because of its high angular resolution, CMB-S4 will significantly improve current constraints on the scale dependence of the primordial power spectrum of scalar perturbations, on departures from Gaussianity, and on departures from adiabatic perturbations.

## 5.1 The power spectrum of primordial density perturbations

The density perturbations are close to scale invariant but not exactly so. In the context of $\Lambda$CDM, *Planck* has measured the scalar spectral index to be $n_s = 0.9677 \pm 0.0060$ and has established $n_s - 1 < 0$ at more

than $5\,\sigma$. CMB-S4 will improve current constraints on the spectral index by more than a factor two to $\sigma(n_s) = 0.0028$, and will provide valuable constraints on the space of inflationary models.

As mentioned in section 3, a measurement of the running of the scalar spectral index with a precision of a few parts in ten thousand would allow a measurement of $p$ in equation (1.23), or equivalently $\mathcal{N}_\star$. This precision cannot be achieve with CMB-S4, but with a precision of one part in a thousand, it will test the idea that the lack of power on large angular scales might be explained by scale dependence of the spectral index [**?**].

Models of inflation that achieve super-Planckian inflaton displacements from repeated circuits of a sub-Planckian fundamental period may give rise to oscillatory features in the spectrum or primordial perturbations. The features may arise either from instanton effects or from periodic bursts of particle or string production. A search for such features is well motivated even though the amplitude is model-dependent and may be undetectably small. A detection would provide clues about the microscopic origin of the inflaton, the absence of a detection can constrain the parameters space of these models in interesting ways. CMB-S4 would tighten the constraints on the amplitude of features in the primordial power spectrum by a factor three.

## 5.2   Higher order correlations

Any detection of departures from Gaussianity would shed light on the interactions either of the inflaton with itself or between the inflaton and other degrees of freedom. The lowest order correlation function that encodes departures from Gaussianity is the $3pt$-function

$$\langle \zeta(\vec{k}_1)\zeta(\vec{k}_2)\zeta(\vec{k}_3) \rangle = (2\pi)^3 \delta(\vec{k}_1 + \vec{k}_2 + \vec{k}_3) B(k_1, k_2, k_3) \,, \tag{1.31}$$

where invariance under rotations and translations guarantee that the bispectrum $B(k_1, k_2, k_3)$ only depends on the magnitudes $k_1$, $k_2$, and $k_3$. A model independent search for the bispectrum, or equivalently the angular bispectrum $b_{\ell_1 \ell_2 \ell_3}$, is not computationally tractable, and in practice searches place constraints on the amplitudes $f_{\rm NL}$ of certain theoretically motivated functional forms, or shapes.

A detection of the most widely studied local shape would have far reaching theoretical implications. A detection of this shape would rule out all models of single clock inflation [97]. In addition, such a signal would open the door to significant cosmic variance on all scales from coupling of fluctuations within our observed volume to any super-Hubble modes [236, 206, 237]. Indeed, there would be room for a significant shift between the observed amplitude of scalar fluctuations (and so the observed $r$) and the mean value of fluctuations on much larger scales. Any scenario that predicts local non-Gaussianity together with fluctuations on scales much larger than our observed volume predicts a probability distribution for our observed $f_{\rm NL}^{\rm local}$. Many well-motivated scenarios predict a small mean value. These include the simplest modulated reheating scenario [300] and ekpyrotic cosmology [199], both of which predict mean values of $f_{\rm NL}^{\rm local} \sim 5$. Currently the strongest constraints on the local shape come from the *Planck* 2015 temperature and polarization analysis which give $f_{\rm NL}^{\rm local} = 0.8 \pm 5.0$ [14]. A noise-free cosmic variance limited CMB experiment is expected to produce constraints on $f_{\rm NL}^{\rm local}$ with $1\sigma$ error bars of about 3 [193]. Therefore the improvement expected of CMB-S4 over current limits is slightly less than a factor of two. This is not sufficient to reach the interesting theoretical threshold around $|f_{\rm NL}^{\rm local}| \lesssim 1$ [24], but will still reduce the space of viable models or hint at a detection. CMB-S4 could, for example, provide hints for the modulated reheating scenario or ekpyrotic cosmology at roughly $2\,\sigma$. The simplest curvaton scenario, which predicts $f_{\rm NL} = -5/4$ [209], will unfortunately be out of reach.

Current constraints on the equilateral shape are $f_{\mathrm{NL}}^{\mathrm{equil}} = -4 \pm 43$ (68% CL) [14]. An improvement by a factor of 2 would further tighten existing constraints on the speed of sound during inflation and the strong coupling scale in single-clock models of inflation. In addition, it would constrain scenarios with secondary production of gravitational waves.

**(Mention other shapes)**
**(Beyond the bispectrum)**

## 5.3   Isocurvature

**To be added**

# 6   Improved constraints on anomalies, birefringence, cosmic strings, axions...

## 6.1   Spatial Curvature

Despite the fact that inflation drives the spatial curvature to zero at the level of the background evolution, it predicts small, but non-zero curvature for any observer. The curvature measured in a Hubble patch receives contributions from long wavelength perturbations and is expected to be $|\Omega_k| < 10^{-4}$. A measurements of $\Omega_k$ exceeding this expectation would contain important information about the process responsible for inflation. In particular, if $|\Omega_k|$ is found to be considerably larger than this value, it would tell us that the inflaton was not slowly rolling when scales slightly larger than our observable horizon exited the horizon. Furthermore, observations of large negative $\Omega_k$ would falsify eternal inflation, while observation of positive and large $\Omega_k$ would be consistent with false vacuum eternal inflation.

Current constraints on this parameter from the CMB alone are $\Omega_k = 0.005^{+0.016}_{-0.017}$. Including baryon acoustic oscillation (BAO) data tightens the bound to $\Omega_k = 0.000 \pm 0.005$. CMB-S4 is expected to constrain spatial curvature at a level of $\sigma(\Omega_k) \approx 10^{-3}$. A detection at this level would have profound implications for the inflationary paradigm.

## 6.2   Cosmic Birefringence

The simplest dynamical way to model the accelerated expansion of the universe is to invoke a new slowly evolving scalar field that dominates its energy budget (the quintessence models for DE). Such a field generically couples to photons through the Chern-Simons term in the electromagnetic Lagrangian, causing linear polarization of photons propagating cosmological distances to rotate—the effect known as cosmic birefringence (CB) [81]. In the case of the CMB, such rotation converts the primordial E mode into B mode, producing characteristic TB and EB cross-correlations in the CMB maps [180, 145]. Even though there us no firm theoretical prediction for the size of this effect, if observed, it would be a clear smoking-gun evidence for physics beyond the standard model. Previous studies have used quadratic estimator formalism to constrain this effect [143], with the best current limit coming from sub-degree scale polarization measurements with POLARBEAR [16] ($< 0.33$ deg$^2$ for the amplitude of a scale-invariant rotation-angle power spectrum). A

promising way to pursue search for CB in the future is measurement of the off-diagonal EB cross correlations on small angular scales. **Put in more specific predictions for S4?**

## 6.3    Cosmic Strings

Cosmic strings can contribute no more than O(1%) to the total CMB temperature anisotropy [12, 205, 198], however, they can still generate observable B-modes. As shown in [231], the bounds on cosmic strings obtained solely from the POLARBEAR [10] and BICEP2 [11] B-mode spectra are comparable to those from temperature spectra. An S4 CMB polarization experiment should be able to reveal the presence of cosmic strings through their B-mode signature even if strings contribute as little as 0.1% to the CMB temperature anisotropy [37].

## 6.4    Anomalies

**Expect text from Glenn Starkman, Dominik Schwarz, ....**
**Add connections to axion physics. eg 1601.03049**

# 7    Summary

**Add some inspiring summarizing text**

# 2

# Neutrino Physics from the Cosmic Microwave Background

## 1 Introduction

Direct interactions between neutrinos and observable matter effectively ceased about one second after the end of inflation. Nevertheless, the total energy density carried by neutrinos was comparable to other matter sources through today. As a result, the gravitational effect of the neutrinos is detectable both at the time of recombination and in the growth of structure at later times [2], leaving imprints in the temperature and polarization spectrum as well as in CMB lensing.

CMB-S4 can improve our understanding of neutrino physics in regimes of interest for both cosmology and particle physics. Arguably the most important parameters of interest will be the sum of the neutrino masses $\sum m_\nu$ and the effective number of neutrino species, $N_{\text{eff}}$. These two parameters have natural targets that are within reach of a CMB-S4 experiment:

- $\sum m_\nu \gtrsim 58$ meV is the lower bound guaranteed by observations of solar and atmospheric neutrino oscillations. A CMB experiment with $\sigma(\sum m_\nu) < 20$ meV would be guaranteed a detection of at least $3\sigma$.

- $\Delta N_{\text{eff}} > 0.027$ is predicted for any light particle that was in thermal equilibrium with the standard model. A CMB experiment producing $\sigma(N_{\text{eff}}) \lesssim 0.01$ would be sensitive to all models in this very broad class of extensions of the Standard Model, which includes a wide range of axions and axion-like particles.

Current CMB data already provides a robust detection of the cosmic neutrino background at $> 10\sigma$. A CMB-S4 experiment will provide an order of magnitude improvement in sensitivity that opens a new window back to the time of neutrino decoupling and beyond.

Section 2 will review the motivation for studying neutrino masses with cosmological probes, and specifically with the CMB. We will explain why cosmology is sensitive to $\sum m_\nu$ via different probes and how it is complementary to the experimental neutrino effort. Section 3 will review the physics of $N_{\text{eff}}$ and its role as probe of the C$\nu$B and as sensitive tool for beyond the Standard model physics. We will emphasize the unique impact $N_{\text{eff}}$ has on the CMB that makes it distinguishable from other extensions of $\Lambda$CDM. In Section 4, we will discuss the implications for a variety of well motivated models, including sterile neutrinos and axions. In Section 5, we will discuss the relation between CMB and BBN based constraints.

# 2  Neutrino Mass

## 2.1  Theory Review

*Subsection to be completed by Marilena Loverde*

Cosmic background neutrinos are nearly as abundant in the universe as CMB photons. In the standard cosmological model, neutrinos cease to scatter with other particles at temperatures $\sim 1$MeV. The relic neutrinos are relativistic at decoupling but as the universe expands and cools the neutrino momenta redshift as $p_\nu \propto 1/a$ and eventually the energy of relic neutrinos comes to be dominated by their rest mass, rather than the momentum. The energy density in nonrelativistic neutrinos therefore contributes to the matter budget of the universe today. The neutrinos, however, were relativistic for much of the history of the Universe so their gravitational clustering is qualitatively different from that of cold dark matter (CDM) particles. This difference can be used to distinguish the neutrino and cold dark matter contributions to the matter density [170, 201, 5]. In this section, we review how neutrino mass affects the evolution of the neutrino energy density and the gravitational clustering of matter in the universe.

As discussed more detail in the $N_{eff}$ section, cosmic background neutrinos have been detected indirectly through their contribution to the energy density in radiation in the early universe. The current CMB constraints from $N_{eff}$ are in excellent agreement with the standard model expectation of three neutrino and anti-neutrino states each described by a relativistic thermal Fermi-Dirac distribution [13]. The phase space for each neutrino and anti-neutrino state is given by

$$f_\nu(p) = \frac{1}{e^{ap/(k_B T_\nu)} + 1} \tag{2.1}$$

where $T_\nu \approx 1.95K$ or $k_B T_\nu \approx 1.68 \times 10^{-4}$eV is the temperature today. Note that the spectral shape of the neutrino phase space distribution is preserved with the expansion of the universe so relic neutrinos will retain the relativistic Fermi-Dirac momentum distribution inherited from decoupling even if the individual neutrinos become non-relativistic.

The neutrino energy density is given by

$$\rho_\nu = \sum_i \int \frac{d^3\mathbf{p}}{(2\pi\hbar)^3} \frac{\sqrt{p^2 + m_{\nu i}^2}}{e^{ap/(k_B T_\nu)} + 1} \tag{2.2}$$

where $m_{\nu i}$ are the three neutrino mass eigenstates. For $T_\nu/a \gg m_{\nu i}$ the neutrino energies are dominated by their momenta and the total energy density behaves like radiation

$$\rho_\nu \Big|_{\text{early}} \approx \frac{7\pi^2}{40} \frac{(k_B T_\nu)^4}{\hbar^3 c^3} \frac{1}{a^4} \tag{2.3}$$
$$\propto a^{-4}$$

While for $T_\nu/a \ll m_{\nu i}$ the energy density behaves like matter

$$\rho_\nu \Big|_{\text{late}} \approx \sum_i m_{\nu i} \bar{n}_\nu \tag{2.4}$$
$$\propto a^{-3}$$

where $\bar{n}_\nu$ is the number of neutrinos and antineutrinos in each mass eigenstate

$$\bar{n}_\nu = \int \frac{d^3\mathbf{p}}{(2\pi\hbar)^3} \frac{2}{e^{ap/(k_B T_\nu)} + 1} \approx \frac{113}{a^3} \text{cm}^{-3} \, . \tag{2.5}$$

For a neutrino of mass $m_{\nu i}$ the transition between these two regimes $(T_\nu(a) \sim m_{\nu i})$ occurs at redshift $z_{nr} \sim 300(m_{\nu i}/0.05\text{eV})$. Using Eq. (2.4) the fractional energy density in neutrinos today can be written as

$$\Omega_\nu h^2 \approx \frac{\sum_i m_{\nu i}}{93\,\text{eV}} \, . \tag{2.6}$$

The individual masses of the neutrino states are unknown but neutrino oscillation data specifies the square of two mass splittings $\Delta m_{12}^2 = 7.54 \times 10^{-5}\text{eV}$, $|\Delta m_{13}^2| \approx 2.4 \times 10^{-3}\text{eV}$ [239]. These mass splittings, in combination with the neutrino number density, give a lower limit on the contribution of neutrinos to the cosmic energy budget

$$\Omega_\nu h^2 \gtrsim 0.0006 \, . \tag{2.7}$$

At $z \ll z_{NR}$ the matter density of the universe, which enters into the Hubble equation, is the sum of the CDM, baryon, and massive neutrino energy densities $\Omega_m = \Omega_c + \Omega_b + \Omega_\nu$. Whereas, at $z \gg z_{nr}$ the matter density is solely the baryon and CDM parts and neutrinos contribute to the radiation density.

Neutrinos do not participate in gravitational collapse until late times when they have become nonrelativistic. Prior to this transition, the neutrinos *free-stream* out of gravitational wells, leaving the CDM and baryons behind [64, 210, 169, 170]. Primordial fluctuations in the neutrino density are therefore damped away on scales smaller than the horizon at $z_{nr}$. In comoving units, this scale corresponds to a wave number

$$k_{nr} \equiv a_{nr} H(a_{nr})/c \approx 0.003 \left( \frac{\Omega_m}{0.3} \frac{m_\nu}{0.05\,\text{eV}} \right)^{1/2} h/\text{Mpc} \, . \tag{2.8}$$

Once the neutrinos are non-relativistic, their finite velocity dispersion still prevents them from clustering on scales smaller than the typical distance a neutrino travels in a Hubble time, $v_\nu/H(a)$ where $v_\nu \approx 3.15 T_\nu/(a m_\nu)$ the mean neutrino velocity. In analogy with the Jeans criterion for gravitational collapse, the neutrino free-streaming scale is defined by [64, 201]

$$k_{fs}(a) \equiv \sqrt{\frac{3}{2}} \frac{aH(a)}{v_\nu(a)} \approx 0.04 \, a^2 \sqrt{\Omega_m a^{-3} + \Omega_\Lambda} \left( \frac{m_\nu}{0.05\text{eV}} \right) h/\text{Mpc} \tag{2.9}$$

in comoving coordinates.

On scales larger than $k_{nr}$ (adiabatic) perturbations in the density of neutrinos, baryons, and CDM are coherent and can be described by a single perturbation to the total matter density $\delta_m = \delta\rho_m/\rho_m$. On smaller scales where the neutrino perturbations have decayed, only the perturbations to the CDM and baryons remain so that $\delta_m = (\Omega_c + \Omega_b)/\Omega_m \delta_{cb}$. The remaining CDM and baryon perturbations also grow more slowly because the neutrino energy density contributes to the expansion rate, but not to the source potentials. These two effects cause a suppression in the amplitude and the growth rate of matter perturbations wavenumbers $k > k_{fs}$ relative to a universe with massless neutrinos (and also relative to density perturbations with $k < k_{nr}$). The net change in the amplitude of perturbations with $k > k_{nr}$ primarily depends on the fractional energy density in massive neutrinos but retains a small sensitivity to the individual neutrino masses through a dependence on $a_{nr}$. Add a figure

An estimate of the effect of massive neutrinos on the growth of structure can be made by studying the evolution of matter perturbations in the two regimes $k \ll k_{fs}$ and $k \gg k_{fs}$. In the synchronous gauge, linear

perturbations to the matter density with wavenumbers $k \ll k_{fs}$ evolve as

$$\ddot{\delta}_m + 2H(a)\dot{\delta}_m - \frac{3}{2}\Omega_m H_0^2 a^{-3}\delta_m = 0 \quad \text{for} \quad k \ll k_{nr} \tag{2.10}$$

which has solutions $\delta_m \propto a, a^{-\frac{3}{2}}$ during the matter dominated era.

On scales where the neutrino perturbations have decayed, perturbations to matter density are just in the CDM and baryon components

$$\delta_m(k \gg k_{fs}) \approx (\delta\rho_c + \delta\rho_b)/\rho_m = (1 - f_\nu)\delta_{cb} \tag{2.11}$$

where $f_\nu = \Omega_\nu/\Omega_m$ and $\delta_{cb} = (\delta\rho_c + \delta\rho_b)/(\rho_c + \rho_b)$, but the neutrino energy density still contributes to the Hubble friction. In this limit, linear perturbations to the CDM and baryon density evolve as

$$\ddot{\delta}_m + 2H(a)\dot{\delta}_m - \frac{3}{2}\Omega_{cb} H_0^2 a^{-3}\delta_m = 0 \quad \text{for} \quad k \gg k_{fs} \tag{2.12}$$

where $\Omega_{cb} = \Omega_c + \Omega_b$ and $\Omega_{cb} < \Omega_m$ for a cosmology with massive neutrinos. Equation (2.12) has the approximate solutions during the matter dominated era of $\delta_{cb} \propto a^{1-\frac{3}{5}f_\nu}, a^{-\frac{3}{2}+\frac{3}{5}f_\nu}$ for $f_\nu \ll 1$.

The matter dominated solutions give a simple estimate of the net effects of massive neutrinos on the amplitude of matter perturbations. For fixed $\Omega_c h^2$, the evolution of perturbations in a cosmology with $f_\nu \neq 0$ is the same as a cosmology with $f_\nu = 0$. After $a_{nr}$, the perturbations with $k \gg k_{fs}$ grow more slowly (according to Eq. (2.12), the growing mode solution grows as $\propto a^{1-3/5f_\nu}$) than those with $k \ll k_{fs}$ (according to Eq. (2.10), $\propto a$). At scale-factor $a$ during the matter dominated era, the total difference in growth or perturbations with $k \gg k_{fs}$ is roughly

$$\frac{\delta_{cb}(k \gg k_{fs}, a|f_\nu)}{\delta_{cb}(k \gg k_{fs}, a|f_\nu = 0)} \sim \left(\frac{a}{a_{nr}}\right)^{-3/5f_\nu}. \tag{2.13}$$

The resulting difference in the amplitude of the matter power spectra is then

$$\frac{P_{mm}(k \gg k_{fs}, a|f_\nu)}{P_{mm}(k \gg k_{fs}, a|f_\nu = 0)} \sim (1 - 2f_\nu)\frac{P_{cc}(k \gg k_{fs}, a|f_\nu)}{P_{cc}(k \gg k_{fs}, a|f_\nu = 0)} \sim \left(1 - 2f_\nu - \frac{6}{5}f_\nu \ln(a/a_{nr})\right). \tag{2.14}$$

On the other hand, the evolution of the large scale modes is identical,

$$\frac{P_{mm}(k \ll k_{fs}, a|f_\nu)}{P_{mm}(k \ll k_{fs}, a|f_\nu = 0)} = 1. \tag{2.15}$$

The above expression overestimates the effect of neutrino mass by assuming the transition from relativistic to non-relativistic is instantaneous. It also ignores the effects of the cosmological constant at late times. Using the true evolution of $\delta_{cb}$ through $a_{nr}$ and allowing for the cosmological constant gives

$$\frac{P_{mm}(k \gg k_{fs}|f_\nu)}{P_{mm}(k \gg k_{fs}|f_\nu = 0)} \approx 1 - 6f_\nu \tag{2.16}$$

at $a = 1$. Note that this expression assumes fixed $\Omega_c h^2$, $\Omega_b h^2$ so that matter-radiation equality is not changed by neutrino mass and that and $\Omega_\Lambda = 1 - \Omega_m$ is fixed by adjusting $h$ so that the onset of cosmological constant domination is also unchanged. Alternatively, assuming fixed $\Omega_m$ and decreasing $\Omega_{cb}$ to account for $\Omega_\nu$ makes matter-radiation equality, which occurs while the neutrinos are relativistic, slightly later so that the suppression is increased to

$$\frac{P_{mm}(k \gg k_{fs}|f_\nu)}{P_{mm}(k \gg k_{fs}|f_\nu = 0)} \approx (1 - 8f_\nu). \tag{2.17}$$

## 2.2   Observational Signatures and Target

Massive neutrinos contribute to the critical density as

$$\Omega_\nu h^2 \simeq \frac{\sum m_\nu}{93\,\text{eV}} \ . \tag{2.18}$$

As discussed above, the signature of massive neutrinos manifests through the energy density $\Omega_\nu$ making its transition from relativistic radiation to non-relativistic matter as its temperature drops; the transition occurs at around $z_{\text{nr}} \sim 2000 m_\nu / 1\,\text{eV}$. During the epoc when neutrinos are relativistic, they free-stream out of the over-dense regions and washes out the matter fluctuations on small scales. This effect turns off roughly at scales larger than the horizon scale at the redshift $z_{\text{nr}}$. Thus, comparison of the amplitudes of the fluctuations at large and small scales probes neutrino mass.

The amplitudes at large scales are precisely measured through primordial CMB fluctuations in both TT and EE power spectra, except for the uncertainty from the optical depth $\tau$, which we discuss later. The large scale structure (LSS) measures the small scales; this is the area where we expect significant improvement through CMB S4.

## 2.3   CMB Lensing and Spectra

Likely the cleanest probe of the neutrino mass in the CMB is through gravitational lensing, which directly measures the matter distribution along the line of sight. To be concrete, in the limber approximation, the lensing power spectrum is given by

$$C_\ell^{\phi\phi} = \frac{8\pi^2}{\ell^2} \int_0^{\chi_\star} \chi d\chi P_\Psi(\ell/\chi; \eta_0 - \chi) \frac{(\chi_\star - \chi)^2}{\chi_\star \chi} \tag{2.19}$$

$$P_\psi(k; \eta) = \frac{9\Omega_m^2(\eta) H^4(\eta)}{8\pi^2} \frac{P_{mm}(k; \eta)}{k} \tag{2.20}$$

where $\chi$ ($\chi_\star$) is the co-moving distance (to the last scattering surface) and $\eta$ ($\eta_0$) is conformal time (today). More details regarding CMB lensing, including current and future measurements, will be discussed in Chapter **.

For the purposes of the neutrino mass measurement, the advantage of lensing over other probes is that it is largely free of astrophysical uncertainties. As we see from the lensing power spectrum, we are directly sensitive to the matter power spectrum (rather than a biased tracer) and the relevant scales are in the linear regime where modeling should be reliable.

The primary challenges for the lensing measurement are degeneracies with other cosmological parameters. The two primary degeneracies in $\Lambda$CDM are

- Optical depth, $\tau$: The suppression of small scale power at low redshift requires a reliable measurement of the amplitude of the power spectrum at high redshift. In principle, this is measured by the primary CMB anisotropies, but the overall normalization is degenerate with $\tau$ for $\ell \gtrsim 20$. A precise measurement of $\tau$ is therefore crucial to calibrate the suppression at low redshifts. This degeneracy can be broken by ... .

- $\Omega_m$ : The amount of lensing is controlled by the total amount of matter. Therefore, we can compensate for a suppression from neutrinos by increasing the matte power spectrum. This degeneracy will be broken by DESI BAO measurements of the expansion history.

In addition to degeneracies in $\Lambda$CMB there can be degeneracies with possible extensions. Most noteablebly:

- $N_{\rm eff}$: The density of neutrinos after they become non-relativistic is given by $\rho_\nu \simeq m_\nu n_\nu$ where $n_\nu$ is the number density. Therefore, we only measure the mass if we know the number density to sufficient accuracy. Fortunately, as we will discuss in the next section, measurements of the neutrino energy density from the primary CMB will be sufficiently accurate as to make this degeneracy insignificant under plausible assumptions

In principle, measurement of the free streaming scale directly in the matter power spectrum would separate the neutrino mass for most other physical quantities. Unfortunately, given current limits on the neutrino mass, the change to the shape of the potential is not expected to drive future constraints.

Enumerate current measurements. Mention future prospects.?

Neutrino mass can also be probed through the early Integrated Sachs Wolfe (ISW) effect in the primordial TT and EE power spectra, since massive neutrinos changes the expansion history by affecting the duration of the radiation dominant era. This measurement is already cosmic-variance limited and only marginal improvement is possible in future.

### 2.3.1    SZ Cluster Abundance

Abundance of galaxy clusters also gives us a measure of the amplitudes at small scales ($\simeq 0.1h{\rm Mpc}^{-1}$). CMB datasets can be used to measure the abundance through the Sunyaev-Zel'dvich (SZ) effect. However, the interpretation of this dataset to derive the neutrino mass requires an accurate understanding of the non-trivial mass-observable relation. [Mention mass-observable relation study works in progress ...]

### 2.3.2    Cross-correlations with External Datasets

Redshift tomography? Calibrating optical surveys to help them measuring neutrino mass? (Remember LSST is a DOE project and thus helping them makes a good case.)

## 2.4    Forecasts

## 2.5    Relation to Lab Experiments

Relation between lab measurements of neutrino masses and the cosmological measurements.

*Subsection to be completed by Clarence Chang*

CMB-S4 will explore neutrino physics through precision measurements of the impact of the Cosmic Neutrino Background on the CMB. There are two primary areas in which CMB-S4 provides interesting neutrino constraints. 1) The first is using precision measurements of the radiation energy density in the early Universe to constrain neutrino physics beyond the 3-neutrino paradigm. The relativistic energy density in the early Universe is uniquely probed by the CMB and provides a critical constraint on any model for the neutrinos and their interactions. It is a highly complementary probe to terrestrial approaches to non-standard neutrino

phenomena (e.g., sterile neutrinos) such as short baseline neutrino experiments. 2) The second is constraining the sum of the neutrino masses through precision measurements of the growth of large scale structure. The CMB-S4 mass sensitivity of 16 meV (1-sigma) is especially interesting as it corresponds to a 3-sigma measurement of the minimum predicted value. Fig. 4 shows the complementarity of the projected CMB-S4 neutrino mass constraints to the neutrino oscillation experiments of the Intensity Frontier (Dune) as well as Katrin mass limits. The oscillation experiments measure the angles and phases of the neutrino mixing matrix and are insensitive to the absolute neutrino mass scale. CMB-S4 measures the sum of the neutrino masses in a manner that is independent of the neutrino oscillation parameters. Results from Intensity Frontier experiments together with CMB-S4 will provide precision measurements of the full neutrino mixing matrix (angles, phases, and masses).
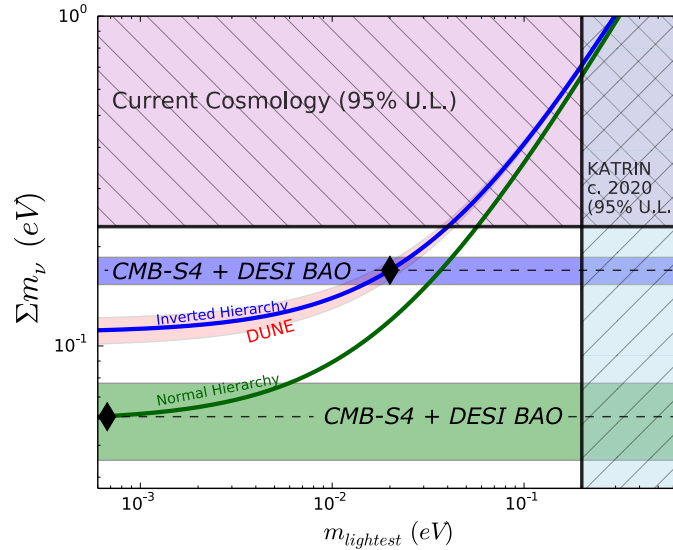


**Figure 4.** *Shown are the current constraints and forecast sensitivity of cosmology to the neutrino mass in relation to the neutrino mass hierarchy. In the case of an "inverted hierarchy," with an example case marked as a diamond in the upper curve, the CMB-S4 (with DESI BAO prior) cosmological constraints would have a very high-significance detection, with $1\sigma$ error shown as a blue band. In the case of a normal neutrino mass hierarchy with an example case marked as diamond on the lower curve, CMB-S4 would detect the lowest $\sum m_\nu$ at $\gtrsim 3\sigma$. Also shown is the sensitivity from the long baseline neutrino experiment (DUNE) as the pink shaded band, which should be sensitive to the neutrino hierarchy. Figure adapted from the Snowmass CF5 Neutrino planning document.*

# 3 Effective Number of Neutrinos

## 3.1 Theory Review

*Subsection to be completed by Joel Meyers with a contribution from George Fuller*

The angular power spectrum of the cosmic microwave background (CMB) at small angular scales is quite sensitive to the radiation content of the early universe, usually parametrized by a quantity $N_{\rm eff}$ which will be defined more precisely below. In the standard models of cosmology and particle physics, $N_{\rm eff}$ is a measure of the energy density of the cosmic neutrino background. More generally, however, $N_{\rm eff}$ receives contributions

from all forms of radiation apart from photons which are present in the early universe. Due to its sensitivity to $N_{\rm eff}$, the CMB can be used as a tool to probe physics of the standard model and beyond which are difficult to measure through other means. Here we will give an overview of the theoretical issues related to $N_{\rm eff}$ and outline the expectations from the standard model.

## 3.2    Thermal History of the Early Universe

In this section, we will give a sketch of the thermal history of the standard hot big bang universe when the temperature of the plasma was falling from about $10^{11}$ K to about $10^8$ K following Section 3.1 of [294]. For other reviews see [116, 239]. During this era, there are two events of particular interest: neutrinos decoupled from the rest of the plasma, and a short time later electrons and positrons annihilated, heating the photons relative to the neutrinos. Our task is to follow how these events impact the evolution of the energy densities of the photons and neutrinos.

For massless particles described by the Fermi-Dirac or Bose-Einstein distributions, the energy density is given by

$$\rho(T) = \begin{cases} g \frac{\pi^2 k_B^4}{30 \hbar^3 c^3} T^4 & \text{Boson} \\ \frac{7}{8} g \frac{\pi^2 k_B^4}{30 \hbar^3 c^3} T^4 & \text{Fermion} \end{cases} \tag{2.21}$$

where $g$ counts the number of distinct spin states. The entropy density for massless particles is given by

$$s(T) = \frac{4\rho(T)}{3T} . \tag{2.22}$$

It is convenient to define a quantity $\mathcal{N}$ which counts the spin states for all particles and antiparticles, with an additional factor $\frac{7}{8}$ for fermions. With this definition, the total energy density and entropy density of the universe during radiation domination are given by

$$\rho(T) = \mathcal{N} \frac{\pi^2 k_B^4}{30 \hbar^3 c^3} T^4 ,$$
$$s(T) = \frac{4}{3} \mathcal{N} \frac{\pi^2 k_B^4}{30 \hbar^3 c^3} T^3 . \tag{2.23}$$

In an expanding universe, the first law of thermodynamics implies that for particles in equilibrium, the comoving entropy density is conserved

$$a^3 s(T) = \text{const} . \tag{2.24}$$

One straightforward consequence of this conservation is that for radiation in free expansion, the temperature evolves as the inverse of the scale factor

$$T \propto \frac{1}{a} . \tag{2.25}$$

Let us now apply this to the physics of the early universe.

At a temperature of $10^{11}$ K ($k_B T \sim 10$ MeV), the universe was filled with photons, electrons and positrons, and neutrinos and antineutrinos of three species, all in thermal equilibrium with negligible chemical potential, along with a much smaller density of baryons and dark matter both of which are unimportant for the present discussion. As the temperature of the plasma dropped below about $10^{10}$ K (about 1 second after the end of inflation), the rate of collisions between neutrinos and electrons and positrons could no longer keep up with the expansion rate of the universe, and neutrinos began to fall out of equilibrium and begin a free expansion. This is just above the temperature for which $m_e c^2 \sim k_B T$, and so for slightly lower temperatures

electrons and positrons rapidly disappeared from equilibrium. We will simplify the discussion by assuming that neutrinos decoupled instantaneously before electron-positron annihilation and comment below how a more detailed calculation modifies the results. Non-zero neutrino masses can safely be neglected here as long as $m_\nu c^2 \lesssim 1$ keV which is guaranteed by current observational bounds.

From this point on, we will distinguish the temperature of neutrinos $T_\nu$ from that of the photons $T_\gamma$. Before neutrino decoupling, frequent interactions kept neutrinos and photons in equilibrium, ensuring they had a common falling temperature. After the universe became transparent to neutrinos, the neutrinos kept their relativistic Fermi-Dirac distribution with a temperature which fell as the inverse of the scale factor. The photons, on the other hand, were heated by the annihilation of the electrons and positrons. Comoving entropy conservation allows us to compute the relative temperatures at later times.

After neutrino decoupling, but before electron positron annihilation, the thermal plasma contained two spin states of photons, plus two spin states each of electrons and positrons, which means that during this period,

$$\mathcal{N}_{\text{before}} = 2 + \frac{7}{8}(2+2) = \frac{11}{2}\,. \tag{2.26}$$

After electron positron annihilation, only the two spin states of photons remained, and so

$$\mathcal{N}_{\text{after}} = 2\,. \tag{2.27}$$

Since $T_\nu \propto a^{-1}$ during this period, we can express the condition of comoving entropy conservation as follows

$$\frac{\mathcal{N}_{\text{before}}T_{\gamma,\text{before}}^3}{T_{\nu,\text{before}}^3} = \frac{\mathcal{N}_{\text{after}}T_{\gamma,\text{after}}^3}{T_{\nu,\text{after}}^3}\,. \tag{2.28}$$

Using the fact that $T_{\gamma,\text{before}} = T_{\nu,\text{before}}$, we find as a result

$$\frac{T_{\gamma,\text{after}}}{T_{\nu,\text{after}}} = \left(\frac{11}{4}\right)^{1/3}\,. \tag{2.29}$$

We find that in the instantaneous neutrino decoupling limit, the annihilation of electrons and positrons raised the photons relative to the neutrinos by a factor of $(11/4)^{1/3} \simeq 1.401$.

After electron positron annihilation, assuming three species of light neutrinos and antineutrinos, each with one spin state, the radiation density of the universe is

$$\rho_r = \frac{\pi^2 k_B^4}{30\hbar^3 c^3}\left[2T_\gamma^4 + 3\frac{7}{8}T_\nu^4\right] = \frac{\pi^2 k_B^4}{15\hbar^3 c^3}\left[1 + 3\frac{7}{8}\left(\frac{4}{11}\right)^{4/3}\right]T_\gamma^4\,. \tag{2.30}$$

It is conventional to define a quantity $N_{\text{eff}}$ which gives the radiation energy density in terms of the effective number of neutrino species as

$$\rho_r = \frac{\pi^2 k_B^4}{15\hbar^3 c^3}\left[1 + \frac{7}{8}\left(\frac{4}{11}\right)^{4/3}N_{\text{eff}}\right]T_\gamma^4\,. \tag{2.31}$$

In the instantaneous neutrino decoupling approximation described above, we found $N_{\text{eff}} = 3$. In the real universe, however, decoupling of neutrinos is not instantaneous, and the residual coupling of neutrinos at the time of electron positron annihilation increases $N_{\text{eff}}$ by a small amount in the standard model.

The current best estimate of $N_{\text{eff}}$ in the standard model is $N_{\text{eff}} = 3.046$ [216]. Very unlike photon decoupling at temperature $T \sim 0.2$ eV, active neutrino decoupling at $T \sim 10\,\text{MeV} - 0.1\,\text{MeV}$ takes place

over many tens of Hubble times, with the result that we expect distortions in the relic neutrino energy spectra relative to thermal-shaped, Fermi-Dirac black bodies. Standard model physics Boltzmann neutrino transport calculations show that these distortions could change $N_{\text{eff}}$ from 3 to something close to 3.05. This result is largely due to (1) the incomplete decoupling of neutrinos during electro-positron annihilation and (2) QED plasma effects. While both effects have been calculated independently quite accurately, there is some theoretical uncertainty in this quantity due to the various numerical approximations that are made in the calculations when both effects are included simultaneously (see e.g. [154] for discussion).

## 3.3   Natural Target

As will be discussed in more detail below, the CMB angular power spectrum is sensitive to the value of $N_{\text{eff}}$ in our universe. Measurement of the value of $N_{\text{eff}}$ provides a huge amount of insight into the early universe, and is in fact an observational probe of the conditions at very early times, well before recombination. Even within the standard model, $N_{\text{eff}}$ provides an observational handle on the thermal history back to about one second after the end of inflation. The true power of measuring $N_{\text{eff}}$, however, comes from the realization that it is sensitive not just to the neutrinos of the standard model, but it in fact receives contributions from all forms of radiation apart from photons present in the early universe and is thus a probe of new physics.

Collider experiments are known to provide a measurement of the number of neutrino species (or more precisely the number of species of fermions coupling to the $Z$ boson with mass below $m_Z/2$) and find very close agreement with three families of light active neutrinos [265]. Cosmological measurements of $N_{\text{eff}}$ provide complimentary constraints and are sensitive to the total energy density of radiation whether constituted of active neutrinos or other light species.

If the measured value of $N_{\text{eff}}$ exceeds the standard model prediction, it would be an indication that there is additional radiation content in the early universe or that the thermal history is somehow modified. Additional radiation which contributes to $N_{\text{eff}}$ is often referred to as dark radiation. There is a huge number of possible sources for dark radiation, including sterile neutrinos [3, 281, 65], gravitational waves [67, 278, 224], dark photons [7, 182, 103], and many more [76, 295]. It is also possible that the measured value of $N_{\text{eff}}$ could be found below the standard model prediction. This can happen if for example photons are heated relative to neutrinos after decoupling [277, 63].

One of the features that make $N_{\text{eff}}$ a compelling theoretical target, is the degree to which broad classes of models fall into two basic levels of $\Delta N_{\text{eff}}$. As illustrate in Figure 5, any species that was in thermal equilibrium with the Standard model produces a characteristic correction to $N_{\text{eff}}$ that depends only on its spin and its freeze-out temperature. For freeze-out after the QCD phase transition, one finds $\Delta N_{\text{eff}} \gtrsim 0.3$. Freeze-out before the QCD phase transition instead produces $\Delta N_{\text{eff}} > 0.027$. This first category has been tested by Planck. The second category, which is sensitive freeze-out temperatures as early as reheating, falls into the level of sensitivity compatible CMB Stage IV experiment.

The contributions to $N_{\text{eff}}$ from hot thermal relics are relatively easy to understand from the discussion of neutrino decoupling. After freeze-out, the temperature of a relativistic specifics redshift like $a^{-1}$ and therefore is only diluted relative to the Standard model when energy is injected. The annihilation of heavy standard model particles into photons conserves the comoving entropy and therefore, the diluted temperature of a relic before neutrino decoupling is given by

$$\left(\frac{T_{\text{relic}}}{T_\nu}\right)^3 = \frac{g_\star(T_{\nu-\text{freeze}-\text{out}})}{g_\star(T_{\text{relic freeze}-\text{out}})} = \frac{43/4}{g_\star(T_{\text{freeze}-\text{out}})} \tag{2.32}$$
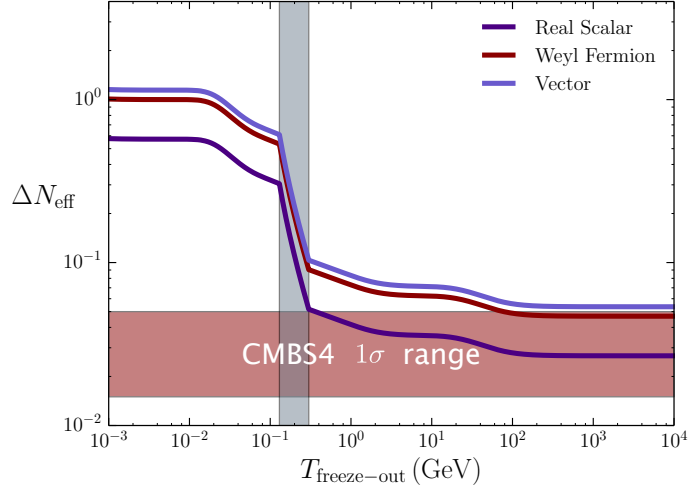
**Figure 5.** *Contribution to $N_{\text{eff}}$ from a massless field that was in thermal equilibrium with the Standard model at temperatures $T > T_{\text{freeze}}$. For $T_{\text{freeze}} \gg m_{\text{top}}$, these curves saturate with $\Delta N_{\text{eff}} > 0.027$. The region in red shows the range of forecasts for $\sigma(N_{\text{eff}})$ for plausible CMB-S4 configurations.*

The order of magnitude difference in $\Delta N_{\text{eff}}$ before and after the QCD phase transition is from order of magnitude drop in $g_\star$ below the QCD scale.

Even a measurement of $N_{\text{eff}}$ which agrees with the standard model prediction to high precision would be very interesting due to the constraints it would place on physics beyond the standard model. Some specific implications for sterile neutrinos, axions and other popular models will be discussed below. Broadly speaking, contraining $\Delta N_{\text{eff}}$ at the $10^{-2}$ level would broadly constrain a wide variety of models that are consistent with current cosmology, astrophysical and lab based constraints. Furthermore, because of the sharp change in $\Delta N_{\text{eff}}$ at the QCD phase transition, in the improvement from current constraints to projections for CMB-Stage IV can be quite dramatic.

For the minimal scenario of a single real scalar, reaching $\sigma(N_{\text{eff}}) \sim 1 \times 10^{-2}$ would push the constraint on freeze-out temperatures from electroweak scale to the reheat temperature. Nevertheless, a measurement a factor of a few times larger would still be extraordinarily valuable, for higher spin fields, multiple light scalars and modifications to the thermal history up to the electroweak scale. This broad reach to extremely high energies and very early times demonstrates the discovery potential for a precision measurement of $N_{\text{eff}}$ with the CMB. Furthermore, the CMB power spectrum has the ability to distinguish among certain types of dark radiation based on the behavior of its density perturbations [82, 47]. This point will be discussed further below.

## 3.4 Observational Signatures

Cosmic neutrinos play to two important roles in the CMB that are measured by $N_{\text{eff}}$. They contribute to the total energy in radiation which controls the expansion history and, indirectly, the damping tail. The

fluctuations of neutrinos and any other free streaming radiation also produces a constant shift in the of the acoustic peaks. These two effects drive both current and future constraints on $N_{\rm eff}$.

The effect of neutrinos on the damping tail has dominated has historically driven the constraint on $N_{\rm eff}$ in the CMB. The largest effect is from the mean-free path of photons, which introduces a suppression $e^{-(k/k_d)^2}$ to short wavelengths, with [301]

$$k_d^{-2} = \int \frac{da}{a^3 \sigma_T n_e H} \frac{R^2 + \frac{16}{15}(1+R)}{6(1+R)^2} \ , \tag{2.33}$$

where $R$ is the ratio of the energy in baryons to photons, $n_e$ is the density of free electrons and $\sigma_T$ is the Thompson cross-section. The damping scale is sensitive to the energy in all radiation through $H \propto \sqrt{\rho_{\rm radiation}}$ during radiation domination (which is applicable at high $\ell$, and is therefore sensitive to $N_{\rm eff}$ or any form of dark radiation. At this level, this also illustrates the degeneracy with $n_e$ which may be altered by the helium fraction, $Y_p$.

In reality, the effect on the damping tail is actually subdominant to the change to the scale of matter radiation equality and the location of the first acoustic peak [168]. As a result, the effect on neutrinos on the damping tail is more accurately represented by holding the first acoustic peak fixed. This changes the sign of the effect on the damping tail, but the intuition for the origin of the effect (and degeneracy) remain applicable.

In addition to the effect on the Hubble expansion, perturbations in neutrinos effect the photon-baryon fluid through their gravitational influence. The contributions from neutrinos are well described by a correction to the amplitude and the phase of the acoustic peaks in both temperature and polarization [44]. The phase shift is a particularly compelling signature as it is not degenerate with other cosmological parameters [44, 47]. This effect is the result of the free-streaming nature of neutrinos that allows propagation speeds of effectively the speed of light (while the neutrinos are relativistic). This effect is sensitive to any gravitationally coupled light thermal relics.

E-mode polarization will play an increasingly important role for several reasons. First of all, the acoustic peaks are sharper in polarization which makes measurements of the peak locations more precise, and therefore aid the measurement of the phase shift. The second reason is that polarization breaks a number of degeneracies that would also affect the damping tail [47].

*Status of current observations* – Planck has provided a strong constraint on $N_{\rm eff} = 3.15 \pm 0.23$ when combining both temperature and polarization data. The addition of polarization data has both improved the constraint on $N_{\rm eff}$ and reduced the impact of the degeneracy with $Y_p$. Recently, the phase shift from neutrinos has also been established direction in the Planck temperature data [137]. This provides the most direct evidence for presence of free-steaming radiation in the early universe, consistent with the cosmic neutrino background.

## 3.5   Forecasts

# 4   Sterile Neutrinos and Axions

## 4.1   Sterile Neutrinos

*Subsection to be completed by Kevork Abazajian*

A number of recent neutrino oscillation experiments have anomalies that are possible indications of four or more mass eigenstates. The first set of anomalies are in short baseline oscillation experiments: first, in the Liquid Scintillator Neutirno Detector (LSND) experiment, where electron antineutrinos were observed in a pure muon antineutrino beam [35]. The MiniBooNE Experiment also sees an excess of electron neutrinos and antineutrinos in their muon neutrino beam [21]. Two-neutrino oscillation interpretations of the results indicate mass splittings of $\Delta m^2 \approx 1 \text{ eV}^2$ and mixing angles of $\sin^2 2\theta \approx 3 \times 10^{-3}$ [21]. Another anomaly arises from re-evaluations of reactor antineutrino fluxes that indicate a an increased flux of antineutrinos as well as a lower neutron lifetime and commensurately increase the antineutrino events from nuclear reactors by 6%. This brought previous agreement of reactor antineutrino experiments to have a $\sim$6% deficit [227, 171]. Another indication consistent with sterile neutrinos are in radio-chemical gallium experiments for solar neutrinos. In their callibrations, a 5-20% deficit of the measured count rate was found when intense sources of electron neutrinos from electron capture nuclei were placed in proximity to the detectors. Such a deficit could be produced by a > 1 eV sterile neutrino with appreciable mixing with electron neutrinos [39, 141]. Some simultaneous fits to the short baseline anomalies and reactor neutrino deficits, commensurate with short baseline constraints, appear to prefer at least two extra sterile neutrino states [91, 195], but see Ref. [140]. Because such neutrinos have relatively large mixing angles, they would be thermalized in the early universe with a standard thermal history, and affect primordial nucleosynthesis [4].

In addition, there are combinations of CMB plus LSS datasets that are in tension, particularly with a smaller amplitude of fluctuations at small scale than that inferred in zero neutrino mass modesl. This would be alleviated with the presence of massive neutrinos, extra neutrinos, or both. In particular, cluster abundance analyses [299, 15] and weak lensing analyses [46] indicate a lower amplitude of fluctuations than zero neutrino mass [142]. Baryon Acoustic Oscillation measures of expansion history are affected by the presence of massive neutrinos, and nonzero neutrino mass may be indicated [55], though 2015 Planck results show a lack of such alleviation in cases with massive or extra neutrinos [13].

There is a potential emergance of both laboratory and cosmological indications of massive and, potentially, extra neutrinos. However, the combined requirements of the specific masses to produce the short baseline results, along with mixing angles that require thermalized sterile neutrino states, are inconsistent at this point with cosmological tension data sets [176, 27]. The tension data sets are not highly significant at this point ($\lesssim 3\sigma$), and there are a significant set of proposals for short baseline oscillation experiment follow up [1]. Future high-sensitivity probes of neutrino mass and number such as CMB-S4 will be able to definitively test for the presence of extra neutrino number and mass consistent with sterile neutrinos.

## 4.2 Axion-like Particles

*Subsection to be completed by Dan Green*

A ubiquitous component of extensions of the Standard model is axions and/or axion-like particles (ALPs). Axions have been introduced to solve the strong-CP problem [246], the hierarchy problem [152] and the naturalness of inflation [139]. Furthermore, they appear generically in string theory, in large numbers, leading to the qualitative phenomena describe as the string axiverse [32].

ALPS typically appear as (pseudo)-Goldstone bosons of some high energy global symmetry. At low energy, the mass of the ALP is protected by an approximate shift symmetry of the general form $a \to a + c$ where $a$ is the axion and $c$ is a constant (for non-abelian Goldstone bosons, this transformation will include higher order terms in $a$). We will define an ALP to be any such particle where all of the couplings of the axion to the Standard model respect such a symmetry. This symmetry may be softly broken with an explicit mass term, although this is highly restricted in the case of the QCD axion.

Two couplings of particular interest for axion phenomenology are the coupling to gluons and photons,

$$\frac{1}{4} g_{a\gamma\gamma} a \tilde{F}_{\mu\nu} F^{\mu\nu} \ , \qquad\qquad \frac{1}{4} g_{agg} a \tilde{G}_{\mu\nu} G^{\mu\nu} \ . \qquad\qquad (2.34)$$

These couplings typically appear as the consequence of chiral anomalies. The coupling of the axion to gluons is what makes the solution to the strong-CP problem possible. The coupling to photons is somewhat model dependent but typically arises in conjunction with the gluon coupling. In addition or instead of these coupling, a variety of possible couplings to matter may also be included.

Two very common features of these models is that the axions as typically light (in many cases, $m \ll 1$ eV) and their interactions are suppressed by powers of $f_a$. These two features make ALPS are particularly compelling target. Because of the small masses, they will often behave as relativistic species in the CMB. Furthermore, because their production rate will scale as $T^{2n+1}/f_a^{2n}$ for some $n \geq 1$, they are likely to be thermalized at high temperatures. Given that $\Delta N_{\text{eff}} > 0.027$ under such circumstances, a CMB experiment with sensitivity at this level will be sensitive to a very wide range of ALP models.

*Status of current observations* – Current constrains on ALPs arise from a combination of experimental [151], astrophysical [257] and cosmological [218] probes. Current cosmological constraints are driven by several effects that depend on the mass of the axion. For axion masses greater than 100 eV, stable thermal ALPs are easily excluded because they produce dark matter abundances inconsistent with observations. By including the free streaming effects of thermal QCD-axions, Planck data [112] combined with local measurements provide the constrain $m_a < 0.525$ eV (95 % CL). At larger masses, ALPs become unstable and can be constrained by the change to $N_{\text{eff}}$ from energy injection as well as from spectral distortions and changes to BBN [77, 137]

*Implications for CMB Stange IV* – Sensitive to $N_{\text{eff}}$ of order $\sigma(N_{\text{eff}}) \simeq 10^{-2}$ has the sensitive to probe then entire mass range of ALPs down to $m_a = 0$ under the assumption that it thermalized in the early universe. Interpreting such bounds in terms of the couplings of axions is more complicated [74] and can depend on assumptions about the reheating temperature. For high (but plausible) reheat temperatures of $10^{10}$ GeV, CMB stage IV would be sensitive to $g_{a\gamma\gamma}, g_{agg} \gtrsim 10^{-13} \text{GeV}^{-1}$ [], which exceeds current constraints and future probes for a range possible axions masses (including the QCD axion).

# 5   Complementarity of CMB and BBN

## 5.1   Introduction

Primordial light element abundances have historically been an interesting observational test of hot big bang cosmology. The process by which light elements form in the early universe known as big bang nucleosynthesis (BBN) was worked out theoretically in the early days of the development of the hot big bang model of cosmology [23]. It is a process which depends on all four fundamental forces, that unfolded during the first three minutes of our current phase of expansion, and which has long provided a useful constraint on physics beyond the standard model. The current observational limits on primordial abundances overall show good agreement with the predictions of standard BBN. Primordial light element abundances are sensitive to the radiation content of the universe as measured through $N_{\text{eff}}$, which also affects the angular power spectrum of the CMB. Combining these two probes provides useful insight into the physics of the early universe which neither could achieve alone.

## 5.2   Standard Big Bang Nucleosynthesis

In this section, we will briefly review the physics of big bang nucleosynthesis in the standard model. For more extensive reviews see for example [294, 239, 101].

At temperatures above $k_B T \sim 1$ MeV, weak interactions kept neutrons and protons in thermal equilibrium, fixing their number densities to have the ratio $n_n/n_p = e^{-Q/k_B T}$, where $Q = 1.293$ MeV is the mass difference between neutrons and protons. At lower temperatures, interactions which convert protons to neutrons could not keep up with the expansion rate, leaving free neutron beta decay as the only channel by which protons and neutrons interconverted. The initial ratio of their number densities at the freeze-out temperature $k_B T_{\rm fr} \simeq 0.8$ MeV was therefore

$$n_n/p_n = e^{-Q/k_B T_{\rm fr}} \simeq 1/5 \,. \tag{2.35}$$

After freeze-out, neutrons decayed until becoming bound into nuclei. This process proceeded primarily through two-body processes, starting with the formation of deuterium. The very small number density of baryons compared to that of photons (parametrized through $\eta \equiv n_b/n_\gamma$) delayed the start of these nuclear reactions until well after the temperature dropped below the binding energy of deuterium due to photo-dissociation of deuterium. The condition of the onset of deuterium formation is set by requiring that the number of photons per baryon with energy above the binding energy of deuterium drops below unity

$$\eta^{-1} e^{-|B_D|/k_B T_D} \simeq 1 \,. \tag{2.36}$$

With the deuterium binding energy given by $|B_D| = 2.23$ MeV, and $\eta \sim 6 \times 10^{-10}$, we find that deuterium begins to form when the temperature drops below about $k_B T_D \simeq 0.1$ MeV. By this time, due to free neutron decay, the neutron to proton ratio had dropped to about $n_n/n_p \simeq 1/7$. Once deuterium was able to form, nearly all of the neutrons quickly became bound into the most energetically favorable light nucleus, which is $^4$He. We can estimate the mass fraction of primordial $^4$He, $Y_p \equiv \dfrac{\rho\left(^4{\rm He}\right)}{\rho_b}$ to be

$$Y_p = \frac{2(n_n/n_p)}{1 + n_n/n_p} \simeq 0.25 \,. \tag{2.37}$$

In addition to $^4$He, BBN produces a small amount of D, $^3$He, $^6$Li, and $^7$Li (and also $^7$Be which subsequently decays by electron capture to $^7$Li). While $Y_p$ is primarily sensitive to the neutron lifetime, the primordial abundances of the other light elements depend in complicated ways various nuclear rates and generally require numerical computation (see for example [292, 100, 247]).

Standard BBN is a one parameter model, depending only on the baryon to photon ratio $\eta$. The theory predicts several abundances which can be used to fix $\eta$ and check the consistency of the theory, or alternatively, to constrain new physics. Current observations agree quite well with the predictions of standard BBN, with the exception of $^7$Li. It is unclear whether this disagreement points to a problem with the astrophysical determination of the primordial abundance or a problem with the standard theory. The cosmological lithium problem remains unsolved [133]. From here on, however, we will ignore the lithium problem and focus on how measurements of the other abundances (primarily D and $^4$He) can be used to constrain the physics of the early universe.

## 5.3    Beyond the Standard Model

Moving beyond standard BBN, measurements of primordial abundances have the ability to constrain many deviations from the standard thermal history and the standard model of particle physics. Because BBN is sensitive to all fundamental forces, changes to any force can in principle impact light element abundances. Of primary interest for our purpose is that BBN is sensitive to the expansion rate between about one second and a few minutes after the end of inflation. The expansion rate is in turn determined by the radiation content of the universe during this period, and thus BBN is sensitive to $N_{\rm eff}$.

More specifically, the expansion rate determines the freeze-out temperature setting the initial ratio of neutrons to protons and the amount of time free neutrons have to decay. Additional radiation compared to the standard model gives a higher expansion rate, which leads to a higher freeze-out temperature and less time for free neutron decay, leading to a larger primordial $^4$He abundance. The freeze-out temperature also depends weakly on the distribution function of electron neutrinos, though this is subdominant to the dependence $N_{\rm eff}$ for small non-thermal distortions [270].

Historically, $Y_p$ had provided the best constraint on $N_{\rm eff}$. Recent advancements in the determination of primordial deuterium abundance have made constraints on $N_{\rm eff}$ from deuterium competitive with those from $Y_p$ [94]. The precision with which primordial abundances constrain $N_{\rm eff}$ is now comparable to that of constraints the CMB power spectrum, and there is no evidence for deviation from the standard model [13].

## 5.4    Complementarity with the CMB

The CMB can be used to quite precisely constrain $\eta$ by measurement of the baryon fraction of the critical density, which is related to $\eta$ by

$$\Omega_b h^2 \simeq \frac{\eta \times 10^{10}}{274} \, . \tag{2.38}$$

Using the value of $\eta$ determined from CMB measurements as an input for BBN makes standard BBN a theory without free parameters which agrees very well with all observations (apart from the aforementioned disagreement with the observed lithium abundance). The CMB and BBN are sensitive to the baryon density measured at different times. While BBN is sensitive to the baryon to photon ratio up to a few minutes after the end of inflation, the CMB is sensitive to the baryon density at much later times, closer to recombination about 380,000 years later. Combining constraints from BBN and CMB on the baryon fraction therefore allows constraints on models where the photon or baryon density changes between these times.

The precision with which the CMB can constrain $N_{\rm eff}$ will soon come to surpass the constraints from BBN, but the value of the latter will not be totally eclipsed. BBN and the CMB probe the physics at different times, and so combining constraints can give insight into models where $N_{\rm eff}$ changes in time. If it were measured for example that $N_{\rm eff}^{\rm BBN} < N_{\rm eff}^{\rm CMB}$, this could be explained by the late decay of some unstable particles [135, 226, 165]. Alternatively, if observations revealed that $N_{\rm eff}^{\rm BBN} > N_{\rm eff}^{\rm CMB}$, this might signal late photon heating [76, 228].

The power spectrum of the CMB is also directly sensitive to $Y_p$. Since helium recombines earlier than hydrogen, the density of helium present at the time of recombination affects the free electron density, and thereby affects the damping tail of the CMB (though in a way which can be distinguished from the effects of $N_{\rm eff}$) [44, 168, 137, 47]. The degeneracy between $Y_p$ and $N_{\rm eff}$ is more strongly broken with precise CMB polarization data.

CMB-Stage IV (Check for consistent notation) will provide constraints on $N_{\rm eff}$ which are about an order of magnitude better than the current best constraints, and will also improve on the measurement of $Y_p$ by about a factor of two compared to the current best astrophysical measurements. Combined with measurements of other primordial abundances, this will help to provide a very thorough check of our understanding of the early universe and provide the opportunity to discover physics beyond the standard model.

# 3

---

# Dark Energy / Gravity / Dark Matter

## 1   Introduction

Here is an intro. Test commit

## 2   Dark Matter

We have learned from many different experiments (weak and strong lensing, studies of the Bullet Cluster, the Cosmic Microwave Background, etc) that approximately 84% of all the matter in the universe is composed of dark matter, which is not accounted for by the Standard Model of particles. However, the particle nature of dark matter remains unknown.

There are various types of experiments trying to shed light on this question: direct detection experiments, indirect detection experiments, and collider experiments. An alternative observable where Dark Matter interactions can modify the Standard Model prediction is the CMB power spectrum. CMB-Stage IV will have the sensitivity to detect new cosmological signatures originating from various types of dark matter interaction. In the sections below, we will discuss some of these possible scenarios.

### 2.1   Dark Matter Annihilation

One of the leading candidates for dark matter are the Weakly Interactive Massive Particles (WIMPs). If dark matter consists of WIMPs, we would expect these particles to self-annihilate. The annihilation of dark matter produces a shower of very energetic particles, that injects energy into the universe, ionizing the matter in it.

This extra source of ionization has distinctive effects on the Cosmic Microwave Background (CMB): it suppresses the CMB temperature and polarization fluctuations at small angular scales, and it enhances the CMB polarization fluctuations at large angular scales due to the extra scattering of photons off free electrons [?, ?]. CMB temperature and polarization spectra can constrain the parameter $p_{\mathrm{ann}} = f \langle \sigma v \rangle / m_{\mathrm{DM}}$, where $f$ is the fraction of energy deposited into the plasma, $\langle \sigma v \rangle$ is velocity-weighted cross section, and $m_{\mathrm{DM}}$ is the mass of the DM particle. Current constraints coming from WMAP 9-year data, Planck, ACT, SPT, BAO, HST and SN data excluded Dark Matter masses below 26 GeV at the $2\sigma$ level, assuming that all the energy is deposited in the plasma [?]. CMB-Stage IV is expected to tighten these constraints by a factor of 10 [?]. Dark-matter annihilation also leads to growing ionization fraction perturbations and amplified small-scale cosmological perturbations, leaving an imprint on the CMB bispectrum [?].

## 2.2   Non-Standard Dark Matter Physics

Near the epoch of CMB last scattering, dark matter (DM) accounts for about 65% of the energy budget of the Universe, hence making the CMB a particularly good probe of potential new physics in the DM sector. Of particular relevance to CMB studies, the presence of new DM interactions with light degrees of freedom [148, 80, 150, 211, 110, 36, 153, 256, 70, 62, 215, 271, 223, 290, 298, 297, 121, 61, 125, 138, 8, 29, 131, 181, 51, 182, 290, 89, 166, 107, 104, 113, 40, 128, 127, 222, 102, 88, 87, 71, 86, 28, 258, 75, 200, 85] can leave subtle imprints on the temperature and polarization CMB power spectra. The introduction of such non-minimal DM models has been primarily (but not exclusively) motivated in the literature by potential shortcomings of the standard cold DM scenario at small sub-galactic scales [108, 191, 230, 302, 238, 66, 243, 293, 245, 190, 240, 244]. While these issues are far from settled, they motivate the search for other non-minimal DM signatures in complementary data sets (such as the CMB) that could indicate whether or not DM can be part of the solution. In addition, DM interacting with light (or massless) dark radiation (DR) has been put forward [75, 200] has a potential solution to the small discrepancy between the amplitude of matter fluctuations inferred from CMB measurements and those inferred from cluster number counts and weak lensing measurements. As we discuss below, CMB-S4 measurements of the CMB lensing and the lensed B-mode power spectra have the potential to significantly improve constraints on DM interacting with light degrees of freedom in the early Universe.

The key equations governing the evolution of cosmological fluctuations for this broad class of non-minimal DM models are presented in Ref. [106]. Essentially, the new DM physics enters entirely through the introduction of DM and DR opacities, which, similarly to the photon-baryon case, prohibit DR free-streaming at early times and provides a pressure term that opposes the gravitational growth of DM density fluctuations. The impact of this new physics on CMB fluctuations has been studied in detail in Ref. [102] and we briefly review it here. First, the presence of extra DR mimics the presence of extra neutrino species and affects the expansion history of the Universe, possibly modifying the epoch of matter-radiation equality, the CMB Silk damping tail, and the early Integrated Sachs-Wolfe effect. However, unlike standard free-streaming neutrinos, the DR forms a tightly-coupled fluid at early times, leading to distinct signatures on CMB fluctuations which include a phase and amplitude shift of the acoustic peaks (see e.g. Ref. [44, 105, 137]). Second, the DR pressure prohibits the growth of interacting DM fluctuations on length scales entering the causal horizon before the epoch of DM kinematic decoupling. This weakens the depth of gravitational potential fluctuations on these scales, hence affecting the source term of CMB temperature fluctuations. Finally, the modified matter clustering in the Universe due to nonstandard DM properties will affect the lensing of the CMB as it travel from the last-scattering surface to us.

**CD: More comments:**

**- At what ell does the DR mainly affect the CMB?**

**- How important is the effect on the B-mode lensing?  Could you be a bit more quantitative here?**

**- How relevant would it be for CMB-S4?  You should think about a full-sky experiment with 1-4 arcmins beam and a detector noise of DeltaP 0.5-1 muK-arcmin.**

**- How big is the degeneracy expected to be with neutrino mass?**

**- Mention that these DM constraints are a lot more sensitive to $\ell_{\max}$ than $\ell_{\min}$.**

**Briefly discuss the possible degeneracy between the impact of interacting DM and massive neutrinos on the matter power spectrum.**

## 2.3 Ultralight axions

Here is the updated text and I've made changes to the .bib file to include those references.

Ultralight axions (ULAs) with masses in the range $10^{-33}$ eV $\leq m_a \leq 10^{-20}$ eV are well motivated by string theory, can contribute to either the dark matter or dark energy components of the Universe, depending on their masses, and are distinguishable from DE and CDM in cosmological observables. The current best constraints from the primary CMB TT power, and WiggleZ galaxy redshift survey were made in [**?**].

The degeneracies of the axions with other cosmological parameters, such as $N_{\text{eff}}$ or neutrino mass $\sigma$ $m_\nu$ vary depending on the axion mass assumed. Dark energy-like axions with masses around $10^{-33}$ eV change the late-time expansion rate and therefore the sound horizon, changing the location of the acoustic peaks. This has degeneracies with the matter and curvature content. Axions that behave more like dark matter (for masses around $m_a \gtrsim 10^{-26}$ eV) start oscillating in the radiation era and reduce the angular scale of the diffusion distance, leading to a boost in the higher acoustic peaks, which has a degeneracy with $N_{eff}$. In both of these cases, improved errors on the temperature and polarization power spectrum, coupled with constraints on the Hubble constant (for the lightest axions) from Baryon Acoustic Oscillations, lead to improvements in the error on allowed axion energy density of a factor of three. In the matter power spectrum, and thus CMB lensing power, light axions suppress clustering power, suggesting a degeneracy with effects of massive neutrinos that must be broken to make an unambiguous measurement of neutrino mass using the CMB. The above mentioned effects in the expansion rate likely break this degeneracy.

Adding in information from the lensing reconstruction using S4 will improve constraints on axion DM significantly, and allow one to break the degeneracy between dark-matter like axions and massive neutrinos. A percent-level measurement of the lensing deflection power at multipoles L > 1000 leads to an improvement in the error on the axion energy density of a factor of eight relative to the current Planck constraints, for an axion mass of $m_a = 10^{-26}$ eV. Furthermore, S4 will improve the maximum axion mass constrainable by the CMB by up to two orders of mangitude from $m_a = 10^{-24}$ eV to $m_a = 10^{-22}$ eV. Achieving this improvement in the mass constraint will require improved understanding of non-linear clustering of axions. If realized it will begin to make contact to the preferred axion model to solve the CDM small scale crises [**?**, **?**].

# 4

# CMB Lensing

# 6   Systematic Effects and Mitigation

## 6.1   Astrophysical Foregrounds

## 6.2   Instrumental Effects

# 7   Instrument, Survey, and Simulation Requirements

# 5

# Experimental Approach
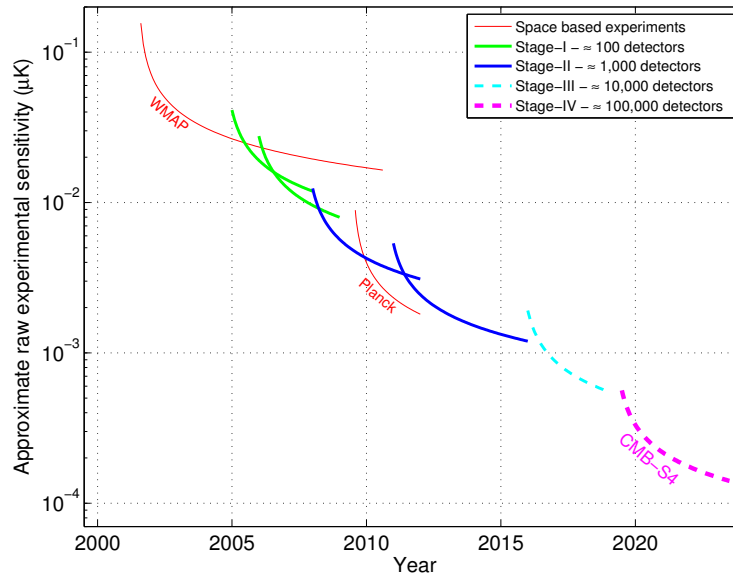
## 1   Introduction



**Figure 6.**   *Plot illustrating the evolution of the raw sensitivity of CMB experiments, which scales as the total number of bolometers. Ground-based CMB experiments are classified into Stages with Stage II experiments having O(1000) detectors, Stage III experiments having O(10,000) detectors, and a Stage IV experiment (such as CMB-S4) having O(100,000) detectors. Figure from Snowmass CF5 Neutrino planning document.*

Experiment design from science goals

- depth

- sky area

- resolution

- ell space coverage

-frequency coverage
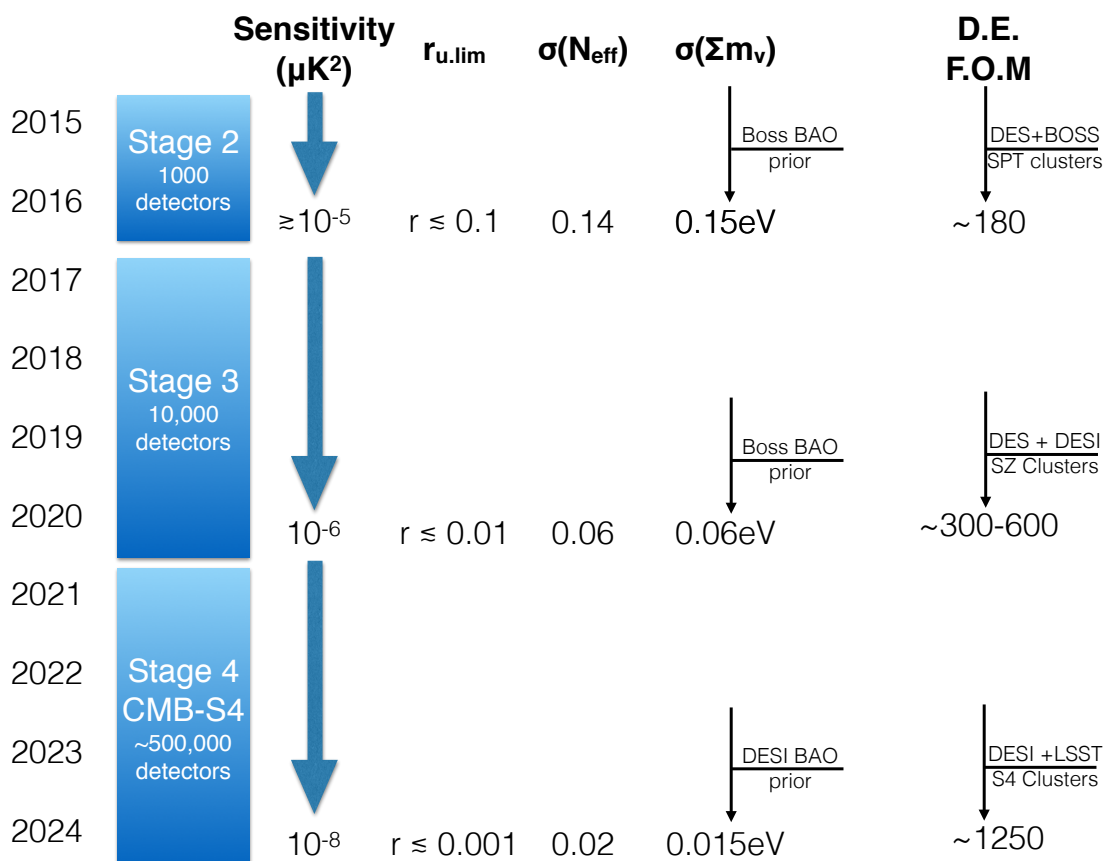
**Figure 7.** *Schematic timeline of evolution of Stage 3 and CMB-S4 sensitivity in $\mu K^2$ and the expected improvement in a few of the key cosmological parameters.*

# 2 Complementarity of Ground and Space

# 3 Detector Arrays

- Superconducting Arrays

- TES

# 4   Multiplexer technologies

# 5   Telescopes and Optics

- Polarization modulators

# 6   Sites

- Chile + Pole

- Northern Site

# 6

# Simulations and Data Analysis

## 1  Introduction

Extracting science from a CMB dataset is a complex, iterative process requiring expertise in both physical and computational sciences. In this chapter we start by outlining the data analysis pipeline and describing how this is complicated by various real-world issues ranging from instrument systematics to computational tractability. We then discuss the drivers for, and corresponding structure of, the simulation pipeline. Next we couple these into an overall simulation and data analysis pipeline, and motivate the division of this pipeline into 5 subsets based on the challenges they pose and the expertise required to meet these. Finally we consider each of these subsets in turn, sketching their current state of the art and noting the prospects for addressing their challenges in the context of the CMB-S4 mission.

## 1.1  Data Analysis

The reduction of a CMB data set typically proceeds in a sequence of steps:

**Pre-processing:** The raw time-ordered detector data are calibrated and gross time-domain systematics are either removed (typically by template subtraction, filtering or marginalization) or flagged. The goal here is to make the real data match a model that will underpin all subsequent analyses.

**Map-making:** At each observing frequency, estimates of the intensity I and the Stokes Q- and U-polarizations of the sky signal are extracted from the cleaned time-ordered data based on their spatial stationarity, typically using some degree of knowledge of the instrument's noise properties.

**Component separation:** If sufficient frequenciy maps are available, the CMB can be separated from the various foreground sky components based on its unique spectral invariance (in CMB units).

**Power spectrum estimation:** The six auto- and cross-angular power spectra of the CMB temperature T and E- and B-mode polarizations are estimated from the CMB and/or frequency maps, and corrected for E- to B-mode lensing.

**Parameter estimation:** The best-fit parameters for any cosmological model are derived by comparing the theoretical TT, TE, EE and BB CMB power spectra that they would induce with the data and their uncertainties.
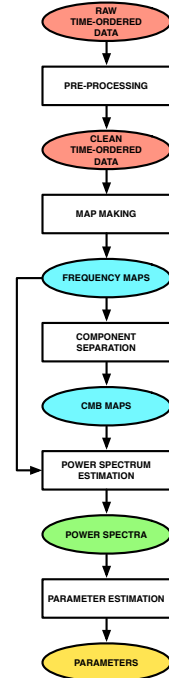


**Figure 8.**  *CMB data reduction*

This reduction essentially consists of a series of changes of basis for the data, from time samples (red) to map pixels (blue) to spectral multipoles (green) to cosmological parameters (yellow), with each basis-change reducing the data volume, increasing the signal-to-noise, and exposing a different class of systematic effects for mitigation.

Note however that the data can only remain a sufficient statistic at each step in the reduction if we also propagate its full covariance matrix. Since this is an $\mathcal{N}_b \times \mathcal{N}_b$ matrix in the dimension of the basis, its construction, manipulation and reduction pose the greatest computational challenge to this analysis. In particular the full pixel-domain data covariance matrix is generally dense and unstructured, requiring $O(\mathcal{N}_p^3)$ operations to build and $O(\mathcal{N}_p^2)$ bytes to store. All the major drivers of CMB science - polarization sensitivity, higher resolution, larger sky coverage - push us towards larger pixel counts, with an instrument mapping a fraction of the sky $f_{sky}$ with a beam of $b$ arcminutes covering $O(10^9 f_{sky}/b^2)$ pixels per IQU-component. For the last decade or more the computational intractability of the resulting pixel-domain matrices has forced us to replace explicit covariance propagation with Monte Carlo methods in all but a limited set of small sky fraction/low resolution cases.
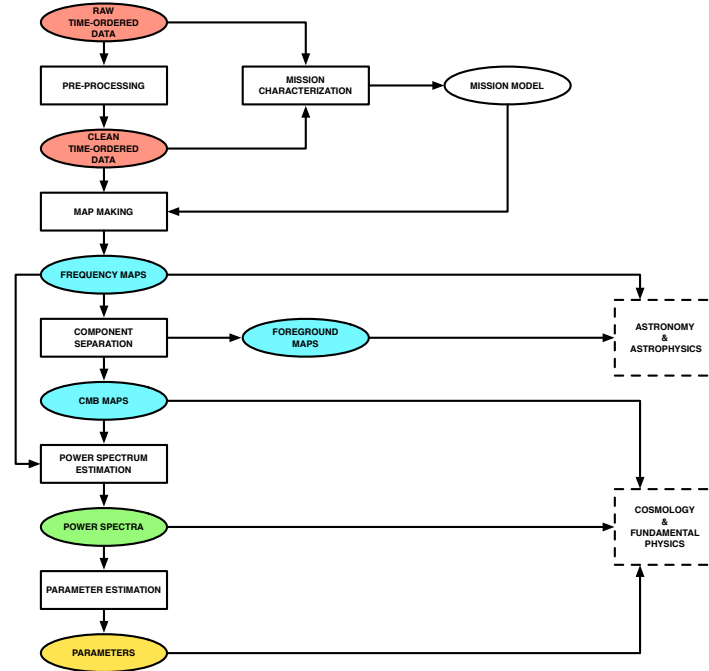


**Figure 9.**   *The CMB data analysis pipeline*

Beyond this basic data reduction, the full analysis pipeline (Figure 9) also includes mission characterization and science exploitation branches. Time domain data are extensively used to build a model of the mission, which we take to comprise the instrument and the observation. For the instrument this modeling can include such steps as determining beam profiles from planet crossings, and estimating noise properties (including cross-correlations) from calibrated, signal-subtracted, detector data; for the observation, it includes reconstructing the detector pointing and polarization orientation from telescope sensor data ,and incorporating atmosphere records in the data-flagging. The resulting mission model then feeds back into all of the ensuing data reduction and interpretation. The primary science exploitation derives cosmology and fundamental physics results from the various correlation functions of the CMB maps, from the power spectra's energy scale of inflation and neutrino mass to the higher-order statistics' measures of non-Gaussianity and the lensing

potential. In addition the frequency maps represent important astronomical and astrophysical observations, particularly when the frequency sampling is sufficient to isolate individual foreground components along with the CMB.

## 1.2 Simulation

Simulations of a CMB mission's data play a number of critical roles; specifically they are required for

- The design and development of both the instrument and the observation, to ensure that the mission is capable of meeting its science goals.

- The validation and verification of all data analysis tools, including those used in data reduction, mission charaterization and science exploitation.

- Monte Carlo based uncertainty quantification and debiasing, particularly when the full data covariance matrix is computationally intractable.

As shown in Figure 10, given a mission model (both instrument and observation) and a sky model (both CMB and foregrounds) we can generate a simulation of the mission data in any of its domains. However, there is an inevitable trade-off between how representative the simulation is of real data and the complexity of the input models and computational cost of generating the simulation. The choice of the simulation data domain will then be determined by the balance between the realism requirements and the complexity/cost constraints for the particular task at hand.
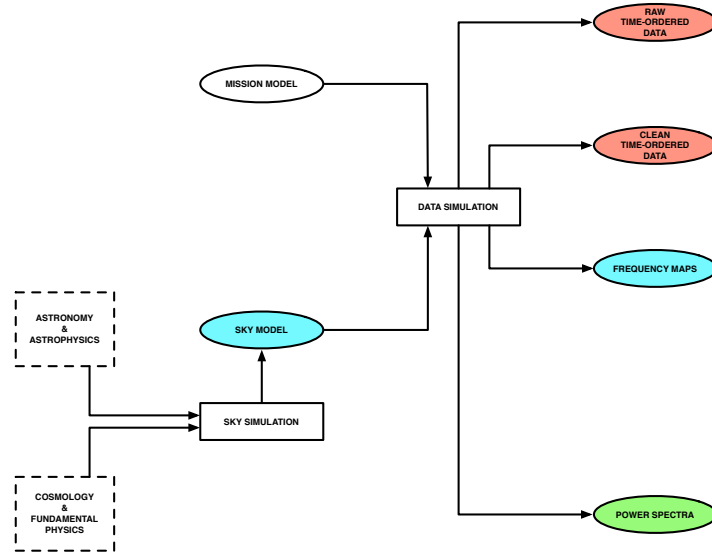


**Figure 10.** *The CMB simulation pipeline*

Note that the generation of the input mission and sky models are themselves far from trivial tasks. The mission model is typically derived from pre-deployment measurements of the instrument properties refined by characterization from the data themselves, together with ancilliary telescope and environmental data characterizing the observation; the sky model requires its own dedicated simulation capability which - since it is independent of the details of any single mission - can be a community-wide endeavor.

## 1.3 The Simulation and Data Analysis Pipeline

Coupling the above, the overall simulation and data analysis pipeline (Figure 11) can now be seen as both a top-down data reduction process and a wrap-around refinement of our mission and sky modeling. Typically the two phases are interleaved, with each new data reduction improving our mission and sky models, which are in turn fed back into an improved data reduction.
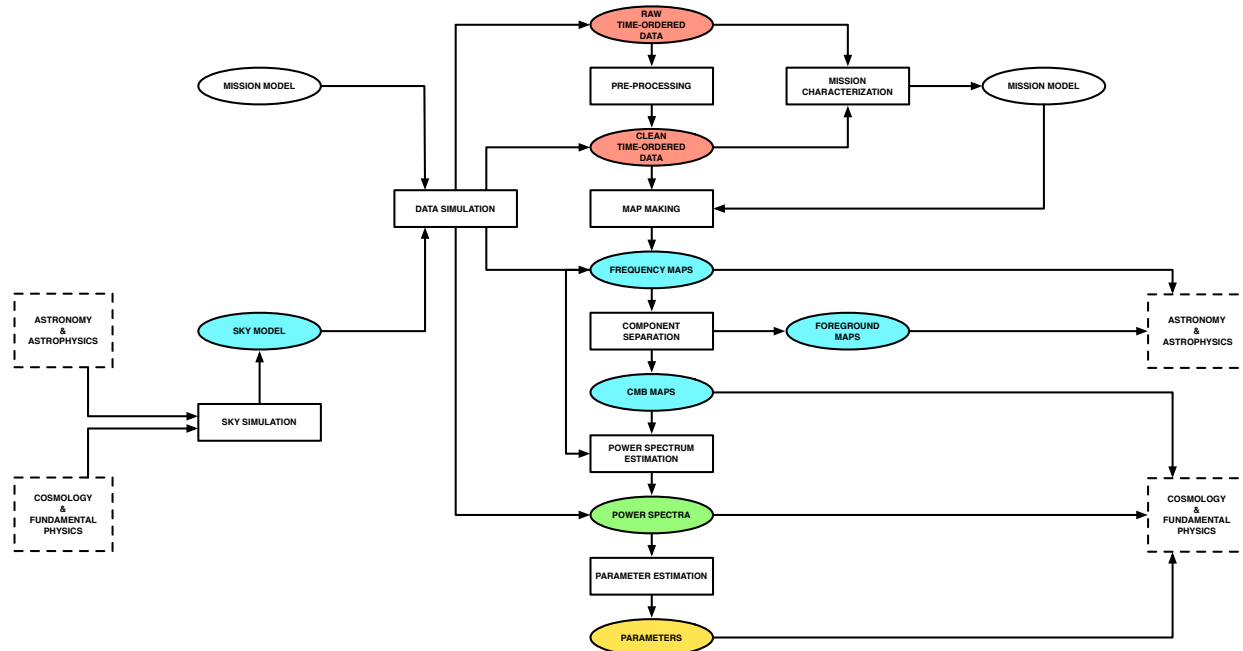


**Figure 11.**  *The full CMB simulation and data analysis pipeline*

The implementation and execution of this pipeline still poses many challenges to the CMB community, and we can subdivide it into 5 subsets based on the nature of these challenges and the expertise and activity required to address them:

**Forecasting:** Rapid assessment of nominal scientific performance under sufficiently simplifying mission and sky models that all analysis can be done in the spectral domain.

**Sky modeling:** Mission-independent modeling of the CMB (scalar, tensor and non-Gausian) and the astrophysical foregrounds (galactic and extra-galactic), including the couplings between them.

**Time-ordered data processing:** All processes that require the manipulation of time-domain data, dominated by the associated 'Big Data' challenges.

**Component separation:** Separation of the CMB from the foreground sky, ideally also including separation of the individual foreground components to feed back into improved sky modeling.

**Statistics and parameters:** Derivation of CMB map statistics, including the 2-, 3-, and 4-point correlation functions, together with the parameters of cosmology and fundamental physics that they constrain.

# 2 Forecasting

Here we describe the main approaches used by our community for forecasting the expected performance of CMB-S4. For assessing the expected performance for large-scale B-modes, two central considerations are Galactic foregrounds and ability to delens the data, as well as a realistic assessment of instrument noise at large scales.

To assess the science return from the smaller-scale polarization two-point functions (TE,EE), and from the lensing four-point function ($\kappa\kappa$), extragalactic foregrounds and instrumental noise are the key considerations.

To forecast the return of the thermal Sunyaev-Zel'dovich effects, an estimate of the expected cluster counts as a function of mass and redshift is the core statistic, combined with an estimate of how well the masses can be calibrated using overlaps with weak lensing surveys. For the kinetic Sunyaev-Zeldovich effect, extragalactic foregrounds and overlap with spectroscopic surveys must all be considered.
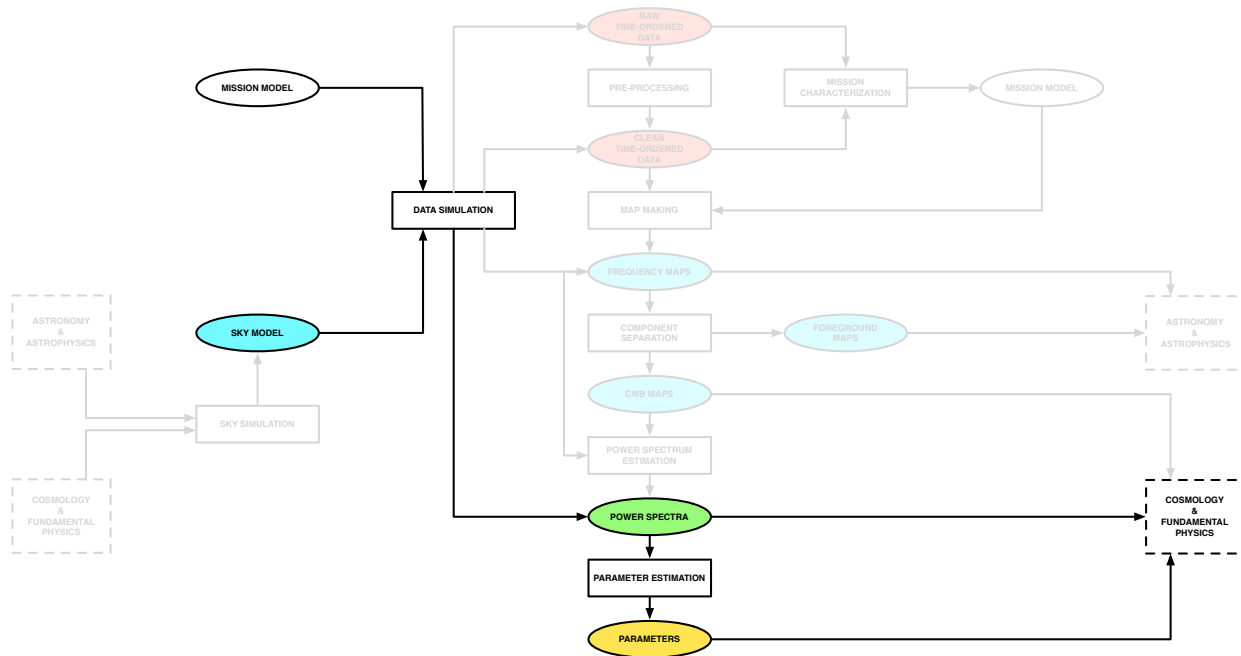


**Figure 12.** *The forecasting subset of the CMB simulation and data analysis pipeline*

## 2.1 Limits on the tensor-to-scalar ratio

### 2.1.1 Spectrum-based domain forecasting

**Forecasting in spectral domain coming from John Kovac**

### 2.1.2 Map-based domain forecasting

Foregrounds are intrinsically non-Gaussian, so it is beneficial to consider approaches directly in map space, to check the robustness of spectrum-based approaches, in particular in the case of pessimistic foregrounds where the spectral indices or dust emissivities have non-trivial spatial variation. Here one of the approaches our community uses is a Bayesian model fitting method, where the foregrounds are described parametrically using a physical model for each component.

Using this method, maps of the CMB plus Galactic foreground sky and expected noise are simulated at each of the CMB-S4 frequencies and integrated across the expected bandpasses, using Galactic models as described for example in Section **??**. Simulations at ancillary frequencies that might be provided by other experiments, for example the Planck data, can also be included in the same way. A parameterized model is then fit to the simulated maps, for example fitting the CMB, thermal dust, and synchrotron in small pixels, and typically the synchrotron spectral index and dust emissivity and temperature in larger pixels of order degree-scale or larger. The BB power spectrum of the foreground-marginalized CMB map is then estimated using e.g., the Master algorithm or a pixel-based likelihood, and converted into an estimate of $r$ and its uncertainty. Our community has at least two such codes that can perform this procedure (Commander and BFoRe).

This method allows for an assessment of the expected bias on $r$ if the model does not match the simulation, and shows how much the expected uncertainty on $r$ would increase if more complicated foreground models are explored e.g. [**?**, **?**]. It is more computationally expensive than spectral-domain forecasts though, so we limit this approach to a smaller subset of explorations.

## 2.2 Limits on parameters from TT/TE/EE/$\kappa\kappa$

To forecast the expected constraints on cosmological parameters from TT/TE/EE and $\kappa\kappa$ for CMB-S4, many of our community's codes use a Fisher matrix method, which assumes that the resulting parameter distributions are close to Gaussian. Some forecasts are performed using full MCMC simulations if the parameters are known to be highly non-Gaussian.

For CMB-S4, the method we follow is to combine CMB-S4 specifications with other available datasets, for example the data from Planck and expected measurements of Baryon Acoustic Oscillations and other low redshift data.

For the noise levels of Planck, we assume that a data release including reliable polarization data will have happened before CMB-S4 data is taken, and forecast results that include TE and EE data and also large-scale polarization from HFI at multipoles lower than CMB-S4 is expected to reach. This follows approaches in e.g. [**?**].

Our community uses two approaches to these Fisher forecasts, either considering the unlensed maps and the lensing convergence map as the basic statistics, or the lensed power spectra of those maps together with the reconstructed $\kappa\kappa$ spectrum. In the case of the power spectrum approach, to compute the Fisher matrix for the CMB we use the lensed power spectrum between each pair of fields $X, Y$:

$$\hat{C}_\ell^{XY} = \frac{1}{2\ell+1} \sum_{m=-\ell}^{m=\ell} x_{\ell m}^* y_{\ell m}. \tag{6.1}$$

The estimated power spectrum is Gaussian distribution to good approximation at small scales. In this case a full-sky survey has

$$-2\ln\mathcal{L}(\boldsymbol{\theta}) = -2\sum_\ell \ln p(\hat{C}_\ell|\boldsymbol{\theta}) = \sum_\ell \left[(\hat{C}_\ell - C_\ell(\boldsymbol{\theta}))^\top \mathbb{C}_\ell^{-1}(\boldsymbol{\theta})(\hat{C}_\ell - C_\ell(\boldsymbol{\theta})) + \ln\det(2\pi\mathbb{C}_\ell(\boldsymbol{\theta}))\right] \qquad (6.2)$$

where $\hat{C}_\ell = (\hat{C}_\ell^{TT}, \hat{C}_\ell^{TE}, ...)$ contains auto- and cross-spectra and $\mathbb{C}_\ell$ is their covariance matrix. Discarding any parameter dependence in the power spectrum covariance matrix gives

$$F_{ij} = \sum_\ell \frac{\partial C_l^\top}{\partial\theta_i}\mathbb{C}_\ell^{-1}\frac{\partial C_l}{\partial\theta_j}. \qquad (6.3)$$

Here the covariance matrix for the power spectra has elements

$$\mathbb{C}(\hat{C}_l^{\alpha\beta}, \hat{C}_l^{\gamma\delta}) = \frac{1}{(2l+1)f_{\text{sky}}}\left[(C_l^{\alpha\gamma} + N_l^{\alpha\gamma})(C_l^{\beta\delta} + N_l^{\beta\delta}) + (C_l^{\alpha\delta} + N_l^{\alpha\delta})(C_l^{\beta\gamma} + N_l^{\beta\gamma})\right], \qquad (6.4)$$

where $\alpha, \beta, \gamma, \delta \in \{T, E, B, \kappa_c\}$ and $f_{\text{sky}}$ is the effective fractional area of sky used.

The second approach we consider is to construct the Fisher matrix using the unlensed temperature and polarization fields, and the lensing convergence field, rather than the suite of lensed two-point spectra and the lensing four-point function. Both approaches give consistent estimates.

The CMB lensing reconstruction noise is calculated using the [?] quadratic-estimator formalism. Our nominal approach is to neglect non-Gaussian terms in the power spectrum covariance. We also avoid including information from both lensed BB and the four-point $\kappa\kappa$, as they are covariant. The BB spectrum will not contribute as significantly to S4 constraints, compared to $\kappa\kappa$, and has a highly non-Gaussian covariance [?].

To address the issue of possible extragalactic foregrounds, we set a maximum multipole for the recoverable information of $\ell_{\text{max}}^T = 3000$ and $\ell_{\text{max}}^P = 4000$ for CMB-S4, as foregrounds are expected to be limiting at smaller scales. We also set a minimum multipole due to the challenge of recovering large-scales from the ground, and consider in general $\ell = 50$. We include Planck data at the scales $\ell < \ell_{\text{min}}$.

When relevant, we can also add information from Baryon Acoustic Oscillation (BAO) experiments. This can be done by adding the BAO Fisher matrix

$$F_{ij}^{\text{BAO}} = \sum_k \frac{1}{\sigma_{f,k}^2}\frac{\partial f_k}{\partial\theta_i}\frac{\partial f_k}{\partial\theta_j} \qquad (6.5)$$

where $f_k = r_s/d_V(z_k)$ is the sound horizon at photon-baryon decoupling $r_s$ over the volume distance $d_V$ to the source galaxies at redshift $z_k$. We also follow standard approaches to including other low redshift probes.

### 2.2.1 Instrument and atmospheric noise

Noise spectra are generated assuming the sum of white noise and atmospheric noise. The white noise part is given by

$$N_\ell^{\alpha\alpha} = (\Delta T)^2 \exp\left(\frac{\ell(\ell+1)\theta_{\text{FWHM}}^2}{8\ln 2}\right) \qquad (6.6)$$

for $\alpha \in \{T, E, B\}$, where $\Delta T$ ($\Delta P$ for polarization) is the map sensitivity in $\mu$K-arcmin and $\theta_{\text{FWHM}}$ is the beam width.

To estimate the atmospheric noise level in intensity, we consider levels at the South Pole and in Chile. For Chile, we base this estimate on current data from ACT and POLARBEAR. for the South Pole, we use data from SPT and BICEP as a guide. We then make the assumption that the atmospheric noise will scale down with observation time for detector arrays within a telescope, and will be uncorrelated for physically separated telescopes. For polarization our nominal estimate is white noise, assuming that use of modulators minimizes atmospheric contamination.

## 2.3   Limits on parameters from tSZ/kSZ

To estimate the expected tSZ cluster counts from S4, we use.

# 3   Sky Modeling

The capability of CMB-S4 to address its science program crucially depends on the possibility to separate the signals of interest from astrophysical emission originating from various astrophysical processes, and on the accuracy of the characterization of foreground residuals after such cleaning is performed.

The polarised CMB is mostly contaminated by diffuse emission from the interstellar medium of our own Milky Way. Both synchrotron and thermal dust are highly polarised (at the level of tens of per cents, depending on the observed region). Their integrated emission dominates over both the CMB E-modes and the CMB B-modes on large angular scales, and cannot be safely neglected at scales where B-modes from gravitational lensing dominate without robust analyses of their impact on lensing science. Other components, such as spinning dust, free-free emission, emission of molecular lines such as CO, could in principle be polarized at a lower level, of order 1-2 per cent or less, but measurements or upper limits are scarce, and not sufficient at this stage for robust predictions of the polarized amplitude of their emission over large patches of sky. For low angular resolution observations, the presence of polarized extragalactic radio and infrared sources constitutes an additional source of contamination, which must be removed with a combination of masking or subtracting individual sources, and modeling residuals at the power-spectrum level.

Massive clusters are easily detected in atmospheric windows below 217 GHz (and in particular around 150 GHz) as decrements in high angular resolution maps of total sky emission fluctuations. The detection of low-mass, distant galaxy clusters, however, will suffer from confusion with fluctuations of the CIB emission (which can be locally positive or negative), and from contamination by radio and infrared sources in the cluster halos. Accurate determination of the clusters profiles, of their integrated Compton parameter $Y$ that serves as a mass-proxy for cosmological constraints, and of cluster peculiar velocities along the line of sight via the kinematic SZ effect, will require sufficient frequency coverage at high angular resolution (of order 1-2′) to separate the various SZ components (thermal SZ, relativistic corrections, and kinematic SZ) as well as sources of astrophysical confusion. In particular, it is plausible that high angular resolution observations of the positive side of the SZ effect (at frequencies above 217 GHz) will be required to fully exploit the sensitivity of CMB-S4 for galaxy cluster science.

More precise estimations of the impact of foreground emission on these main science targets of CMB-S4 hence require realistic simulations of the sky emission, that can be used to investigate the effectiveness of component separation techniques and assess the impact of residual contamination from foregrounds on the main scientific products (degradation of the error bars and possible biases). The place of such modelling in the CMB simulation and data analysis pipeline is shown in Figure 13.

A sky model is useful only as far as it captures adequately the characteristics of real sky emission that play an essential role in the performance of cleaning techniques and on the amplitude and statistical properties of residual contamination after such cleaning is performed. The key characteristics of sky emission for foreground cleaning are:

- The coherence and decoherence of diffuse emission across observed frequencies, which is key to identifying foreground emission in the form of patterns that scale with an emission law different from that of the CMB;

- The existence or not of a simple parametric emission law for each component emission, such as power laws (for synchrotron) or modified blackbody emission (for dust components);

- The absolute level of foreground emission (in particular for those components that do not scale simply as a function of frequency, such as the superposition of many individual sources with a specific emission law each);
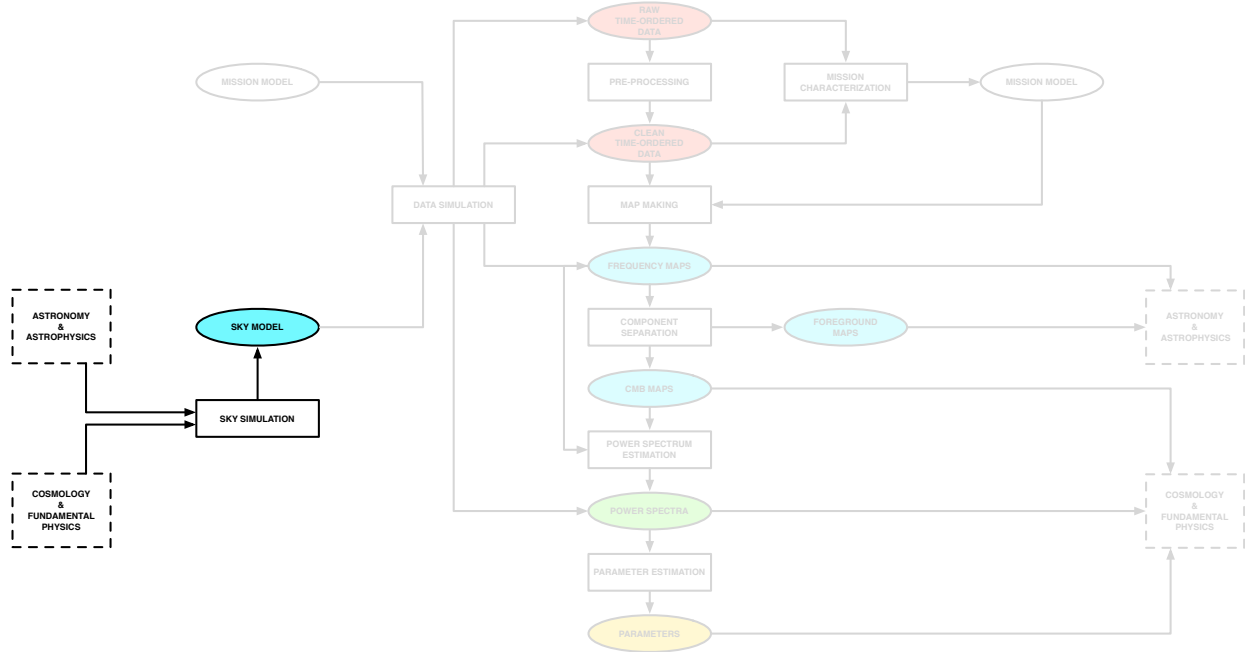
**Figure 13.** *The sky modeling subset of the CMB simulation and data analysis pipeline*

- Whether or not emissions for which the level of polarization is unknown or unclear (including possible surprises) are above the sensitivity objectives of CMB-S4, or can be safely neglected;

- The self-consistency of extragalactic emission (in particular CIB and SZ clusters) and CMB lensing. In particular, CIB as observed by Planck and by future instruments can be used to generate a proxy for the lensing potential, which can be used to partially de-lens the CMB B-modes.

The key challenges for a usable sky model are hence:

- The reliability of models based on observations at angular resolution lower than that of CMB-S4, integrated in broad frequency bands, and with a sensitivity limit at least an order of magnitude worse than what will be achieved with CMB-S4; the complexity of sky emission below current sensitivity limits must be extrapolated on the basis of existing knowledge and theoretical models, taking into account past experience when orders of magnitude in sensitivity were gained;

- The self-consistency of CMB secondary anisotropies (lensing, SZ emission from hot intra-cluster gaz and filaments, late ISW) and extra-Galactic foregrounds (CIB, radio and infrared sources) is crucial to both de-lensing, and to extragalactic science; generating reliable models over the entire Hubble volume is challenging, the evaluation of errors of such models even more so;

- The practical usability of the model (software engineering aspects for generating many simulations).

## 3.1 The sky modeling pipeline

The emission of the sky will be modeled as the sum of emission of different components, identified either by their emission process (e.g. Galactic synchrotron, due to electrons spiralling in the Galactic magnetic field), or by their region of origin (e.g. emission of a particular extragalactic source). These emissions, as a function of sky pixel and frequency, must then be band-integrated and beam-integrated to produce total emission maps as observed by the instrument. We decompose this simulation pipeline into two main steps: the multicomponent model of sky emission, which does not depend on the instrument, and the integration of this emission in the instrumental response.

### 3.1.1 The multi-component sky model

### 3.1.2 Sky emission observations

## 3.2 The Galactic interstellar medium

Strong evidence exists for variability of the physical properties of the interstellar medium as a function of the line of sight, and hence as a function of region of emission. Hence, in each line of sight the total ISM emission is the superposition of emission from various regions. Even assuming that each such region has a simple parameteric emission law, such as a power law or a modified blackbody, the superposition of such emission cannot be modeled with a single simple emission law. Modeling the Galactic ISM for future sensitive surveys such as CMB-S4 requires modeling this complexity at the appropriate level. It seems reasonable to use a multi-layer approach, in which each ISM component is modeled as a superposition of several layers, with a simple (although pixel-dependent and polarization dependent) emission law for each such layer.

### 3.2.1 Synchrotron

A baseline model we use here has a power law scaling with a modestly spatially varying spectral index. The emission templates are the Haslam 408 MHz data reprocessed by [**?**], and the WMAP 7-year 23 GHz Q/U maps [**?**] smoothed to 3 degree FWHM and with smaller scales added using the PSM code [**?**] The spectral index map is derived using a combination of the Haslam 408 MHz data and WMAP 23 GHz 7-year data [**?**] The same scaling is used for intensity and polarization. This is the same prescription as used in the Planck Sky Model's v1.7.8 'power law' option, but with the Haslam map updated to the Remazeilles version.

Extensions to this model that we are exploring include a curved power law model with a single isotropic curvature index, and a polarization spectral index that steepens with Galactic latitude by $\delta\beta \sim 0.2$ from low to high latitude, as this is currently consistent with WMAP and Planck data.

### 3.2.2 Thermal dust

A baseline model we consider has thermal dust modelled as a single component modified blackbody. We use dust templates for emission at 545 GHz in intensity and 353 GHz in polarisation from the Planck-2015 analysis, and scale these to different frequencies with a modified black-body spectrum using the spatially varying dust temperature and emissivity obtained from the Planck data using the Commander code (Planck

Collaboration 2015, arXiv:1502.01588). This therefore assumes the same spectral index for polarization as for intensity. These templates are smoothed to degree scale.

Variations on this model that appear consistent with current data are a more strongly varying emissivity, e.g. up to $\sigma \sim 0.2$ dispersion on degree scales, in addition to different prescriptions for small-scale behaviour that account for turbulence in the magnetic field. A two (or more) component model for the dust, composed of the spatially varying sum of silicon and carbonaceous dust, each with a different emissivity, is also physically motivated.

### 3.2.3 Spinning dust

In polarization the spinning dust, or anomalous microwave emission, is nominally unpolarized, but a fractional polarization of a few percent is physically possible and not excluded by current data. We construct a possible polarized model for this using the intensity templates for spinning dust from the Planck-2015 Commander fits, combined with the thermal dust polarization angles and an overall polarization fraction.

### 3.2.4 Free-free

### 3.2.5 Atomic and molecular lines

## 3.3 CMB Secondary Anisotropies and Extragalactic Sources

The key challenges for the extragalactic sky models of CMB-S4 are to provide fast and self-consistent simulations of CMB secondary anisotropies and extragalactic sources. These models will allow us to make more realistic forecasts. In our cosmological analyses they will allows us to Monte Carlo over the underlying astrophysical uncertainties of these secondaries and sources. Our plan to meet these challenges is modular and can be broken down as follows:

- We will use full hydrodynamical simulations of cosmological volume as the basis to parametrically model the complicated *gastrophysical* processes associated with extragalactic foregrounds.

- As the backbone of our model we will require fast simulations of growth of structure that generate halo catalogs for a large set of cosmological parameters.

- To have self-consistent maps we will have a flexible pipeline that generates simulated all sky maps which applies the parametric models from the hydrodynamical simulations to our backbone large-scale structure simulations and halo catalogs.

Hydrodynamical simulations of cosmological volumes are currently available which we can already used to model extragalactic foregrounds. These simulations will be used for the development and testing phases of the simulation pipeline. However, they are limited in their size, sub-grid modeling accuracy, thus will not meet our accuracy requirements of CMB-S4. We will develop new full hydrodynamical simulations of cosmological volumes that include a variety of physical processes. An essential requirement of these simulations will be to capture growth and evolution of galaxies to clusters size halos throughout cosmic time at a sufficient spacial resolution. Hydrodynamic simulations of this size and scale are already computationally feasible, the challenges will be the appropriate modeling of radiative cooling, star formation, and feedback processes in order to capture the global stellar and gas contents of these halos.

There are many different approaches already developed to provide us with the underlying large-scale structure simulations that will we build our extragalactic model upon. They vary in speed which tend to inversely scale with accuracy. A benefit of our modular and flexible approach is that we do not need to limit ourselves to one approach. In fact we will compare the various approaches to see how they bias our answers. It is in these simulations where we will vary cosmological parameters assuming that they only affect the growth of structure and not the *gastrophysical* properties of extragalactic foregrounds.

Our final product will be all sky maps. They will be in HEALPIX format (or some other format) to seamlessly interface with galactic and CMB simulated maps. The map products will include:

- Optical galaxies that correspond to the various overlapping surveys including LSST.

- Radio and dusty star-forming galaxy point sources.

- Unresolved CIB.

- Projected density maps (both total and gas) of the large-scale structure.

- Thermal and kinetic SZ maps.

We will explore the parameter space for each of the maps listed above and provide a sufficient number of realization that we will marginalize over the many model uncertainties. For example, the lensing field can be constructed through a proper ray-tracing method from the projected density maps or via the born approximation. Our self-consistent extragalactic sky model allows us to test various sources of contamination and systematic biases in our estimators. Additionally, any cross-correlation analyses can easily be checked and evaluated using these maps. **All the simulation products we create will become public.**

# 4 Time-Ordered Data Processing

## 4.1 Overview

The time-ordered data processing elements of the CMB simulation and analysis pipeline – simulation, pre-processing and mission characterization, and map-making – are grouped as a subset due to the unique computational challenges posed by the volume of data that they must process.
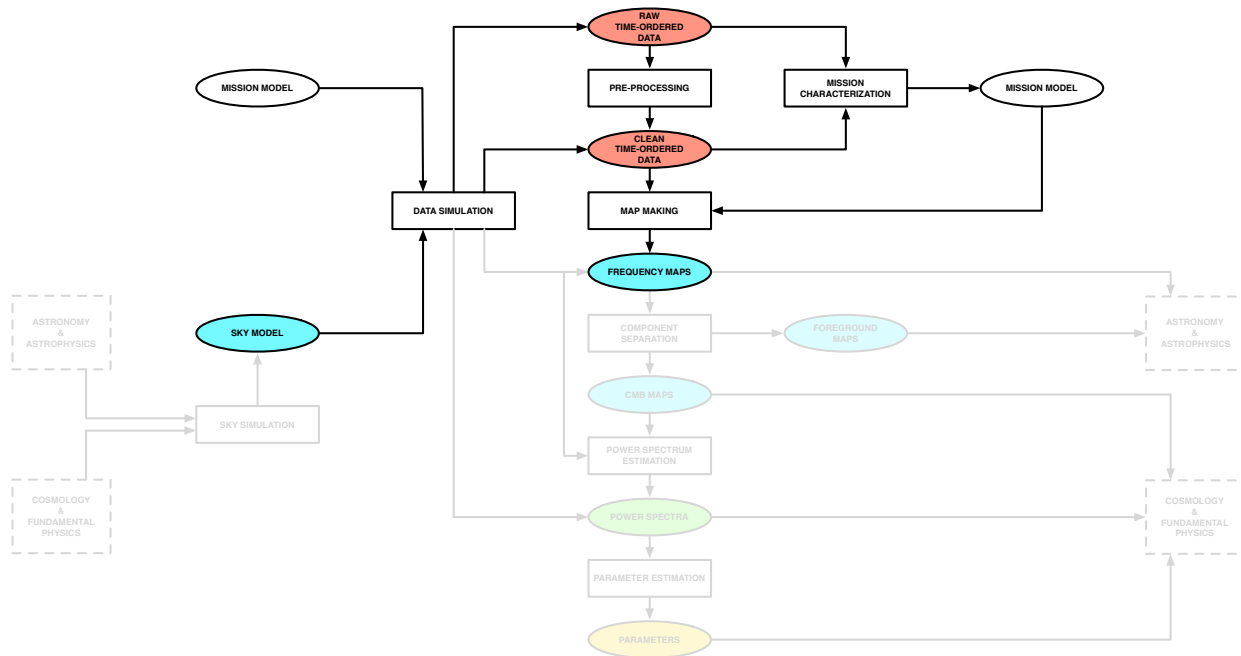


**Figure 14.** *The time-ordered data processing subset of the CMB simulation and data analysis pipeline*

## 4.2 Simulation

sky signal to instrument readout

instrument - beam, bandpass, noise; calibration, electronics

observation – pointing, polarization (hwp), flagging, atmosphere

V & V for other TOD processing elements

effective beam convolution

## 4.3 Pre-Processing and Mission Characterization

systematics mitigation: filtering, template-subtraction, marginalization

mission model building: pointing, beam, noise, systematics

## 4.4 Map-Making

Map-making is the stage of the analysis when the major compression of the time-ordered data happens and some estimate of the sky signal is produced at each observing frequency. It is usually a linear operation, characterized by some operator, $\mathbf{L}$, which transforms the input time-ordered data, $\mathbf{d}$, into a pixel domain map, $\mathbf{m}$, e.g., [283],

$$\mathbf{m} = \mathbf{Ld}, \tag{6.7}$$

typically under the condition that the estimator is unbiased over the statistical ensemble of instrumental noise realizations, i.e.,

$$\langle \mathbf{m} - \mathbf{s} \rangle = 0, \tag{6.8}$$

where $\mathbf{s}$ is the underlying pixelized sky signal. Given the usual model for the time-ordered data as the sum of sky-synchonous signal and time-varying noise,

$$\mathbf{d} = \mathbf{As} + \mathbf{n}, \tag{6.9}$$

for a pointing matrix $\mathbf{A}$, this condition leads to,

$$\langle \mathbf{m} - \mathbf{s} \rangle = (\mathbf{LA} - \mathbf{1})\mathbf{s} + \langle \mathbf{n} \rangle = (\mathbf{LA} - \mathbf{1})\mathbf{s}, \tag{6.10}$$

as the average noise is assumed to vanish. Hence,

$$\mathbf{LA} = \mathbf{1}, \tag{6.11}$$

which is solved by,

$$\mathbf{L} = (\mathbf{A}^{\mathrm{T}}\mathbf{WA})^{-1}\mathbf{A}^{\mathrm{T}}\mathbf{W}. \tag{6.12}$$

Here the matrix $\mathbf{W}$ is an arbitrary positive definite weight matrix, and different choices of $\mathbf{W}$ lead to different estimates of the sky signal.

- If $\mathbf{W}$ is taken to be the inverse of the time-domain noise covariance, i.e., $\mathbf{W} = \mathbf{N}^{-1}$, then the sky signal estimate, $\mathbf{m}$, will correspond to the **maximum likelihood** and **minimum variance** solution.

- If $\mathbf{W}$ is taken to be proportional to some diagonal matrix minus some low-rank correction, i.e. $\mathbf{W} \propto \mathbf{1} - \mathbf{TT}^{\mathrm{T}}$, with $\mathbf{T}$ assumed to be column-orthogonal, then the modes defined by its columns are marginalized over, effectively removing them from the solution. This approach includes as a special case so-called **destriping** map-making, e.g., [254, 186], which has gained recognition thanks to its successful applications to the Planck data, e.g., [185, 287, 252, 249], and is therefore of potential interest to any experiments aiming to cover a large fraction of the sky. More generally, however $\mathbf{T}$ can be constructed to remove any unwanted modes present in the time domain data, e.g., [280, 78, 119].

- If **W** is taken to be diagonal, then the map-making solution corresponds to **binning**, i.e. the weighted co-addition of the samples falling within each pixel.

If the instrument beams display complex, non-axially symmetric structure, the proper estimation of the sky signal may require correcting for their effects at the map level, leading to the so-called **deconvolution** map-making [31, 156, 187]. However, further work is needed to demonstrate the effectiveness of such an approach in general.

If map-making is used primarily as a data compression operation on the way to deriving constraints on the statistical properties of the sky signal (such as its power spectra), one may choose to relax the condition in Eq. (6.8) in favor of the more computationally tractable, albeit potentially biased, sky estimate,

$$\mathbf{m} = (\mathbf{A}^\mathrm{T}\mathrm{diag}(\mathbf{W})\mathbf{A})^{-1}\mathbf{A}^\mathrm{T}\mathbf{W}\mathbf{d}, \tag{6.13}$$

where $\mathrm{diag}(\mathbf{W})$ denotes the diagonal part of **W**. In this approach any bias is then corrected at the next level of the data processing, e.g., [164]. This approach has been proven to be very effective, at least in the context of experiments with small sky coverage, e.g., [99, 266, 285, 56].

Formally the linearity of the mapmaking operation permits the propagation of the uncertainty due to the instrumental noise from time- to pixel-domain as

$$\hat{\mathbf{N}} = \mathbf{L}\mathbf{N}\mathbf{L}^\mathrm{T}, \tag{6.14}$$

which leads to a particularly simple expression for maximum likelihood estimators

$$\hat{\mathbf{N}} = (\mathbf{A}^\mathrm{T}\mathbf{N}^{-1}\mathbf{A})^{-1}. \tag{6.15}$$

However, as noted above, due its size the computational cost involved in computating such pixel-domain noise correlations make them impractical for all but special cases today, and the uncertainty is either carried over to the next stages of the data processing in implicit form or the final uncertainty is estimated using Monte Carlo simulations.

## 4.5 Computational Constraints

The computational requirements here are for both capacity and capability. To support the iterative exploration of the time-ordered data required by the pre-processing and mission characterization steps we need many analysts to be able to process the full data simultaneously, with each seeing no worse than order 1-day turnaround time for their jobs to complete. Conversely, to support the massive Monte Carlo simulation and map-making required for percent level uncertainty quantification in the absence of a full data covariance matrix, we need to be able to perform occasional runs of up to $10^4$ realizations within the total cycles available to us.

As Figure 15 shows, the size of ground-based, balloon-borne and satellite CMB data sets exhibit exponential growth over a 40 year period. Moreover, for suborbital experiments the exponent exactly matches that of Moore's Law, where we us as a proxy the peak performance of the flagship high performance computing (HPC) system at the DOE's National Energy Research Scientific Computing (NERSC) Center at any epoch (this choice reflecting the widespread use of NERSC for CMB data analyses over the last 20 years).

As noted above, the intractability of pixel-domain data covariance matrices pushes us to use Monte Carlo (MC) methods for uncertainty quantification and debiasing, and the computational cost of the data analysis
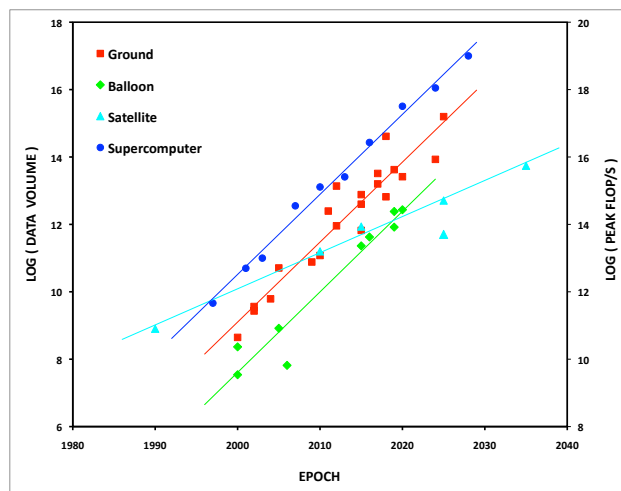
**Figure 15.** *Exponential growth of CMB time-ordered data volume and HPC capability: 1990 – 2030.*

is dominated by the generation and reduction of sufficient MC realizations of the data for the resulting statistical error to be subdominant (typically assumed to be $10^4$ realizations for percent level uncertainty).

Key challenges:

- computational tractability due to data volume and complexity of next-generation supercomputers

- mitigating raw data systematics and developing sufficient mission and data models

All algorithmic and implementation choices we make must first and foremost be informed by their impact on computational tractability.

# 5 Component Separation

**Authors: Mark Ashdown, Jonathan Aumont, Carlo Baccicalupi, Josquin Errard, Maude Le Jeune**

Key challenges:

- validation - are we using the right algorithms for the (as yet unknown) real foregrounds

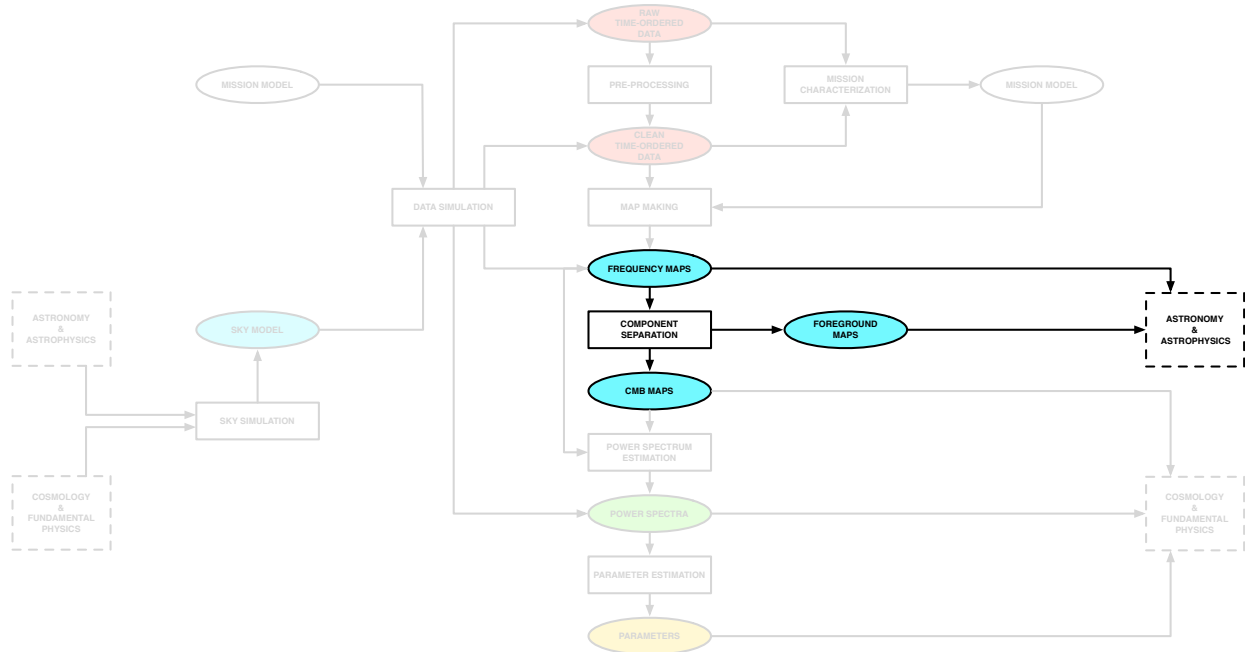- verification - are these algorithms right given our (as yet flawed) simulations



**Figure 16.** *The component separation subset of the CMB simulation and data analysis pipeline*

This section discusses the algorithms and methods for disentangling different sources of sky emission in multi-frequency maps. We first present the motivations and the general ideas of existing approaches. We then give some specifics of parametric and blind methods. Finally, we summarize several questions which might be answered by follow-up studies.

## 5.1 Introduction

### 5.1.1 Motivations

Recent measurements by BICEP2/Keck/Planck [57] confirm that on degree scales, where CMB-S4 is expected to search for the imprint of $B$ modes from primordial GWs, the contamination from polarized foreground emission is comparable to or higher than the cosmological signal at 150 GHz and in one of the cleaner
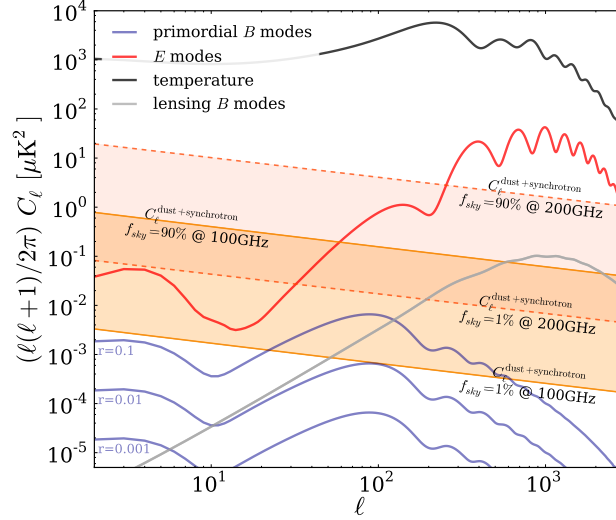
**Figure 17.** *Angular power spectra showing primordial B modes, lensing B modes, total intensity, and E modes, as well as the total contribution of polarized B-mode foregrounds (dust plus synchrotron), expected on the cleanest $1 - 90\%$ of the sky, at 100 and 200 GHz. Note that, as these results are derived from Planck data at intermediate and high Galactic latitudes, sensitive primarily to the large scale foreground pattern in polarization and are not therefore optimized for high-resolution, small scale instruments, there is potential for discovery of small patches of sky (e.g., $f_{sky} \leq 5\%$) with a signal differing than those indicated here. From [124].*

patches of the sky. Given that 150 GHz is expected to be close to the minimum of foreground contamination vs. CMB signal, this is likely to be the case at all frequencies and all but the smallest fractions of the sky. Given the power law behavior in $\ell$ found on larger scales by Planck and WMAP [248, 241], foregrounds are expected to be even more relevant at larger angular scales. Foregrounds are expected to be subdominant with respect to the $B$-mode lensing signal on the scale of a few arcminutes (see Fig.17); nevertheless, dust polarization fractions around 10% (comparable to observed levels) have been shown to have non-negligible impact on the 4-point function used for achieving lensing extraction [129]. Therefore, component separation is a necessary and important step in gaining insight into the amplitude of primordial GWs, as well as the neutrino masses and dark energy abundances through CMB lensing studies.

### 5.1.2   Definition of component separation

Broadly defined, the process of component separation would generally

- include any data processing that characterizes and exploits correlations between observations at multiple frequencies

- use external constraints and physical modeling

- aim at distinguishing between different physical sources of emission.

The general data modeling reads

$$d_p = \sum_{\text{comp,p}} a_p^{\text{comp}} s_p^{\text{comp}} + n_p \equiv \mathbf{A}\, s_p + n_p \tag{6.16}$$

where the vector $d_p$ contains the measured signal in each observing band, $\mathbf{A}$ is the so-called mixing matrix which encapsulates the emission law $a_p^{\text{comp}}$ of each component, $s_p$ is a vector containing the unknown CMB and foregrounds amplitude and $n_p$ is a vector containing the noise level at each observing band. The index $p$ refers to sky pixels $(\theta, \phi)$, or modes of a spherical harmonic decomposition $(\ell, m)$, or a set of Fourier modes $(k_x, k_y)$, etc. Note that this modeling assumes spatial templates $s_p$ that are the same in all observing bands.

Component separation aims at inverting Eq. 6.16, to estimate the foregrounds-disentangled CMB signal encapsulated in $s_p$, as well as the foreground templates which are relevant for testing and updating our knowledge of astrophysical processes (and hence improve the sky model), as illustrated in Fig. 16. The estimate $\tilde{s}_p$ of the true sky templates $s_p$ — given $\mathbf{A}$, $d_p$ and the statistical properties of the noise — minimizes the following $\chi^2$:

$$\chi^2 \equiv \sum_p |s_p - \tilde{s}_p|^2 \tag{6.17}$$

and can be taken to have the following general form

$$\tilde{s}_p = \mathbf{W} \, d_p \tag{6.18}$$

where the weighting operator $\mathbf{W}$ is chosen to optimize some criterion regarding $\tilde{s}_p$ and $s_p$ (variance of the cleaned map, unbiasedness, etc.) while keeping statistical consistency and robustness. In particular, a common requirement for all component separation algorithms is the ability of propagating errors due to foreground subtraction, while having the flexibility of including foreground modeling and external constraints in a transparent way.
Component separation is then defined as a method of estimating the mixing matrix $\mathbf{A}$ and finding the weighting $\mathbf{W}$ that provides closest possible estimate $\tilde{s}_p$ to the true sky signal.

For example, a solution to Eqs. 6.17 and 6.18 is obtained by taking $\mathbf{W} \equiv \left(\mathbf{A}^T \mathbf{N}^{-1} \mathbf{A}\right)^{-1} \mathbf{A}^T \mathbf{N}^{-1}$ with $\mathbf{N} \equiv \langle n_p^T n_p \rangle$, leading to an unbiased estimate of the sky. As mentioned below, this expression can be changed (see, e.g., [111]), depending on the desired level of generality and complexity and on the level of prior knowledge of the sky signal.

Studies have demonstrated the applicability of classes of component separation algorithms to certain simulated multi-frequency datasets, either balloon-borne or ground-based, and targeting limited frequency ranges and sky areas [279, 130, 129]. Results indicate that generally, for a frequency range extending from 90 to 250 GHz, polarized foregrounds may be removed effectively through a multi-frequency combination, at the price of enhancing the white noise contribution due to channel mixing; moreover, a possible bias may be introduced if, at the lowest frequency interval edge, the synchrotron component is not negligible: lower frequency templates/data are required to avoid such a contribution [126]. The most comprehensive application of component separation to data, in terms of completeness of algorithms and frequency range, is represented by Planck [248], although the targeted CMB components in that analysis (total intensity and $E$-mode polarization) are not the same as in the CMB-S4 case.

## 5.2 Description of methods

The CMB extraction may be achieved essentially through two basic concepts: the fitting of foreground unknowns along with CMB, or the minimization of the variance of a linear combination of the data, constrained to have the frequency scaling of a black body. The first class of algorithms, known as "parametric", makes the maximum use of prior knowledge of foreground emission. By contrast, the second class, known as "blind",

makes the minimum set of assumptions. These two broad classes and other possibilities are discussed in turn below.

- **Parametric** – The overall idea of these methods boils down to two steps: 1) the estimation of the mixing matrix, $\mathbf{A}$; and 2) the inversion of Eq. 6.16 to recover an estimate of the sky signal, $s_p$. Parametric methods assumes that the mixing matrix, used in Eq. 6.16, has a functional form which is known and which can be parametrized by so-called "spectral" parameters $\beta$, i.e. $\mathbf{A} = \mathbf{A}(\beta)$. The functional form of $\mathbf{A}$ being fixed, the estimation of the mixing matrix is therefore equivalent to an estimation of the parameters $\beta$. The parameters of the model are determined via a fitting procedure, often performed over sky pixels. This can be achieved by maximizing the following so-called "spectral" likelihood [69, 122]:

$$-2\log\mathcal{L}(\beta) = -\sum_p \left(\mathbf{A}^T\mathbf{N}^{-1}d\right)^T \left(\mathbf{A}^T\mathbf{N}^{-1}\mathbf{A}\right)^{-1} \left(\mathbf{A}^T\mathbf{N}^{-1}d\right). \tag{6.19}$$

  Any deviation between the true mixing matrix $\mathbf{A}$ and the estimated $\tilde{\mathbf{A}} \equiv A(\tilde{\beta})$ leads to the presence of foreground residuals in the reconstructed component maps.

- **Blind** – By assuming that sky components are statistically independent, blind methods aim at recovering these with an a priori unknown mixing matrix. Blind methods make minimal assumptions about the foregrounds and focus on the CMB reconstruction from its well known black body spectral energy distribution. The Internal Linear Combination (ILC, [284]) belongs to this class of methods. It only uses the CMB column of the mixing matrix elements (noted $a$ hereafter) to perform the minimum variance reconstruction, cf. Eq. 6.18:

$$\tilde{s}_p = \sum_{i=0}^{i=m} w_i d_{p,i} \tag{6.20}$$

  with $\sum_i w_i a_i = 1$, leading to the following solution:

$$w_i = a^T N^{-1} (a^T N^{-1} a)^{-1} \tag{6.21}$$

In this scheme, no attempt is made to design a foreground model. The decorrelation property between CMB and foregrounds alone is used to project out the contamination into a $m$-1 subspace (with $m$ being the number of frequency maps).

The main caveat in this method is its well known bias ([161, 111], etc) which comes from empirical correlation between the CMB and the foregrounds. The ILC bias is proportional to the number of detectors $m$ and inversely proportional to the number of pixels used to compute $N$. In order to reduce this effect, one could think of reducing the foreground subspace size by adding further constraints. The SEVEM template fitting method ([219], etc) follows this idea, by building some foreground templates with a combination of a subset of the input frequency maps.

The semi-blind SMICA method [79] also works at containing the foreground in a smaller dimension space, but in a more general way. The idea of Independent Component Analysis (ICA) is to blindly recover the full mixing matrix $\mathbf{A}$ by using the independence property of the different components. As we know that they are spatial correlations between the foregrounds, the ICA principle is used to disentangle the CMB from the noise and the foregrounds taken as a whole.

The main advantage of such blind of semi-blind methods is their ability to face any unknown and/or complex foreground contamination, to reconstruct a clean CMB signal. This is a big advantage when real data comes, one can then focus on instrumental effects, or data set combination issues at first, and leave the complex task of the foreground modeling and reconstruction for a future analysis step.

Moreover, in a framework like SMICA, the level of blindness can be adjusted via the plugin of any parametric component to its flexible engine as described in [79], allowing for a step by step fine grain design of the foreground model.

- **Template fitting** – In this variant, emission laws are not modeled, and the analysis is reduced to the maximisation of a likelihood over the CMB contribution and the amplitudes of each foreground component (see, e.g., [184]).

For all of the approaches discussed above, Eq. 6.18 can be implemented equivalently with any representations of the map—i.e. pixel, harmonic, wavelet, etc. The resulting component separation is independent of this choice as long as the linear data modeling (Eq. 6.16) holds. This complementarity, and the internal comparison of results through these pipelines has been proven to be relevant in actual analysis of Planck data [248]. That said, the difference between domain of application will lie in the computational needs: for high number of sky pixels, the implementation of Eq. 6.18 might be significantly more efficient in harmonic space.

## 5.3 Questions to be addressed during follow-up studies

- **E/B or Q/U basis of analysis** – Component separation between CMB radiation and its foregrounds can be performed either dealing with Stokes parameters $Q$ and $U$ maps of the sky in real space or Fourier space, and either before or after the separation between the $E$ and $B$ modes. Several approaches have been followed by CMB experiments so far [147, 253, 57], and each of them has some advantages and some caveats. For example, processing $Q/U$ data in the map domain simplifies the treatment of foreground components that have non-Gaussian and/or non-stationary spatial distributions. However, in the $Q$ and $U$ basis, the CMB $E$ and $B$ modes are mixed and the CMB $E$ modes will be the dominant contribution to the variance at intermediate and small scales in the CMB observing frequencies, limiting the accuracy of the separation. To overcome this limitation, $E$ and $B$ observables can be constructed in Fourier space. The separation of the $B$-mode components (primordial CMB, Galactic foregrounds, lensing, etc.) can then be done in the angular power spectrum domain (where the final accuracy might be limited by the cosmic variance associated to foregrounds), in the two-dimensional, phase-full Fourier domain (where the treatment of non-stationary components will be complicated) or in the map domain (where the final accuracy might be limited by ringing of the foregrounds due to the non-local transformation). While for $Q$ and $U$ the problem we face is analogous in terms of foreground vs CMB balance, for $E$ and $B$ that is not: $E$ is more similar to $Q$ and $U$, but in the $B$ channel separation is more challenging. We have the capability and will analyze in both domains, to validate and cross-check the stability of the mixing matrix recovery. Although these different approaches are currently giving satisfactory results on simulated data, these effects will become crucial at the sensitivity of CMB-S4 and merit a dedicated study.

- **Combining data from multiple instruments** – Ground-based instruments heavily filter time streams because of atmosphere contamination, ground emission, etc to perform projections on the sky. In particular, large angular scales are usually suppressed anisotropically, and this suppression is corrected in the power spectrum estimate. In order to perform component separation using various observations, component separation methods will require the use of maps derived from common filters. As stressed already, in recent analysis a first $B$ modes foreground cleaning was implemented in a multi-site fashion, i.e. by combining different probes, i.e. BICEP2, Keck Array and Planck [57]. A template fitting analysis was implemented with the primary objective to minimize the variance in the CMB

solution, by achieving a linear combination of the data, which turned out in a reduction of the power observed from the ground, which is interpreted as cleaning of the Galactic dust, and sets the current limit on $B$ modes from primordial GWs. The independent reduction of the data required an additional layer in the analysis, made by the simulated scans of the Planck data through the filtering by the ground observatories, along with validation through simulations of the whole procedure. The necessity for CMB-S4 will be to have a combined data reduction, a single pipeline reducing and combining different datasets. With a common filtering implemented from scratch in a multi-site experiment, the latter a posteriori combination would be built-in, thus avoiding the extra layer and increasing confidence and robustness of results.

- **Various resolutions** – under the approximation that the mixing matrix is not significantly varying under the largest resolution, the impact of various resolutions can be propagated to the noise level of the final CMB map through the CMB x CMB term of $\left( \mathbf{A}^T \mathbf{N}^{-1} \mathbf{A} \right)^{-1}$ as given by Eq. 6.18 with $\mathbf{W} \equiv \left( \mathbf{A}^T \mathbf{N}^{-1} \mathbf{A} \right)^{-1} \mathbf{A}^T \mathbf{N}^{-1}$. Beam for each frequency channel would appear in the expression of the noise covariance matrix

$$\mathbf{N}(i) \equiv \mathbf{N}(i)_\ell = (\sigma_i)^2 \exp \left[ \frac{\ell(\ell+1)\theta_{\mathrm{FWHM}}^2}{8 \log(2)} \right] \tag{6.22}$$

where $i$ is a frequency channel and $\sigma_i$ is the noise level in the corresponding map. The noise variance in the reconstructed CMB map, i.e. after component separation, would then be given by

$$N_\ell^{\mathrm{post\ comp\ sep}} = \left[ \left( \mathbf{A}^T \left( \mathbf{N}_\ell \right)^{-1} \mathbf{A} \right)^{-1} \right]_{\mathrm{CMBxCMB}} \tag{6.23}$$

The effective beam of this noise is degraded compared to a simple quadratically combined noise, but this obviously depends on the involved beams sizes and on the importance of given channels to perform the foregrounds cleaning.

- **Atmosphere residuals** – Atmosphere residuals appear at large scales in ground-based CMB observations, and they scale with frequency in a similar way as dust, $\propto \nu^\beta$ [123]. Having redundant frequencies among the different observatories could help mitigating the atmospheric and astrophysical foregrounds. Furthermore, the small intrinsic polarization of the atmosphere [45, 123] will limit the contamination to component separation of the polarized signals. Still, this effect will have to be investigated quantitatively with realistic simulations.

# 6   Statistics and Parameters

In this section, we discuss the process of going from sky maps at different frequencies—or, in light of the previous section, foreground-cleaned CMB maps and an estimate of foreground residuals—to post-map products such as angular power spectra, estimates of lensing potential $\phi$, and finally cosmological parameters, as well as covariance estimates for all of these quantities. We briefly describe the current practice for this process, then we address specific challenges anticipated in the CMB-S4 era.

## 6.1   Current practice

Early measurements of CMB temperature anisotropy, with comparatively few map pixels or angular modes measured, often used maximum-likelihood methods to produce maps of the sky (e.g., [**?**]) and either a direct evaluation of the full likelihood or a quadratic approximation to that likelihood to go from maps to angular power spectra (e.g., [**?**]). With the advent of the WMAP and Planck space missions, which would map the entire sky at sub-degree resolution, it became apparent that computing resources could not compete with the $\mathcal{O}(N^3)$ scaling of the full-likelihood approach (e.g., [**?**]). The solution for power spectrum analysis that has been adopted by most current CMB experiments is a Monte-Carlo-based approach advocated in [**?**]. In this approach, a biased estimate of the angular power spectrum of the data is obtained by simply binning and averaging the square of the spherical harmonic transform of the sky map. That estimate (known as the "pseudo-$C_\ell$ spectrum") is related to the unbiased estimate that would be obtained in a maximum-likelihood procedure through the combined effect of noise bias, sky windowing, and any filtering applied to the data before or after mapmaking (including the effects of instrument beam and pixelization). These effects are estimated by "observing" and analyzing simulated data and constructing a matrix describing their net influence on simulated data is computed and inverted. This inverse matrix is applied to the pseudo-$C_\ell$s to produce the final data product. It is expected that some version of this Monte-Carlo treatment will also be adopted for CMB-S4.

Pseudo-$C_\ell$ methods are also now commonly used in analysis of CMB polarization anisotropy [253, **?**, **?**]. An added complication in polarization analyses is that pseudo-$C_\ell$ methods do not cleanly separate $E$ and $B$ modes (e.g., [**?**]). "Pure" $B$-mode estimators can be constructed that suppress the spurious $B$-mode contribution from estimating $E$ and $B$ on a cut sky with pseudo-$C_\ell$ methods [**?**]), but other analysis steps (such as particular choices of filtering) can produce spurious $B$ modes that are immune to the pure estimators [**?**]. These can also be dealt with using Monte-Carlo methods, either by estimating the statistical bias to the final $B$-mode spectrum or by constructing a matrix representing the effect of any analysis steps on the true sky [56]. The latter approach involves constructing an $N_{\rm pixel}$-by-$N_{\rm pixel}$ matrix, equal in size to the full pixel-pixel covariance, and will not be feasible for high-resolution CMB-S4 data but could be used in analyzing lower-resolution data.

In addition to the two-point function of CMB maps, higher-order statistics of the maps have recently been of great interest to the community. In particular, the four-point function encodes the effect of gravitational lensing, and estimators can be constructed to go from CMB temperature and polarzation maps to estimates of CMB lensing $\phi$ and the associated covariance (e.g., [**?**, **?**]). These quadratic estimators are the first step in an iterative estimation of the true likelihood, and in the weak-lensing limit they are nearly optimal; as a result, they remain the state of the art for estimating the large-scale $\phi$ from CMB lensing (e.g., [251]). The computational burden involved in this step of the analysis is unlikely to be significantly greater for CMB-S4 than for Planck.

The final step in the analysis of a CMB data set is the estimation of cosmological parameters from the various post-map statistics discussed above. This involves estimating the likelihood of the data given a model parameterized by the standard six $\Lambda$CDM parameters, possible extensions of the cosmological model, and any nuisance parameters involving the instrument, foregrounds, and other sources of systematic uncertainty. The current industry standard for this part of the analysis are Monte-Carlo Markov-Chain (MCMC) methods, in particular the implementation in CosmoMC [**?**].

## 6.2 Challenges

Some of the avenues in the analysis that need to be re-addressed for an experiment such as CMB-S4 are:

- The impact of uncertainties in foreground modeling on cosmological parameters, particularly the tensor-to-scalar ratio $r$.

- The covariance between different observables (i.e., the lensed CMB power spectrum and the reconstructed lensing potential power spectrum)

- The separation of the gravitational lensing signal and the primordial $B$-mode signal, lowering the effective lensing background (these statistical algorithms are known as "delensing"), the impact of delensing on cosmological parameters.

We treat each of these challenges individually in the sections below.

### 6.2.1 Foreground-related uncertainty on cosmological parameters

do frequency-map cross-spectra and fit for foregrounds or do component separation and parameterize foreground residuals. either way, what parameterization? refer to comp sep and sky modeling sections.

### 6.2.2 CMB lensing covariances for CMB S4

The measured lensing power spectrum is given by a 4-point function of the lensed CMB. This is not statistically independent from the lensed CMB 2-point function, because both depend on the same observed, lensed CMB maps. As a consequence, measured lensing power spectra and lensed CMB power spectra may be correlated. This correlation should be taken into account when combining these measurements to avoid spurious double counting of information. For the specific case of Planck is negligible [267]. However, the level of correlation depends on experiment specifications and the multipole range where power spectra have high signal-to-noise. The correlation should thus be included in analyses that combine 2- and 4-point measurements unless it is known to be negligible for a specific experiment.

For CMB-S4, the best lensing measurements are expected to come from the auto-power spectrum of $EB$ reconstruction. Its covariance with the lensed $EE$ and $BB$ power spectra depends on six-point functions of the lensed CMB, e.g. $\langle EBEBEE \rangle$. Although many terms contribute, the dominant effect is expected from only a few contributions [267]:

- First, there are signal contributions to the covariance of the form

$$\text{cov}(\hat{C}_{l,\text{expt}}^{EE}, \hat{C}_L^{\hat{\phi}_{EB}\hat{\phi}_{EB}})_{\text{signal}} = \frac{\partial C_l^{EE}}{\partial C_L^{\phi\phi}} \frac{2}{2L+1} (C_L^{\phi\phi})^2, \tag{6.24}$$

$$\text{cov}(\hat{C}_{l,\text{expt}}^{BB}, \hat{C}_L^{\hat{\phi}_{EB}\hat{\phi}_{EB}})_{\text{signal}} = \frac{\partial C_l^{BB}}{\partial C_L^{\phi\phi}} \frac{2}{2L+1} (C_L^{\phi\phi})^2, \tag{6.25}$$

where we used power spectra of observed (noisy, beam-deconvolved) CMB fluctuations $X \in \{E, B\}$:

$$\langle \hat{C}_{l,\text{expt}}^{XX} \rangle = C_{l,\text{expt}}^{XX} = C_l^{XX} + \left( \frac{\sigma_X}{T_{\text{CMB}}} \right)^2 e^{l(l+1)\sigma_{\text{FWHM}}^2/(8\ln 2)}. \tag{6.26}$$

The signal covariance in Eqs. (6.24) and (6.25) arises because cosmic variance fluctuations of the true lensing potential (i.e. fluctuations of matter along the line of sight) modify the lensing reconstruction power as well as the lensed $EE$ and $BB$ power spectra. Formally, this follows from the connected part of the lensed CMB 6-point function.

- Second, a noise covariance follows from the disconnected 6-point function,

$$\text{cov}(\hat{C}_{l,\text{expt}}^{EE}, \hat{C}_L^{\hat{\phi}_{EB}\hat{\phi}_{EB}})_{\text{noise}} = \frac{2}{2l+1} (C_{l,\text{expt}}^{EE})^2 \frac{\partial(2\hat{N}_L^{(0)})}{\partial \hat{C}_{l,\text{expt}}^{EE}}, \tag{6.27}$$

and similarly for $BB$. This noise covariance arises because fluctuations of the CMB and instrumental noise change both the Gaussian reconstruction noise $N^{(0)}$ and the CMB power spectra. It is however cancelled if the Gaussian $N^{(0)}$ reconstruction noise is subtracted in a realization-dependent way [120, 155, 235, 267]

$$\hat{C}_L^{\hat{\phi}\hat{\phi}} \rightarrow \hat{C}_L^{\hat{\phi}\hat{\phi}} - 2\hat{N}_L^{(0)} + N_L^{(0)}. \tag{6.28}$$

For the specific case of $EBEB$ reconstruction, the realization-dependent $\hat{N}^{(0)}$ is Comment: MS: check

$$\hat{N}_L^{(0)} = \frac{\left| A_L^{EB} \right|^2}{2L+1} \sum_{l_1, l_2} \left| g_{l_1 l_2}^{EB}(L) \right|^2 \frac{1}{2} \left[ \hat{C}_{l_1,\text{expt}}^{EE} C_{l_2,\text{expt}}^{BB} + C_{l_1,\text{expt}}^{EE} \hat{C}_{l_2,\text{expt}}^{BB} \right], \tag{6.29}$$

Comment: CD: Define $g_{l_1 l_2}^{EB}(L)$. where $A^{EB}$ and $g^{EB}$ denote the reconstruction estimator normalization and weight, respectively. In the square brackets one of the CMB power spectra is replaced by a data power spectrum Comment: Are all $\hat{C}_\ell$s data power spectra?. On average, $\langle \hat{N}_L^{(0)} \rangle = N_L^{(0)}$. This realization-dependent $\hat{N}^{(0)}$ subtraction also follows more formally from optimal trispectrum estimation (see Appendix B in [267] and Appendix D in [250]).

- A third covariance contribution arises from the connected trispectrum part of the CMB 6-point function. If realization-dependent $\hat{N}^{(0)}$ subtraction is used, the dominant remaining term is expected to be (at leading order in $\phi$, see also Eq. (D4) of [267]; similarly for $BB$)

$$\text{cov}(\hat{C}_{l,\text{expt}}^{EE}, \hat{C}_L^{\hat{\phi}_{EB}\hat{\phi}_{EB}}) = 2 \frac{C_L^{\phi\phi}}{A_L^{EB}} \frac{\partial(2\hat{N}_L^{(0)})}{\partial \hat{C}_{l,\text{expt}}^{EE}} \frac{2}{2l+1} (C_{l,\text{expt}}^{EE})^2. \tag{6.30}$$

Similarly to avoiding the noise covariance with the realization-dependent $\hat{N}^{(0)}$ subtraction, the signal covariance could in principle also be avoided by delensing CMB power spectra with the estimated lensing reconstruction, e.g. by forming [267]

$$\hat{C}_{l,\text{expt}}^{EE} \rightarrow \hat{C}_{l,\text{expt}}^{EE} - \sum_L \frac{\partial C_l^{EE}}{\partial C_L^{\phi\phi}} \left( \frac{C_L^{\phi\phi}}{\langle \hat{C}_L^{\hat{\phi}\hat{\phi}} \rangle} \right)^2 (\hat{C}_L^{\hat{\phi}\hat{\phi}} - 2\hat{N}_L^{(0)}), \tag{6.31}$$

or by applying more advanced delensing methods. However this has not yet been tested in practice and makes only sense if lensing reconstructions have sufficient signal-to-noise. In general, forming linear combinations of measured lensing and CMB power spectra as in Eqs. (6.28) and (6.31) does simplify covariances, but it cannot add any new information as long as correct covariances are used.

Since more covariance contributions arise from other couplings of the CMB 6-point function, it should be tested against simulations if the above contributions are sufficient. In practice, it is then favorable to use analytical covariances because they are less noisy than those derived from simulations.

On top of the cross-covariance between 2-point CMB power spectra and 4-point lensing power spectra, both power spectra can also have non-trivial auto-covariances. Covariances between CMB power spectra have been computed in [274, 202, 53]. They contain similar building blocks as the covariances above [53]. Covariances between two 4-point lensing power spectra involve the lensed CMB 8-point function. While many covariance contributions are cancelled when using realization-dependent $\hat{N}^{(0)}$ subtraction [155], other contributions may be relevant for future experiments. Finally, the discussion above applies to the standard quadratic lensing reconstruction estimators and may change for maximum-likelihood lensing estimators [163].

### 6.2.3 Delensing

For noise levels below $\Delta_P \simeq 5\mu$K-arcmin, the dominant source of effective noise in $B$-mode maps is the fluctuation induced by the lensing of $E$-modes from recombination. This signal has a well-understood amplitude, and unlike other sources of astrophysical fluctuation in the map, it cannot be removed with multifrequency data. Instead it must be removed using map-level estimates of both the primordial $E$-mode maps and the CMB lensing potential $\phi$.

As discussed in the dedicated CMB lensing chapter, delensing will be a crucial portion of the reconstruction of the CMB lensing field. This is because at low noise levels a quadratic reconstruction of lensing using the $EB$ estimator [**?**] can be improved upon by cleaning the CMB maps of the lens-induced $B$-mode fluctuations, and then performing lens reconstruction again. In effect, the quadratic estimate of [**?**] is effectively the first step in an iterative scheme to find the maximum-likelihood solution for the lensing and primordial fields [163]. CMB maps cleaned of the lensing signals will thus likely be produced as part of the CMB lensing analysis procedure.

The finite noise in the CMB-Stage IV survey will lead to residual lensing $B$-modes which cannot be removed and will act as a noise floor for studying $B$ modes from tensors. The amplitude of these residual lensed $B$-modes are discussed in the dedicated lensing chapter as a function of the angular resolution and the noise level of the S4 survey; in particular, it is crucial to have high-angular resolution maps in order to measure the small-scale $E$- and $B$-modes fluctuations needed for the $EB$ quadratic lensing estimator.

The concerns with the delensing procedure are similar to those for measuring the lensing power spectrum. The impact of polarized dust and synchrotron emission from the Galaxy, and the impact of polarized point sources on small scales on the lensing reconstruction are addressed in chapter IV. Left untreated the effects may be large; however the use of multi-frequency data together with the application of dedicated point-source estimators can mitigate these effects.

Additionally, rather than using an estimate of the CMB lensing field obtained from the CMB itself, it is also possible to use other tracers of large-scale structure which are correlated with CMB lensing [273]. In particular the dusty, star-forming galaxies that comprise the cosmic infrared background (CIB) are strongly correlated with CMB lensing, due to their redshift distribution which peaks near $z \sim 2$ [**?**, **?**]. The level of

correlation is approximately 80% [251] and can in principle be improved using multifrequency maps of the CIB which select different emission redshifts [**?**].

Comment: Add impact of delensing on Neff.

# References

[1] K. N. Abazajian et al. Light Sterile Neutrinos: A White Paper. 2012.

[2] K. N. Abazajian et al. Neutrino Physics from the Cosmic Microwave Background and Large Scale Structure. *Astropart. Phys.*, 63:66–80, 2015.

[3] Kevork Abazajian, George M. Fuller, and Mitesh Patel. Sterile neutrino hot, warm, and cold dark matter. *Phys. Rev.*, D64:023501, 2001.

[4] Kevork N. Abazajian. Telling three from four neutrinos with cosmology. *Astropart. Phys.*, 19:303–312, 2003.

[5] K.N. Abazajian, E. Calabrese, A. Cooray, F. De Bernardis, S. Dodelson, et al. Cosmological and Astrophysical Neutrino Mass Measurements. *Astropart.Phys.*, 35:177–184, 2011.

[6] B. P. et al. Abbott. Observation of gravitational waves from a binary black hole merger. *Phys. Rev. Lett.*, 116:061102, Feb 2016.

[7] Lotty Ackerman, Matthew R. Buckley, Sean M. Carroll, and Marc Kamionkowski. Dark Matter and Dark Radiation. *Phys. Rev.*, D79:023519, 2009. [,277(2008)].

[8] Lotty Ackerman, Matthew R. Buckley, Sean M. Carroll, and Marc Kamionkowski. Dark Matter and Dark Radiation. *Phys. Rev. D*, 79:023519, 2009.

[9] Fred C. Adams, J. Richard Bond, Katherine Freese, Joshua A. Frieman, and Angela V. Olinto. Natural inflation: Particle physics models, power law spectra for large scale structure, and constraints from COBE. *Phys. Rev.*, D47:426–455, 1993.

[10] P. A. R. Ade et al. A Measurement of the Cosmic Microwave Background B-Mode Polarization Power Spectrum at Sub-Degree Scales with POLARBEAR. *Astrophys. J.*, 794(2):171, 2014.

[11] P. A. R. Ade et al. Detection of $B$-Mode Polarization at Degree Angular Scales by BICEP2. *Phys. Rev. Lett.*, 112(24):241101, 2014.

[12] P. A. R. Ade et al. Planck 2013 results. XXV. Searches for cosmic strings and other topological defects. *Astron. Astrophys.*, 571:A25, 2014.

[13] P. A. R. Ade et al. Planck 2015 results. XIII. Cosmological parameters. 2015.

[14] P. A. R. Ade et al. Planck 2015 results. XVII. Constraints on primordial non-Gaussianity. 2015.

[15] P. A. R. Ade et al. Planck 2015 results. XXIV. Cosmology from Sunyaev-Zeldovich cluster counts. 2015.

[16] Peter A. R. Ade et al. POLARBEAR Constraints on Cosmic Birefringence and Primordial Magnetic Fields. *Phys. Rev.*, D92:123509, 2015.

[17] Peter Adshead, Emil Martinec, and Mark Wyman. Gauge fields and inflation: Chiral gravitational waves, fluctuations, and the Lyth bound. *Phys. Rev.*, D88(2):021302, 2013.

[18] Peter Adshead, Emil Martinec, and Mark Wyman. Perturbations in Chromo-Natural Inflation. *JHEP*, 09:087, 2013.

[19] Peter Adshead and Mark Wyman. Chromo-Natural Inflation: Natural inflation on a steep potential with classical non-Abelian gauge fields. *Phys. Rev. Lett.*, 108:261302, 2012.

[20] Peter Adshead and Mark Wyman. Gauge-flation trajectories in Chromo-Natural Inflation. *Phys. Rev.*, D86:043530, 2012.

[21] A. A. Aguilar-Arevalo et al. Improved Search for $\bar{\nu}_\mu \to \bar{\nu}_e$ Oscillations in the MiniBooNE Experiment. *Phys. Rev. Lett.*, 110:161801, 2013.

[22] Stephon Alexander and Jerome Martin. Birefringent gravitational waves and the consistency check of inflation. *Phys. Rev.*, D71:063526, 2005.

[23] R. A. Alpher, H. Bethe, and G. Gamow. The origin of chemical elements. *Phys. Rev.*, 73:803–804, 1948.

[24] Marcelo Alvarez et al. Testing Inflation with Large Scale Structure: Connecting Hopes with Reality. 2014.

[25] Mohamed M. Anber and Lorenzo Sorbo. N-flationary magnetic fields. *JCAP*, 0610:018, 2006.

[26] Aditya Aravind, Dustin Lorshbough, and Sonia Paban. Bogoliubov Excited States and the Lyth Bound. *JCAP*, 1408:058, 2014.

[27] Maria Archidiacono, Nicolao Fornengo, Carlo Giunti, Steen Hannestad, and Alessandro Melchiorri. Sterile neutrinos: Cosmology versus short-baseline experiments. *Phys. Rev.*, D87(12):125034, 2013.

[28] Maria Archidiacono, Steen Hannestad, Rasmus Sloth Hansen, and Thomas Tram. Cosmology with self-interacting sterile neutrinos and dark matter - A pseudoscalar model. *Phys. Rev. D*, 91(6):065021, 2015.

[29] Nima Arkani-Hamed, Douglas P. Finkbeiner, Tracy R. Slatyer, and Neal Weiner. A Theory of Dark Matter. *Phys. Rev. D*, 79:015014, 2009.

[30] Nima Arkani-Hamed, Lubos Motl, Alberto Nicolis, and Cumrun Vafa. The String landscape, black holes and gravity as the weakest force. *JHEP*, 06:060, 2007.

[31] C. Armitage and B. D. Wandelt. Deconvolution map-making for cosmic microwave background observations. *Phys. Rev. D*, 70(12):123007, December 2004.

[32] Asimina Arvanitaki, Savas Dimopoulos, Sergei Dubovsky, Nemanja Kaloper, and John March-Russell. String Axiverse. *Phys. Rev.*, D81:123530, 2010.

[33] Z. Arzoumanian et al. The NANOGrav Nine-year Data Set: Limits on the Isotropic Stochastic Gravitational Wave Background. 2015.

[34] Amjad Ashoorioon, Konstantinos Dimopoulos, M. M. Sheikh-Jabbari, and Gary Shiu. Non-Bunch?Davis initial state reconciles chaotic models with BICEP and Planck. *Phys. Lett.*, B737:98–102, 2014.

[35] C. Athanassopoulos et al. Evidence for nu/mu –¿ nu/e neutrino oscillations from lsnd. *Phys. Rev. Lett.*, 81:1774–1777, 1998.

[36] Fernando Atrio-Barandela and Sacha Davidson. Interacting hot dark matter. *Phys. Rev. D*, 55:5886–5894, 1997.

[37] A. Avgoustidis, E. J. Copeland, A. Moss, L. Pogosian, A. Pourtsidou, and Daniele A. Steer. Constraints on the fundamental string coupling from B-mode experiments. *Phys. Rev. Lett.*, 107:121301, 2011.

[38] Thomas C. Bachlechner, Cody Long, and Liam McAllister. Planckian Axions and the Weak Gravity Conjecture. *JHEP*, 01:091, 2016.

[39] John N. Bahcall, P. I. Krastev, and E. Lisi. Limits on electron-neutrino oscillations from the GALLEX Cr-51 source experiment. *Phys. Lett.*, B348:121–123, 1995.

[40] Marco Baldi. Structure formation in Multiple Dark Matter cosmologies with long-range scalar interactions. *Mon. Not. Roy. Astron. Soc.*, 428:2074, 2013.

[41] Tom Banks, Michael Dine, Patrick J. Fox, and Elie Gorbatov. On the possibility of large axion decay constants. *JCAP*, 0306:001, 2003.

[42] Neil Barnaby, Jordan Moxon, Ryo Namba, Marco Peloso, Gary Shiu, and Peng Zhou. Gravity waves and non-Gaussian features from particle production in a sector gravitationally coupled to the inflaton. *Phys. Rev.*, D86:103508, 2012.

[43] Neil Barnaby and Marco Peloso. Large Nongaussianity in Axion Inflation. *Phys. Rev. Lett.*, 106:181301, 2011.

[44] Sergei Bashinsky and Uros Seljak. Neutrino perturbations in CMB anisotropy and matter clustering. *Phys. Rev.*, D69:083002, 2004.

[45] E. S. Battistelli, G. Amico, A. Baù, L. Bergé, É. Bréelle, R. Charlassier, S. Collin, A. Cruciani, P. de Bernardis, C. Dufour, L. Dumoulin, M. Gervasi, M. Giard, C. Giordano, Y. Giraud-Héraud, L. Guglielmi, J.-C. Hamilton, J. Landé, B. Maffei, M. Maiello, S. Marnieros, S. Masi, A. Passerini, F. Piacentini, M. Piat, L. Piccirillo, G. Pisano, G. Polenta, C. Rosset, M. Salatino, A. Schillaci, R. Sordini, S. Spinelli, A. Tartari, and M. Zannoni. Intensity and polarization of the atmospheric emission at millimetric wavelengths at Dome Concordia. *Mon. Not. Roy. Astron. Soc.*, page 3009, May 2012.

[46] Richard A. Battye and Adam Moss. Evidence for Massive Neutrinos from Cosmic Microwave Background and Lensing Observations. *Phys. Rev. Lett.*, 112(5):051303, 2014.

[47] Daniel Baumann, Daniel Green, Joel Meyers, and Benjamin Wallisch. Phases of New Physics in the CMB. 2015.

[48] Daniel Baumann, Daniel Green, and Rafael A. Porto. B-modes and the Nature of Inflation. *JCAP*, 1501(01):016, 2015.

[49] Daniel Baumann, Hayden Lee, and Guilherme L. Pimentel. High-Scale Inflation and the Tensor Tilt. *JHEP*, 01:101, 2016.

[50] Daniel Baumann and Matias Zaldarriaga. Causality and Primordial Tensor Modes. *JCAP*, 0906:013, 2009.

[51] Siavosh R. Behbahani, Martin Jankowiak, Tomas Rube, and Jay G. Wacker. Nearly Supersymmetric Dark Atoms. *Adv. High Energy Phys.*, 2011:709492, 2011.

[52] Ido Ben-Dayan and Ram Brustein. Cosmic Microwave Background Observables of Small Field Models of Inflation. *JCAP*, 1009:007, 2010.

[53] A. Benoit-Lévy, K. M. Smith, and W. Hu. Non-Gaussian structure of the lensed CMB power spectra covariance matrix. *Phys. Rev.* **D** , 86(12):123008, December 2012.

[54] Marcus Berg, Enrico Pajer, and Stefan Sjors. Dante's Inferno. *Phys. Rev.*, D81:103535, 2010.

[55] Florian Beutler et al. The clustering of galaxies in the SDSS-III Baryon Oscillation Spectroscopic Survey: Signs of neutrino mass in current cosmological datasets. *Mon. Not. Roy. Astron. Soc.*, 444:3501, 2014.

[56] Fedor L. Bezrukov and Mikhail Shaposhnikov. The Standard Model Higgs boson as the inflaton. *Phys. Lett.*, B659:703–706, 2008.

[57] BICEP2 Collaboration, P. A. R. Ade, R. W. Aikin, D. Barkats, S. J. Benton, C. A. Bischoff, J. J. Bock, J. A. Brevik, I. Buder, E. Bullock, C. D. Dowell, L. Duband, J. P. Filippini, S. Fliescher, S. R. Golwala, M. Halpern, M. Hasselfield, S. R. Hildebrandt, G. C. Hilton, V. V. Hristov, K. D. Irwin, K. S. Karkare, J. P. Kaufman, B. G. Keating, S. A. Kernasovskiy, J. M. Kovac, C. L. Kuo, E. M. Leitch, M. Lueker, P. Mason, C. B. Netterfield, H. T. Nguyen, R. O'Brient, R. W. Ogburn, A. Orlando, C. Pryke, C. D. Reintsema, S. Richter, R. Schwarz, C. D. Sheehy, Z. K. Staniszewski, R. V. Sudiwala, G. P. Teply, J. E. Tolan, A. D. Turner, A. G. Vieregg, C. L. Wong, and K. W. Yoon. Detection of B-Mode Polarization at Degree Angular Scales by BICEP2. *Physical Review Letters*, 112(24):241101, June 2014.

[58] BICEP2/Keck and Planck Collaborations, P. A. R. Ade, N. Aghanim, Z. Ahmed, R. W. Aikin, K. D. Alexander, M. Arnaud, J. Aumont, C. Baccigalupi, A. J. Banday, and et al. Joint Analysis of BICEP2/Keck Array and Planck Data. *Physical Review Letters*, 114(10):101301, March 2015.

[59] Jannis Bielefeld and Robert R. Caldwell. Chiral Imprint of a Cosmic Gauge Field on Primordial Gravitational Waves. *Phys. Rev.*, D91(12):123501, 2015.

[60] Jannis Bielefeld and Robert R. Caldwell. Cosmological consequences of classical flavor-space locked gauge field radiation. *Phys. Rev.*, D91(12):124004, 2015.

[61] Ralph Blumenhagen, Cesar Damian, Anamaria Font, Daniela Herschmann, and Rui Sun. The Flux-Scaling Scenario: De Sitter Uplift and Axion Inflation. 2015.

[62] C. Boehm, J. A. Schewtschenko, R. J. Wilkinson, C. M. Baugh, and S. Pascoli. Using the Milky Way satellites to study interactions between cold dark matter and radiation. *Mon. Not. Roy. Astron. Soc.*, 445:L31–L35, 2014.

[63] Celine Boehm, Alain Riazuelo, Steen H. Hansen, and Richard Schaeffer. Interacting dark matter disguised as warm dark matter. *Phys. Rev. D*, 66:083505, 2002.

[64] Cline Boehm, Matthew J. Dolan, and Christopher McCabe. A Lower Bound on the Mass of Cold Thermal Dark Matter from Planck. *JCAP*, 1308:041, 2013.

[65] J.R̃. Bond, A.H̃. Jaffe, and L. Knox. Estimating the power spectrum of the cosmic microwave background. *Phys. Rev.* **D** , 57:2117–2137, February 1998.

[66] J. R. Bond and A. S. Szalay. The Collisionless Damping of Density Fluctuations in an Expanding Universe. *Astrophys. J.*, 274:443–468, 1983.

[67] J. Borrill. The challenge of data analysis for future CMB observations. In L. Maiani, F. Melchiorri, and N. Vittorio, editors, *3K cosmology*, volume 476 of *American Institute of Physics Conference Series*, pages 277–282, May 1999.

[68] Alexey Boyarsky, Oleg Ruchayskiy, and Mikhail Shaposhnikov. The Role of sterile neutrinos in cosmology and astrophysics. *Ann. Rev. Nucl. Part. Sci.*, 59:191–214, 2009.

[69] Michael Boylan-Kolchin, James S. Bullock, and Manoj Kaplinghat. Too big to fail? The puzzling darkness of massive Milky Way subhaloes. *Mon. Not. Roy. Astron. Soc.*, 415:L40, 2011.

[70] Latham A. Boyle and Alessandra Buonanno. Relating gravitational wave constraints from primordial nucleosynthesis, pulsar timing, laser interferometers, and the CMB: Implications for the early Universe. *Phys. Rev.*, D78:043531, 2008.

[71] Latham A. Boyle, Paul J. Steinhardt, and Neil Turok. The Cosmic gravitational wave background in a cyclic universe. *Phys. Rev.*, D69:127302, 2004.

[72] W. N. Brandt, C. R. Lawrence, A. C. S. Readhead, J. N. Pakianathan, and T. M. Fiola. Separation of foreground radiation from cosmic microwave background using multifrequency measurements. *ApJ*, 424:1, 1994.

[73] Torsten Bringmann. Particle Models and the Small-Scale Structure of Dark Matter. *New J. Phys.*, 11:105027, 2009.

[74] Torsten Bringmann, Jasper Hasenkamp, and Jorn Kersten. Tight bonds between sterile neutrinos and dark matter. *JCAP*, 1407:042, 2014.

[75] Jon Brown, William Cottrell, Gary Shiu, and Pablo Soler. Fencing in the Swampland: Quantum Gravity Constraints on Large Field Inflation. *JHEP*, 10:023, 2015.

[76] Jon Brown, William Cottrell, Gary Shiu, and Pablo Soler. On Axionic Field Ranges, Loopholes and the Weak Gravity Conjecture. 2015.

[77] Christopher Brust, David E. Kaplan, and Matthew T. Walters. New Light Species and the CMB. *JHEP*, 12:058, 2013.

[78] Manuel A. Buen-Abad, Gustavo Marques-Tavares, and Martin Schmaltz. Non-Abelian dark matter and dark radiation. *Phys. Rev.*, D92(2):023531, 2015.

[79] Davide Cadamuro, Steen Hannestad, Georg Raffelt, and Javier Redondo. Cosmological bounds on sub-MeV mass axions. *JCAP*, 1102:003, 2011.

[80] Davide Cadamuro and Javier Redondo. Cosmological bounds on pseudo Nambu-Goldstone bosons. *JCAP*, 1202:032, 2012.

[81] C. M. Cantalupo, J. D. Borrill, A. H. Jaffe, T. S. Kisner, and R. Stompor. MADmap: A Massively Parallel Maximum Likelihood Cosmic Microwave Background Map-maker. *The Astrophysical Journal Supplement Series*, 187:212–227, March 2010.

[82] J.-F. Cardoso, M. Le Jeune, J. Delabrouille, M. Betoule, and G. Patanchon. Component Separation With Flexible Models - Application to Multichannel Astrophysical Observations. *IEEE Journal of Selected Topics in Signal Processing*, 2:735–746, November 2008.

[83] E. D. Carlson, M. E. Machacek, and L. J. Hall. Self-interacting dark matter. *Ap. J.* , 398:43–52, October 1992.

[84] S. M. Carroll. Quintessence and the Rest of the World: Suppressing Long-Range Interactions. *Physical Review Letters*, 81:3067–3070, October 1998.

[85] Zackaria Chacko, Yanou Cui, Sungwoo Hong, and Takemichi Okui. Hidden dark matter sector, dark radiation, and the CMB. *Phys. Rev.*, D92:055033, 2015.

[86] A. Challinor and A. Lewis. Lensed CMB power spectra from all-sky correlation functions. *Phys. Rev. D* , 71(10):103010–+, May 2005.

[87] Arindam Chatterjee and Anupam Mazumdar. Bound on largest $r \lesssim 0.1$ from sub-Planckian excursions of inflaton. *JCAP*, 1501(01):031, 2015.

[88] Xue-Lei Chen and Marc Kamionkowski. Particle decays during the cosmic dark ages. *Phys. Rev.*, D70:043502, 2004.

[89] Kiwoon Choi and Sang Hui Im. Realizing the relaxion from multiple axions and its UV completion with high scale supersymmetry. *JHEP*, 01:149, 2016.

[90] Jeremie Choquette and James M. Cline. Minimal non-Abelian model of atomic dark matter. *Phys. Rev.*, D92(11):115011, 2015.

[91] Xiaoyong Chu and Basudeb Dasgupta. Dark Radiation Alleviates Problems with Dark Matter Halos. *Phys. Rev. Lett.*, 113(16):161301, 2014.

[92] James M. Cline, Zuowei Liu, Guy Moore, and Wei Xue. Composite strongly interacting dark matter. *Phys. Rev. D*, 90(1):015023, 2014.

[93] James M. Cline, Zuowei Liu, Guy Moore, and Wei Xue. Scattering properties of dark atoms and molecules. *Phys. Rev. D*, 89(4):043514, 2014.

[94] James M. Cline, Zuowei Liu, and Wei Xue. Millicharged Atomic Dark Matter. *Phys. Rev. D*, 85:101302, 2012.

[95] Hael Collins, R. Holman, and Tereza Vardanyan. Do Mixed States save Effective Field Theory from BICEP? 2014.

[96] J. M. Conrad, C. M. Ignarra, G. Karagiorgi, M. H. Shaevitz, and J. Spitz. Sterile Neutrino Fits to Short Baseline Neutrino Oscillation Measurements. *Adv. High Energy Phys.*, 2013:163897, 2013.

[97] Carlo R. Contaldi, Joao Magueijo, and Lee Smolin. Anomalous CMB polarization and gravitational chirality. *Phys. Rev. Lett.*, 101:141101, 2008.

[98] Jessica L. Cook and Lorenzo Sorbo. Particle production during inflation and gravitational waves detectable by ground-based interferometers. *Phys. Rev.*, D85:023534, 2012. [Erratum: Phys. Rev.D86,069901(2012)].

[99] Ryan Cooke, Max Pettini, Regina A. Jorgenson, Michael T. Murphy, and Charles C. Steidel. Precision measures of the primordial abundance of deuterium. *Astrophys. J.*, 781(1):31, 2014.

[100] Edmund J. Copeland, Robert C. Myers, and Joseph Polchinski. Cosmic F and D strings. *JHEP*, 06:013, 2004.

[101] Paolo Creminelli, Sergei Dubovsky, Diana Lopez Nacir, Marko Simonovic, Gabriele Trevisan, Giovanni Villadoro, and Matias Zaldarriaga. Implications of the scalar tilt for the tensor-to-scalar ratio. *Phys. Rev.*, D92(12):123528, 2015.

[102] Paolo Creminelli and Matias Zaldarriaga. Single-Field Consistency Relation for the 3-Point Function. *JCAP*, 0410:006, 2004.

[103] A. T. Crites, J. W. Henning, P. A. R. Ade, K. A. Aird, J. E. Austermann, J. A. Beall, A. N. Bender, B. A. Benson, L. E. Bleem, J. E. Carlstrom, C. L. Chang, H. C. Chiang, H.-M. Cho, R. Citron, T. M. Crawford, T. de Haan, M. A. Dobbs, W. Everett, J. Gallicchio, J. Gao, E. M. George, A. Gilbert, N. W. Halverson, D. Hanson, N. Harrington, G. C. Hilton, G. P. Holder, W. L. Holzapfel, S. Hoover, Z. Hou, J. D. Hrubes, N. Huang, J. Hubmayr, K. D. Irwin, R. Keisler, L. Knox, A. T. Lee, E. M. Leitch, D. Li,

C. Liang, D. Luong-Van, J. J. McMahon, J. Mehl, S. S. Meyer, L. Mocanu, T. E. Montroy, T. Natoli, J. P. Nibarger, V. Novosad, S. Padin, C. Pryke, C. L. Reichardt, J. E. Ruhl, B. R. Saliwanchik, J. T. Sayre, K. K. Schaffer, G. Smecher, A. A. Stark, K. T. Story, C. Tucker, K. Vanderlinde, J. D. Vieira, G. Wang, N. Whitehorn, V. Yefremenko, and O. Zahn. Measurements of E-Mode Polarization and Temperature-E-Mode Correlation in the Cosmic Microwave Background from 100 Square Degrees of SPTpol Data. *Astrophys. J.*, 805:36, May 2015.

[104] Csaba Csaki, Nemanja Kaloper, Javi Serra, and John Terning. Inflation from Broken Scale Invariance. *Phys. Rev. Lett.*, 113:161302, 2014.

[105] T. Culverhouse, P. Ade, J. Bock, M. Bowden, M. L. Brown, G. Cahill, P. G. Castro, S. E. Church, R. Friedman, K. Ganga, W. K. Gear, S. Gupta, J. R. Hinderks, J. Kovac, A. E. Lange, E. Leitch, S. J. Melhuish, Y. Memari, J. A. Murphy, A. Orlando, R. Schwarz, C. O'Sullivan, L. Piccirillo, C. Pryke, N. Rajguru, B. Rusholme, A. N. Taylor, K. L. Thompson, A. H. Turner, E. Y. S. Wu, M. Zemcov, and QUaD Collaboration. The QUaD Galactic Plane Survey. I. Maps and Analysis of Diffuse Emission. *The Astrophysical Journal*, 722:1057–1077, October 2010.

[106] Richard H. Cyburt, Brian D. Fields, and Keith A. Olive. The NACRE thermonuclear reaction compilation and big bang nucleosynthesis. *New Astron.*, 6:215–238, 2001.

[107] Richard H. Cyburt, Brian D. Fields, Keith A. Olive, and Tsung-Han Yeh. Big Bang Nucleosynthesis: 2015. 2015.

[108] Francis-Yan Cyr-Racine, Roland de Putter, Alvise Raccanelli, and Kris Sigurdson. Constraints on Large-Scale Dark Acoustic Oscillations from Cosmology. *Phys. Rev. D*, 89(6):063517, 2014.

[109] Francis-Yan Cyr-Racine and Kris Sigurdson. Cosmology of atomic dark matter. *Phys. Rev.*, D87(10):103515, 2013.

[110] Francis-Yan Cyr-Racine and Kris Sigurdson. The cosmology of atomic dark matter. *Phys. Rev. D*, 87:103515, 2013.

[111] Francis-Yan Cyr-Racine and Kris Sigurdson. Limits on Neutrino-Neutrino Scattering in the Early Universe. *Phys. Rev.*, D90(12):123533, 2014.

[112] Francis-Yan Cyr-Racine, Kris Sigurdson, Jesus Zavala, Torsten Bringmann, Mark Vogelsberger, and Christoph Pfrommer. ETHOS - An Effective Theory of Structure Formation: From dark particle physics to the matter distribution of the Universe. 2015.

[113] Subinoy Das and Kris Sigurdson. Cosmological limits on hidden sector dark matter. *Phys. Rev. D*, 85:063510, 2012.

[114] W. J. G. de Blok and S. S. McGaugh. The Dark and visible matter content of low surface brightness disk galaxies. *Mon. Not. Roy. Astron. Soc.*, 290:533–552, 1997.

[115] Anton de la Fuente, Prashant Saraswat, and Raman Sundrum. Natural Inflation and Quantum Gravity. *Phys. Rev. Lett.*, 114(15):151303, 2015.

[116] A. A. de Laix, R. J. Scherrer, and R. K. Schaefer. Constraints on Self-interacting Dark Matter. *Ap. J.* , 452:495, October 1995.

[117] J. Delabrouille and J.-F. Cardoso. Diffuse Source Separation in CMB Observations. In V. J. Martínez, E. Saar, E. Martínez-González, and M.-J. Pons-Bordería, editors, *Data Analysis in Cosmology*, volume 665 of *Lecture Notes in Physics, Berlin Springer Verlag*, pages 159–205, 2009.

[118] Eleonora Di Valentino, Elena Giusarma, Massimiliano Lattanzi, Olga Mena, Alessandro Melchiorri, and Joseph Silk. Cosmological Axion and neutrino mass constraints from Planck 2015 temperature and polarization data. *Phys. Lett.*, B752:182–185, 2016.

[119] Roberta Diamanti, Elena Giusarma, Olga Mena, Maria Archidiacono, and Alessandro Melchiorri. Dark Radiation and interacting scenarios. *Phys. Rev. D*, 87:063509, 2013.

[120] Emanuela Dimastrogiovanni, Matteo Fasiello, and Andrew J. Tolley. Low-Energy Effective Field Theory for Chromo-Natural Inflation. *JCAP*, 1302:046, 2013.

[121] Emanuela Dimastrogiovanni and Marco Peloso. Stability analysis of chromo-natural inflation and possible evasion of Lyth?s bound. *Phys. Rev.*, D87(10):103501, 2013.

[122] A. D. Dolgov. Neutrinos in cosmology. *Phys. Rept.*, 370:333–535, 2002.

[123] S. L. Dubovsky. Phases of massive gravity. *JHEP*, 10:076, 2004.

[124] Sergei Dubovsky, Raphael Flauger, Alexei Starobinsky, and Igor Tkachev. Signatures of a Graviton Mass in the Cosmic Microwave Background. *Phys. Rev.*, D81:023523, 2010.

[125] R. Dünner, M. Hasselfield, T. A. Marriage, J. Sievers, V. Acquaviva, G. E. Addison, P. A. R. Ade, P. Aguirre, M. Amiri, J. W. Appel, L. F. Barrientos, E. S. Battistelli, J. R. Bond, B. Brown, B. Burger, E. Calabrese, J. Chervenak, S. Das, M. J. Devlin, S. R. Dicker, W. Bertrand Doriese, J. Dunkley, T. Essinger-Hileman, R. P. Fisher, M. B. Gralla, J. W. Fowler, A. Hajian, M. Halpern, C. Hernández-Monteagudo, G. C. Hilton, M. Hilton, A. D. Hincks, R. Hlozek, K. M. Huffenberger, D. H. Hughes, J. P. Hughes, L. Infante, K. D. Irwin, J. Baptiste Juin, M. Kaul, J. Klein, A. Kosowsky, J. M. Lau, M. Limon, Y.-T. Lin, T. Louis, R. H. Lupton, D. Marsden, K. Martocci, P. Mauskopf, F. Menanteau, K. Moodley, H. Moseley, C. B. Netterfield, M. D. Niemack, M. R. Nolta, L. A. Page, L. Parker, B. Partridge, H. Quintana, B. Reid, N. Sehgal, B. D. Sherwin, D. N. Spergel, S. T. Staggs, D. S. Swetz, E. R. Switzer, R. Thornton, H. Trac, C. Tucker, R. Warne, G. Wilson, E. Wollack, and Y. Zhao. The Atacama Cosmology Telescope: Data Characterization and Mapmaking. *The Astrophysical Journal*, 762:10, January 2013.

[126] C. Dvorkin and K. M. Smith. Reconstructing patchy reionization from the cosmic microwave background. *Phys. Rev.* **D** , 79(4):043003, February 2009.

[127] Cora Dvorkin, Kfir Blum, and Marc Kamionkowski. Constraining Dark Matter-Baryon Scattering with Linear Cosmology. *Phys. Rev. D*, 89(2):023519, 2014.

[128] Cora Dvorkin, Kfir Blum, and Matias Zaldarriaga. Perturbed Recombination from Dark Matter Annihilation. *Phys. Rev.*, D87(10):103522, 2013.

[129] H. K. Eriksen, C. Dickinson, C. R. Lawrence, C. Baccigalupi, A. J. Banday, K. M. Górski, F. K. Hansen, P. B. Lilje, E. Pierpaoli, M. D. Seiffert, K. M. Smith, and K. Vanderlinde. Cosmic Microwave Background Component Separation by Parameter Estimation. *ApJ*, 641:665–682, April 2006.

[130] J. Errard, P. A. R. Ade, Y. Akiba, K. Arnold, M. Atlas, C. Baccigalupi, D. Barron, D. Boettger, J. Borrill, S. Chapman, Y. Chinone, A. Cukierman, J. Delabrouille, M. Dobbs, A. Ducout, T. Elleflot, G. Fabbian, C. Feng, S. Feeney, A. Gilbert, N. Goeckner-Wald, N. W. Halverson, M. Hasegawa, K. Hattori, M. Hazumi, C. Hill, W. L. Holzapfel, Y. Hori, Y. Inoue, G. C. Jaehnig, A. H. Jaffe, O. Jeong, N. Katayama, J. Kaufman, B. Keating, Z. Kermish, R. Keskitalo, T. Kisner, M. Le Jeune, A. T. Lee, E. M. Leitch, D. Leon, E. Linder, F. Matsuda, T. Matsumura, N. J. Miller, M. J. Myers, M. Navaroli, H. Nishino, T. Okamura, H. Paar, J. Peloton, D. Poletti, G. Puglisi, G. Rebeiz, C. L. Reichardt, P. L. Richards, C. Ross, K. M. Rotermund, D. E. Schenck, B. D. Sherwin, P. Siritanasak,

G. Smecher, N. Stebor, B. Steinbach, R. Stompor, A. Suzuki, O. Tajima, S. Takakura, A. Tikhomirov, T. Tomaru, N. Whitehorn, B. Wilson, A. Yadav, and O. Zahn. Modeling Atmospheric Emission for CMB Ground-based Observations. *Astrophys. J.*, 809:63, August 2015.

[131] J. Errard, S. M. Feeney, H. V. Peiris, and A. H. Jaffe. Robust forecasts on fundamental physics from the foreground-obscured, gravitationally-lensed CMB polarization. *ArXiv e-prints*, September 2015.

[132] Miguel Escudero, Olga Mena, Aaron C. Vincent, Ryan J. Wilkinson, and Celine Boehm. Exploring dark matter microphysics with galaxy surveys. *jcap*, 1509(09):034, 2015.

[133] T. Essinger-Hileman, A. Ali, M. Amiri, J. W. Appel, D. Araujo, C. L. Bennett, F. Boone, M. Chan, H.-M. Cho, D. T. Chuss, F. Colazo, E. Crowe, K. Denis, R. Dünner, J. Eimer, D. Gothe, M. Halpern, K. Harrington, G. C. Hilton, G. F. Hinshaw, C. Huang, K. Irwin, G. Jones, J. Karakla, A. J. Kogut, D. Larson, M. Limon, L. Lowry, T. Marriage, N. Mehrle, A. D. Miller, N. Miller, S. H. Moseley, G. Novak, C. Reintsema, K. Rostem, T. Stevenson, D. Towner, K. U-Yen, E. Wagner, D. Watts, E. J. Wollack, Z. Xu, and L. Zeng. CLASS: the cosmology large angular scale surveyor. In *Society of Photo-Optical Instrumentation Engineers (SPIE) Conference Series*, volume 9153 of *Society of Photo-Optical Instrumentation Engineers (SPIE) Conference Series*, page 1, July 2014.

[134] Ji Ji Fan, Andrey Katz, Lisa Randall, and Matthew Reece. Dark-Disk Universe. *Phys. Rev. Lett.*, 110:211302, 2013.

[135] JiJi Fan, Andrey Katz, Lisa Randall, and Matthew Reece. Double-Disk Dark Matter. *Phys. Dark Univ.*, 2:139–156, 2013.

[136] Y. Fantaye, C. Baccigalupi, S. M. Leach, and A. P. S. Yadav. CMB lensing reconstruction in the presence of diffuse polarized foregrounds. *JCAP*, 12:017, December 2012.

[137] Y. Fantaye, F. Stivoli, J. Grain, S. M. Leach, M. Tristram, C. Baccigalupi, and R. Stompor. Estimating the tensor-to-scalar ratio and the effect of residual foreground contamination. *JCAP*, 8:001, August 2011.

[138] Jonathan L. Feng, Manoj Kaplinghat, Huitzu Tu, and Hai-Bo Yu. Hidden Charged Dark Matter. *jcap*, 0907:004, 2009.

[139] Ricardo Z. Ferreira and Martin S. Sloth. Universal Constraints on Axions from Inflation. *JHEP*, 12:139, 2014.

[140] Brian D. Fields. The primordial lithium problem. *Ann. Rev. Nucl. Part. Sci.*, 61:47–68, 2011.

[141] Lee Samuel Finn and Patrick J. Sutton. Bounding the mass of the graviton using binary pulsar observations. *Phys. Rev. D*, 65:044022, Jan 2002.

[142] Willy Fischler and Joel Meyers. Dark Radiation Emerging After Big Bang Nucleosynthesis? *Phys. Rev.*, D83:063520, 2011.

[143] Raphael Flauger, Daniel Green, and Rafael A. Porto. On squeezed limits in single-field inflation. Part I. *JCAP*, 1308:032, 2013.

[144] Raphael Flauger, Liam McAllister, Enrico Pajer, Alexander Westphal, and Gang Xu. Oscillations in the CMB from Axion Monodromy Inflation. *JCAP*, 1006:009, 2010.

[145] Brent Follin, Lloyd Knox, Marius Millea, and Zhen Pan. First Detection of the Acoustic Oscillation Phase Shift Expected from the Cosmic Neutrino Background. *Phys. Rev. Lett.*, 115(9):091301, 2015.

[146] Robert Foot. Mirror matter-type dark matter. *Int. J. Mod. Phys.*, D13:2161–2192, 2004.

[147] Katherine Freese, Joshua A. Frieman, and Angela V. Olinto. Natural inflation with pseudo - Nambu-Goldstone bosons. *Phys.Rev.Lett.*, 65:3233–3236, 1990.

[148] C. Giunti and E. M. Zavanin. Appearancedisappearance relation in $3 + N_s$ short-baseline neutrino oscillations. *Mod. Phys. Lett.*, A31(01):1650003, 2015.

[149] Carlo Giunti and Marco Laveder. Statistical Significance of the Gallium Anomaly. *Phys. Rev.*, C83:065504, 2011.

[150] Elena Giusarma, Eleonora Di Valentino, Massimiliano Lattanzi, Alessandro Melchiorri, and Olga Mena. Relic Neutrinos, thermal axions and cosmology in early 2014. *Phys. Rev.*, D90(4):043507, 2014.

[151] V. Gluscevic, D. Hanson, M. Kamionkowski, and C. M. Hirata. First CMB constraints on direction-dependent cosmological birefringence from WMAP-7. "PRD", 86(10):103529, November 2012.

[152] V. Gluscevic and M. Kamionkowski. Testing parity-violating mechanisms with cosmic microwave background experiments. "PRD", 81(12):123529, June 2010.

[153] V. Gluscevic, M. Kamionkowski, and A. Cooray. Derotation of the cosmic microwave background polarization: Full-sky formalism. *PRD*, 80(2):023510, July 2009.

[154] Vera Gluscevic and Marc Kamionkowski. Testing Parity-Violating Mechanisms with Cosmic Microwave Background Experiments. *Phys. Rev.*, D81:123529, 2010.

[155] B. Gold, N. Odegard, J. L. Weiland, R. S. Hill, A. Kogut, C. L. Bennett, G. Hinshaw, X. Chen, J. Dunkley, M. Halpern, N. Jarosik, E. Komatsu, D. Larson, M. Limon, S. S. Meyer, M. R. Nolta, L. Page, K. M. Smith, D. N. Spergel, G. S. Tucker, E. Wollack, and E. L. Wright. Seven-year Wilkinson Microwave Anisotropy Probe (WMAP) Observations: Galactic Foreground Emission. *Ap. J. Suppl.* , 192:15, February 2011.

[156] Haim Goldberg and Lawrence J. Hall. A NEW CANDIDATE FOR DARK MATTER. *Phys. Lett.*, B174:151, 1986.

[157] A. B. Goncharov and Andrei D. Linde. Chaotic Inflation in Supergravity. *Phys. Lett.*, B139:27, 1984.

[158] B.-A. Gradwohl and J. A. Frieman. Dark matter, long-range forces, and large-scale structure. *Ap. J.* , 398:407–424, October 1992.

[159] Peter W. Graham, Igor G. Irastorza, Steven K. Lamoreaux, Axel Lindner, and Karl A. van Bibber. Experimental Searches for the Axion and Axion-Like Particles. *Ann. Rev. Nucl. Part. Sci.*, 65:485–514, 2015.

[160] Peter W. Graham, David E. Kaplan, and Surjeet Rajendran. Cosmological Relaxation of the Electroweak Scale. *Phys. Rev. Lett.*, 115(22):221801, 2015.

[161] Anne M. Green, Stefan Hofmann, and Dominik J. Schwarz. The First wimpy halos. *JCAP*, 0508:003, 2005.

[162] E. Grohs, G. M. Fuller, C. T. Kishimoto, M. W. Paris, and A. Vlasenko. Neutrino energy transport in weak decoupling and big bang nucleosynthesis. 2015.

[163] D. Hanson, A. Challinor, G. Efstathiou, and P. Bielewicz. CMB temperature lensing power reconstruction. *Phys. Rev.* **D** , 83(4):043005, February 2011.

[164] D. L. Harrison, F. van Leeuwen, and M. A. J. Ashdown. A deconvolution map-making method for experiments with circular scanning strategies. *Astronomy and Astrophysics*, 532:A55, August 2011.

[165] Arthur Hebecker, Jakob Moritz, Alexander Westphal, and Lukas T. Witkowski. Axion Monodromy Inflation with Warped KK-Modes. *Phys. Lett.*, B754:328–334, 2016.

[166] Ben Heidenreich, Matthew Reece, and Tom Rudelius. Sharpening the Weak Gravity Conjecture with Dimensional Reduction. 2015.

[167] Ben Heidenreich, Matthew Reece, and Tom Rudelius. Weak Gravity Strongly Constrains Large-Field Axion Inflation. *JHEP*, 12:108, 2015.

[168] M. B. Hindmarsh and T. W. B. Kibble. Cosmic strings. *Rept. Prog. Phys.*, 58:477–562, 1995.

[169] G. Hinshaw, M. R. Nolta, C. L. Bennett, R. Bean, O. Doré, M. R. Greason, M. Halpern, R. S. Hill, N. Jarosik, A. Kogut, E. Komatsu, M. Limon, N. Odegard, S. S. Meyer, L. Page, H. V. Peiris, D. N. Spergel, G. S. Tucker, L. Verde, J. L. Weiland, E. Wollack, and E. L. Wright. Three-Year Wilkinson Microwave Anisotropy Probe (WMAP) Observations: Temperature Analysis. *Ap. J. Suppl.*, 170:288–334, June 2007.

[170] Kurt Hinterbichler. Theoretical Aspects of Massive Gravity. *Rev. Mod. Phys.*, 84:671–710, 2012.

[171] C. M. Hirata and U. Seljak. Analyzing weak lensing of the cosmic microwave background using the likelihood function. *Phys. Rev.* **D**, 67(4):043001, February 2003.

[172] E. Hivon, K. M. Górski, C. B. Netterfield, B. P. Crill, S. Prunet, and F. Hansen. MASTER of the Cosmic Microwave Background Anisotropy Power Spectrum: A Fast Method for Statistical Analysis of Large and Complex Cosmic Microwave Background Data Sets. *Astrophys. J.*, 567:2–17, March 2002.

[173] Eric Hivon, Krzysztof M. Gorski, C. Barth Netterfield, Brendan P. Crill, Simon Prunet, and Frode Hansen. MASTER of the Cosmic Microwave Background Anisotropy Power Spectrum: A Fast Method for Statistical Analysis of Large and Complex Cosmic Microwave Background Data Sets. *The Astrophysical Journal*, 567(1):2–17, March 2002.

[174] R. Hlozek, D. Grin, D. J. E. Marsh, and P. G. Ferreira. A search for ultralight axions using precision cosmological data. *Phys. Rev.* **D**, 91(10):103512, May 2015.

[175] Dan Hooper, Farinaldo S. Queiroz, and Nickolay Y. Gnedin. Non-Thermal Dark Matter Mimicking An Additional Neutrino Species In The Early Universe. *Phys. Rev.*, D85:063513, 2012.

[176] Dan Hooper, Neal Weiner, and Wei Xue. Dark Forces and Light Dark Matter. *Phys. Rev. D*, 86:056009, 2012.

[177] Shaun Hotchkiss, Anupam Mazumdar, and Seshadri Nadathur. Observable gravitational waves from inflation with small field excursions. *JCAP*, 1202:008, 2012.

[178] Zhen Hou, Ryan Keisler, Lloyd Knox, Marius Millea, and Christian Reichardt. How Massless Neutrinos Affect the Cosmic Microwave Background Damping Tail. *Phys. Rev.*, D87:083008, 2013.

[179] W. Hu, R. Barkana, and A. Gruzinov. Fuzzy Cold Dark Matter: The Wave Properties of Ultralight Particles. *Physical Review Letters*, 85:1158–1161, August 2000.

[180] W. Hu and T. Okamoto. Mass Reconstruction with Cosmic Microwave Background Polarization. *Astrophys. J.*, 574:566–574, August 2002.

[181] Wayne Hu and Daniel J. Eisenstein. Small scale perturbations in a general MDM cosmology. *Astrophys.J.*, 498:497, 1998.

[182] Wayne Hu, Daniel J. Eisenstein, and Max Tegmark. Weighing neutrinos with galaxy surveys. *Phys.Rev.Lett.*, 80:5255–5258, 1998.

[183] Wayne Hu and Takemi Okamoto. Mass reconstruction with cmb polarization. *Astrophys.J.*, 574:566–574, 2002.

[184] Patrick Huber. On the determination of anti-neutrino spectra from nuclear reactors. *Phys. Rev.*, C84:024617, 2011. [Erratum: Phys. Rev.C85,029901(2012)].

[185] Rachel Jeannerot. A Supersymmetric SO(10) model with inflation and cosmic strings. *Phys. Rev.*, D53:5426–5436, 1996.

[186] Rachel Jeannerot, Jonathan Rocher, and Mairi Sakellariadou. How generic is cosmic string formation in SUSY GUTs. *Phys. Rev.*, D68:103514, 2003.

[187] Nicholas T. Jones, Horace Stoica, and S. H. Henry Tye. The Production, spectrum and evolution of cosmic strings in brane inflation. *Phys. Lett.*, B563:6–14, 2003.

[188] Katherine Jones-Smith, Lawrence M. Krauss, and Harsh Mathur. A Nearly Scale Invariant Spectrum of Gravitational Radiation from Global Phase Transitions. *Phys. Rev. Lett.*, 100:131302, 2008.

[189] Shahab Joudaki, Kevork N. Abazajian, and Manoj Kaplinghat. Are Light Sterile Neutrinos Preferred or Disfavored by Cosmology? *Phys.Rev.*, D87:065003, 2013.

[190] Renata Kallosh and Andrei Linde. Universality Class in Conformal Inflation. *JCAP*, 1307:002, 2013.

[191] Nemanja Kaloper, Albion Lawrence, and Lorenzo Sorbo. An Ignoble Approach to Large Field Inflation. *JCAP*, 1103:023, 2011.

[192] Nemanja Kaloper and Lorenzo Sorbo. A Natural Framework for Chaotic Inflation. *Phys. Rev. Lett.*, 102:121301, 2009.

[193] M. Kamionkowski. How to Derotate the Cosmic Microwave Background Polarization. *Physical Review Letters*, 102(11):111302, March 2009.

[194] David E. Kaplan, Gordan Z. Krnjaic, Keith R. Rehermann, and Christopher M. Wells. Atomic Dark Matter. *jcap*, 1005:021, 2010.

[195] David E. Kaplan, Gordan Z. Krnjaic, Keith R. Rehermann, and Christopher M. Wells. Dark Atoms: Asymmetry and Direct Detection. *JCAP*, 1110:011, 2011.

[196] David E. Kaplan and Riccardo Rattazzi. A Clockwork Axion. 2015.

[197] N. Katayama and E. Komatsu. Simple Foreground Cleaning Algorithm for Detecting Primordial B-mode Polarization of the Cosmic Microwave Background. *ApJ*, 737:78, August 2011.

[198] E. Keihänen, R. Keskitalo, H. Kurki-Suonio, T. Poutanen, and A.-S. Sirviö. Making cosmic microwave background temperature and polarization maps with MADAM. *Astronomy and Astrophysics*, 510:A57, February 2010.

[199] E. Keihänen, H. Kurki-Suonio, T. Poutanen, D. Maino, and C. Burigana. A maximum likelihood approach to the destriping technique. *Astronomy and Astrophysics*, 428:287–298, December 2004.

[200] E. Keihänen and M. Reinecke. ArtDeco: a beam-deconvolution code for absolute cosmic microwave background measurements. *Astronomy and Astrophysics*, 548:A110, December 2012.

[201] R. Keisler, S. Hoover, N. Harrington, J. W. Henning, P. A. R. Ade, K. A. Aird, J. E. Austermann, J. A. Beall, A. N. Bender, B. A. Benson, L. E. Bleem, J. E. Carlstrom, C. L. Chang, H. C. Chiang, H-M. Cho, R. Citron, T. M. Crawford, A. T. Crites, T. de Haan, M. A. Dobbs, W. Everett, J. Gallicchio, J. Gao, E. M. George, A. Gilbert, N. W. Halverson, D. Hanson, G. C. Hilton, G. P. Holder, W. L. Holzapfel, Z. Hou, J. D. Hrubes, N. Huang, J. Hubmayr, K. D. Irwin, L. Knox, A. T. Lee, E. M. Leitch, D. Li, D. Luong-Van, D. P. Marrone, J. J. McMahon, J. Mehl, S. S. Meyer, L. Mocanu, T. Natoli, J. P. Nibarger, V. Novosad, S. Padin, C. Pryke, C. L. Reichardt, J. E. Ruhl, B. R. Saliwanchik, J. T. Sayre, K. K. Schaffer, E. Shirokoff, G. Smecher, A. A. Stark, K. T. Story, C. Tucker, K. Vanderlinde, J. D. Vieira, G. Wang, N. Whitehorn, V. Yefremenko, and O. Zahn. Measurements of sub-degree b-mode polarization in the cosmic microwave background from 100 square degrees of sptpol data. *Astrophys. J.*, 807(2):151, 2015.

[202] Justin Khoury, Burt A. Ovrut, Paul J. Steinhardt, and Neil Turok. The Ekpyrotic universe: Colliding branes and the origin of the hot big bang. *Phys. Rev.*, D64:123522, 2001.

[203] Jihn E. Kim, Hans Peter Nilles, and Marco Peloso. Completing natural inflation. *JCAP*, 0501:005, 2005.

[204] Anatoly Klypin, Igor Karachentsev, Dmitry Makarov, and Olga Nasonova. Abundance of Field Galaxies. *Mon. Not. Roy. Astron. Soc.*, 454(2):1798–1810, 2015.

[205] Anatoly A. Klypin, Andrey V. Kravtsov, Octavio Valenzuela, and Francisco Prada. Where are the missing Galactic satellites? *Astrophys. J.*, 522:82–92, 1999.

[206] Lev Kofman, Andrei D. Linde, and Alexei A. Starobinsky. Nonthermal phase transitions after inflation. *Phys. Rev. Lett.*, 76:1011–1014, 1996.

[207] Eiichiro Komatsu and David N. Spergel. Acoustic signatures in the primary microwave background bispectrum. *Phys. Rev.*, D63:063002, 2001.

[208] Karta Kooner, Susha Parameswaran, and Ivonne Zavala. Warping the Weak Gravity Conjecture. 2015.

[209] Joachim Kopp, Pedro A. N. Machado, Michele Maltoni, and Thomas Schwetz. Sterile Neutrino Oscillations: The Global Picture. *JHEP*, 05:050, 2013.

[210] Lawrence M. Krauss. Gravitational waves from global phase transitions. *Phys. Lett.*, B284:229–233, 1992.

[211] Paul D. Lasky et al. Gravitational-wave cosmology across 29 decades in frequency. 2015.

[212] Andrei Lazanu and Paul Shellard. Constraints on the Nambu-Goto cosmic string contribution to the CMB power spectrum in light of new temperature and polarisation data. *JCAP*, 1502(02):024, 2015.

[213] Jean-Luc Lehners and Sebastien Renaux-Petel. Multifield Cosmological Perturbations at Third Order and the Ekpyrotic Trispectrum. *Phys. Rev.*, D80:063503, 2009.

[214] Julien Lesgourgues, Gustavo Marques-Tavares, and Martin Schmaltz. Evidence for dark matter interactions in cosmological precision data? *JCAP*, 1602(02):037, 2016.

[215] Julien Lesgourgues and Sergio Pastor. Massive neutrinos and cosmology. *Phys.Rept.*, 429:307–379, 2006.

[216] A. Lewis and S. Bridle. Cosmological parameters from CMB and other data: A Monte Carlo approach. *Phys. Rev.* **D** , 66(10):103511–+, November 2002.

[217] C. Li, T. L. Smith, and A. Cooray. Non-Gaussian covariance of CMB B modes of polarization and parameter degradation. *Phys. Rev.* **D** , 75(8):083501, April 2007.

[218] Andrei D. Linde. Chaotic Inflation. *Phys.Lett.*, B129:177–181, 1983.

[219] Andrei D. Linde. Particle physics and inflationary cosmology. *Contemp. Concepts Phys.*, 5:1–362, 1990.

[220] Joanes Lizarraga, Jon Urrestilla, David Daverio, Mark Hindmarsh, Martin Kunz, and Andrew R. Liddle. Constraining topological defects with temperature and polarization anisotropies. *Phys. Rev.*, D90(10):103504, 2014.

[221] Marilena LoVerde, Elliot Nelson, and Sarah Shandera. Non-Gaussian Mode Coupling and the Statistical Cosmological Principle. *JCAP*, 1306:024, 2013.

[222] A. Lue, L. Wang, and M. Kamionkowski. Cosmological Signature of New Parity-Violating Interactions. *Physical Review Letters*, 83:1506–1509, August 1999.

[223] Arthur Lue, Li-Min Wang, and Marc Kamionkowski. Cosmological signature of new parity violating interactions. *Phys. Rev. Lett.*, 83:1506–1509, 1999.

[224] David H. Lyth. What would we learn by detecting a gravitational wave signal in the cosmic microwave background anisotropy? *Phys.Rev.Lett.*, 78:1861–1863, 1997.

[225] David H. Lyth and David Wands. Generating the curvature perturbation without an inflaton. *Phys. Lett.*, B524:5–14, 2002.

[226] Chung-Pei Ma. Linear power spectra in cold + hot dark matter models: Analytical approximations and applications. *Astrophys. J.*, 471:13–23, 1996.

[227] M. E. Machacek. Growth of adiabatic perturbations in self-interacting dark matter. *Ap. J.* , 431:41–51, August 1994.

[228] Mathew S. Madhavacheril, Neelima Sehgal, and Tracy R. Slatyer. Current Dark Matter Annihilation Constraints from CMB and Low-Redshift Data. *Phys. Rev.*, D89:103508, 2014.

[229] Juan M. Maldacena and Guilherme L. Pimentel. On graviton non-Gaussianities during inflation. *JHEP*, 09:045, 2011.

[230] Juan Martin Maldacena. Non-Gaussian features of primordial fluctuations in single field inflationary models. *JHEP*, 05:013, 2003.

[231] A. Maleknejad and M. M. Sheikh-Jabbari. Gauge-flation: Inflation From Non-Abelian Gauge Fields. *Phys. Lett.*, B723:224–228, 2013.

[232] Gianpiero Mangano, Alessandro Melchiorri, Paolo Serra, Asantha Cooray, and Marc Kamionkowski. Cosmological bounds on dark matter-neutrino interactions. *Phys. Rev. D*, 74:043517, 2006.

[233] Gianpiero Mangano, Gennaro Miele, Sergio Pastor, Teguayco Pinto, Ofelia Pisanti, et al. Relic neutrino decoupling including flavor oscillations. *Nucl.Phys.*, B729:221–234, 2005.

[234] Fernando Marchesano, Gary Shiu, and Angel M. Uranga. F-term Axion Monodromy Inflation. *JHEP*, 09:184, 2014.

[235] D. J. E. Marsh and J. Silk. A model for halo formation with axion mixed dark matter. *Mon. Not. Roy. Astron. Soc.*, 437:2652–2663, January 2014.

[236] David J. E. Marsh. Axion Cosmology. 2015.

[237] E. Martínez-González, J. M. Diego, P. Vielva, and J. Silk. Cosmic microwave background power spectrum estimation and map reconstruction with the expectation-maximization algorithm. *Mon. Not. Roy. Astron. Soc.*, 345:1101–1109, November 2003.

[238] Liam McAllister, Eva Silverstein, and Alexander Westphal. Gravity Waves and Linear Inflation from Axion Monodromy. *Phys.Rev.*, D82:046003, 2010.

[239] Liam McAllister, Eva Silverstein, Alexander Westphal, and Timm Wrase. The Powers of Monodromy. *JHEP*, 09:123, 2014.

[240] Matthew McCullough and Lisa Randall. Exothermic Double-Disk Dark Matter. *jcap*, 1310:058, 2013.

[241] Samuel D. McDermott, Hai-Bo Yu, and Kathryn M. Zurek. Turning off the Lights: How Dark is Dark Matter? *Phys. Rev. D*, 83:063509, 2011.

[242] P. Daniel Meerburg. Alleviating the tension at low $\ell$ through axion monodromy. *Phys. Rev.*, D90(6):063529, 2014.

[243] P. Daniel Meerburg, Rene Hloek, Boryana Hadzhiyska, and Joel Meyers. Multiwavelength constraints on the inflationary consistency relation. *Phys. Rev.*, D91(10):103505, 2015.

[244] P. Daniel Meerburg and Enrico Pajer. Observational Constraints on Gauge Field Production in Axion Inflation. *JCAP*, 1302:017, 2013.

[245] Justin L. Menestrina and Robert J. Scherrer. Dark Radiation from Particle Decays during Big Bang Nucleosynthesis. *Phys. Rev.*, D85:047301, 2012.

[246] G. Mention, M. Fechner, Th. Lasserre, Th. A. Mueller, D. Lhuillier, M. Cribier, and A. Letourneau. The Reactor Antineutrino Anomaly. *Phys. Rev.*, D83:073006, 2011.

[247] Marius Millea, Lloyd Knox, and Brian Fields. New Bounds for Axions and Axion-Like Particles with keV-GeV Masses. *Phys. Rev.*, D92(2):023010, 2015.

[248] Mehrdad Mirbabayi, Leonardo Senatore, Eva Silverstein, and Matias Zaldarriaga. Gravitational Waves and the Scale of Inflation. *Phys. Rev.*, D91:063518, 2015.

[249] Ben Moore, Sebastiano Ghigna, Fabio Governato, George Lake, Tom Quinn, Joachim Stadel, and Paolo Tozzi. Dark matter substructure in galactic halos. *Ap. J.* , 524:L19–L22, 1999.

[250] Adam Moss and Levon Pogosian. Did BICEP2 see vector modes? First B-mode constraints on cosmic defects. *Phys. Rev. Lett.*, 112:171302, 2014.

[251] Viatcheslav Mukhanov. Quantum Cosmological Perturbations: Predictions and Observations. *Eur. Phys. J.*, C73:2486, 2013.

[252] S. Naess, M. Hasselfield, J. McMahon, M. D. Niemack, G. E. Addison, P. A. R. Ade, R. Allison, M. Amiri, N. Battaglia, J. A. Beall, F. de Bernardis, J. R. Bond, J. Britton, E. Calabrese, H.-m. Cho, K. Coughlin, D. Crichton, S. Das, R. Datta, M. J. Devlin, S. R. Dicker, J. Dunkley, R. Dünner, J. W. Fowler, A. E. Fox, P. Gallardo, E. Grace, M. Gralla, A. Hajian, M. Halpern, S. Henderson, J. C. Hill, G. C. Hilton, M. Hilton, A. D. Hincks, R. Hlozek, P. Ho, J. Hubmayr, K. M. Huffenberger, J. P. Hughes, L. Infante, K. Irwin, R. Jackson, S. Muya Kasanda, J. Klein, B. Koopman, A. Kosowsky,

D. Li, T. Louis, M. Lungu, M. Madhavacheril, T. A. Marriage, L. Maurin, F. Menanteau, K. Moodley, C. Munson, L. Newburgh, J. Nibarger, M. R. Nolta, L. A. Page, C. Pappas, B. Partridge, F. Rojas, B. L. Schmitt, N. Sehgal, B. D. Sherwin, J. Sievers, S. Simon, D. N. Spergel, S. T. Staggs, E. R. Switzer, R. Thornton, H. Trac, C. Tucker, M. Uehara, A. Van Engelen, J. T. Ward, and E. J. Wollack. The Atacama Cosmology Telescope: CMB polarization at $200 < l < 9000$. *JCAP*, 10:7, October 2014.

[253] Ryo Namba, Emanuela Dimastrogiovanni, and Marco Peloso. Gauge-flation confronted with Planck. *JCAP*, 1311:045, 2013.

[254] Ryo Namba, Marco Peloso, Maresuke Shiraishi, Lorenzo Sorbo, and Caner Unal. Scale-dependent gravitational waves from a rolling axion. *JCAP*, 1601(01):041, 2016.

[255] T. Namikawa, D. Hanson, and R. Takahashi. Bias-hardened CMB lensing. *Mon. Not. Roy. Astron. Soc.*, 431:609–620, May 2013.

[256] Elliot Nelson and Sarah Shandera. Statistical Naturalness and non-Gaussianity in a Finite Universe. *Phys. Rev. Lett.*, 110(13):131301, 2013.

[257] Sami Nurmi, Christian T. Byrnes, and Gianmassimo Tasinato. A non-Gaussian landscape. *JCAP*, 1306:004, 2013.

[258] Se-Heon Oh, W. J. G. de Blok, Elias Brinks, Fabian Walter, and Robert C. Kennicutt, Jr. Dark and luminous matter in THINGS dwarf galaxies. *Astron. J.*, 141:193, 2011.

[259] T. Okamoto and W. Hu. Cosmic microwave background lensing reconstruction on the full sky. *Phys. Rev.* **D** , 67(8):083002–+, April 2003.

[260] K. A. Olive et al. Review of Particle Physics. *Chin. Phys.*, C38:090001, 2014.

[261] Kyle A. Oman et al. The unexpected diversity of dwarf galaxy rotation curves. *Mon. Not. Roy. Astron. Soc.*, 452(4):3650–3665, 2015.

[262] Nikhil Padmanabhan and Douglas P. Finkbeiner. Detecting dark matter annihilation with CMB polarization: Signatures and experimental prospects. *Phys. Rev.*, D72:023508, 2005.

[263] L. Page, G. Hinshaw, E. Komatsu, M. R. Nolta, D. N. Spergel, C. L. Bennett, C. Barnes, R. Bean, O. Doré, J. Dunkley, M. Halpern, R. S. Hill, N. Jarosik, A. Kogut, M. Limon, S. S. Meyer, N. Odegard, H. V. Peiris, G. S. Tucker, L. Verde, J. L. Weiland, E. Wollack, and E. L. Wright. Three-Year Wilkinson Microwave Anisotropy Probe (WMAP) Observations: Polarization Analysis. *Ap. J. Suppl.* , 170:335–376, June 2007.

[264] Eran Palti and Timo Weigand. Towards large r from [p, q]-inflation. *JHEP*, 04:155, 2014.

[265] Emmanouil Papastergis, Ann M. Martin, Riccardo Giovanelli, and Martha P. Haynes. The velocity width function of galaxies from the 40% ALFALFA survey: shedding light on the cold dark matter overabundance problem. *Astrophys. J.*, 739:38, 2011.

[266] Papastergis, E., Giovanelli, R., Haynes, M. P., and Shankar, F. Is there a "too big to fail" problem in the field? *A & A* , 574:A113, 2015.

[267] Marcel S. Pawlowski, Pavel Kroupa, and Helmut Jerjen. Dwarf galaxy planes: the discovery of symmetric structures in the local group. *Monthly Notices of the Royal Astronomical Society*, 435(3):1928–1957, 2013.

[268] R. D. Peccei and Helen R. Quinn. CP Conservation in the Presence of Instantons. *Phys. Rev. Lett.*, 38:1440–1443, 1977.

[269] O. Pisanti, A. Cirillo, S. Esposito, F. Iocco, G. Mangano, G. Miele, and P. D. Serpico. PArthENoPE: Public Algorithm Evaluating the Nucleosynthesis of Primordial Elements. *Comput. Phys. Commun.*, 178:956–971, 2008.

[270] Planck Collaboration, R. Adam, P. A. R. Ade, N. Aghanim, M. Arnaud, M. Ashdown, J. Aumont, C. Baccigalupi, A. J. Banday, R. B. Barreiro, and et al. Planck 2015 results. IX. Diffuse component separation: CMB maps. *ArXiv e-prints*, February 2015.

[271] Planck Collaboration, R. Adam, P. A. R. Ade, N. Aghanim, and et al. Planck 2015 results. VIII. High Frequency Instrument data processing: Calibration and maps. *ArXiv e-prints*, February 2015.

[272] Planck Collaboration, P. A. R. Ade, N. Aghanim, C. Armitage-Caplan, M. Arnaud, M. Ashdown, F. Atrio-Barandela, J. Aumont, C. Baccigalupi, A. J. Banday, and et al. Planck 2013 results. XVII. Gravitational lensing by large-scale structure. *A & A* , 571:A17, November 2014.

[273] Planck Collaboration, P. A. R. Ade, N. Aghanim, C. Armitage-Caplan, M. Arnaud, M. Ashdown, F. Atrio-Barandela, J. Aumont, C. Baccigalupi, A. J. Banday, and et al. Planck 2013 results. XVIII. The gravitational lensing-infrared background correlation. *A & A* , 571:A18, November 2014.

[274] Planck Collaboration, P. A. R. Ade, N. Aghanim, M. Ashdown, J. Aumont, C. Baccigalupi, A. J. Banday, R. B. Barreiro, N. Bartolo, E. Battaner, K. Benabed, A. Benoît, A. Benoit-Lévy, J.-P. Bernard, M. Bersanelli, P. Bielewicz, A. Bonaldi, L. Bonavera, J. R. Bond, J. Borrill, F. R. Bouchet, M. Bucher, C. Burigana, R. C. Butler, E. Calabrese, J.-F. Cardoso, A. Catalano, A. Chamballu, R.-R. Chary, P. R. Christensen, S. Colombi, L. P. L. Colombo, B. P. Crill, A. Curto, F. Cuttaia, L. Danese, R. D. Davies, R. J. Davis, P. de Bernardis, A. de Rosa, G. de Zotti, J. Delabrouille, C. Dickinson, J. M. Diego, H. Dole, S. Donzelli, O. Doré, M. Douspis, A. Ducout, X. Dupac, G. Efstathiou, F. Elsner, T. A. Enßlin, H. K. Eriksen, J. Fergusson, F. Finelli, O. Forni, M. Frailis, E. Franceschi, A. Frejsel, S. Galeotta, S. Galli, K. Ganga, M. Giard, Y. Giraud-Héraud, E. Gjerløw, J. González-Nuevo, K. M. Górski, S. Gratton, A. Gregorio, A. Gruppuso, F. K. Hansen, D. Hanson, D. L. Harrison, S. Henrot-Versillé, D. Herranz, S. R. Hildebrandt, E. Hivon, M. Hobson, W. A. Holmes, A. Hornstrup, W. Hovest, K. M. Huffenberger, G. Hurier, A. H. Jaffe, T. R. Jaffe, M. Juvela, E. Keihänen, R. Keskitalo, K. Kiiveri, T. S. Kisner, J. Knoche, M. Kunz, H. Kurki-Suonio, A. Lähteenmäki, J.-M. Lamarre, A. Lasenby, M. Lattanzi, C. R. Lawrence, J. P. Leahy, R. Leonardi, J. Lesgourgues, F. Levrier, M. Liguori, P. B. Lilje, M. Linden-Vørnle, V. Lindholm, M. López-Caniego, P. M. Lubin, J. F. Macías-Pérez, G. Maggio, D. Maino, N. Mandolesi, A. Mangilli, P. G. Martin, E. Martínez-González, S. Masi, S. Matarrese, P. Mazzotta, P. McGehee, P. R. Meinhold, A. Melchiorri, L. Mendes, A. Mennella, M. Migliaccio, S. Mitra, L. Montier, G. Morgante, D. Mortlock, A. Moss, D. Munshi, J. A. Murphy, P. Naselsky, F. Nati, P. Natoli, C. B. Netterfield, H. U. Nørgaard-Nielsen, D. Novikov, I. Novikov, F. Paci, L. Pagano, D. Paoletti, B. Partridge, F. Pasian, G. Patanchon, T. J. Pearson, O. Perdereau, L. Perotto, F. Perrotta, V. Pettorino, E. Pierpaoli, D. Pietrobon, E. Pointecouteau, G. Polenta, G. W. Pratt, G. Prézeau, S. Prunet, J.-L. Puget, J. P. Rachen, R. Rebolo, M. Reinecke, M. Remazeilles, A. Renzi, G. Rocha, C. Rosset, M. Rossetti, G. Roudier, J. A. Rubiño-Martín, B. Rusholme, M. Sandri, D. Santos, M. Savelainen, D. Scott, M. D. Seiffert, E. P. S. Shellard, L. D. Spencer, V. Stolyarov, R. Stompor, D. Sutton, A.-S. Suur-Uski, J.-F. Sygnet, J. A. Tauber, L. Terenzi, L. Toffolatti, M. Tomasi, M. Tristram, M. Tucci, J. Tuovinen, L. Valenziano, J. Valiviita, B. Van Tent, T. Vassallo, P. Vielva, F. Villa, L. A. Wade, B. D. Wandelt, R. Watson, I. K. Wehus, D. Yvon, A. Zacchei, and A. Zonca. Planck 2015 results. VI. LFI mapmaking. *ArXiv e-prints*, February 2015.

[275] Planck Collaboration, N. Aghanim, M. Arnaud, M. Ashdown, J. Aumont, C. Baccigalupi, A. J. Banday, R. B. Barreiro, J. G. Bartlett, N. Bartolo, and et al. Planck 2015 results. XI. CMB power spectra, likelihoods, and robustness of parameters. *ArXiv e-prints*, July 2015.

[276] T. Poutanen, D. Maino, H. Kurki-Suonio, E. Keihänen, and E. Hivon. Cosmic microwave background power spectrum estimation with the destriping technique. *MNRAS*, 353:43–58, September 2004.

[277] Layne C. Price, Hiranya V. Peiris, Jonathan Frazer, and Richard Easther. Gravitational wave consistency relations for multifield inflation. *Phys. Rev. Lett.*, 114(3):031301, 2015.

[278] Stefano Profumo, Kris Sigurdson, and Marc Kamionkowski. What mass are the smallest protohalos? *Phys. Rev. Lett.*, 97:031301, 2006.

[279] Georg G. Raffelt. Neutrinos and the stars. *Proc. Int. Sch. Phys. Fermi*, 182:61–143, 2012.

[280] Lisa Randall and Jakub Scholtz. Dissipative Dark Matter and the Andromeda Plane of Satellites. *jcap*, 1509(09):057, 2015.

[281] Sebastien Renaux-Petel and Krzysztof Turzynski. On reaching the adiabatic limit in multi-field inflation. *JCAP*, 1506(06):010, 2015.

[282] Jonathan Rocher and Mairi Sakellariadou. D-term inflation, cosmic strings, and consistency with cosmic microwave background measurement. *Phys. Rev. Lett.*, 94:011303, 2005.

[283] Diederik Roest. Universality classes of inflation. *JCAP*, 1401:007, 2014.

[284] Tom Rudelius. Constraints on Axion Inflation from the Weak Gravity Conjecture. *JCAP*, 1509(09):020, 2015.

[285] Tom Rudelius. On the Possibility of Large Axion Moduli Spaces. *JCAP*, 1504(04):049, 2015.

[286] D.S. Salopek, J.R. Bond, and James M. Bardeen. Designing Density Fluctuation Spectra in Inflation. *Phys.Rev.*, D40:1753, 1989.

[287] Saswat Sarangi and S. H. Henry Tye. Cosmic string production towards the end of brane inflation. *Phys. Lett.*, B536:185–192, 2002.

[288] S. Schael et al. Precision electroweak measurements on the $Z$ resonance. *Phys. Rept.*, 427:257–454, 2006.

[289] K. K. Schaffer, T. M. Crawford, K. A. Aird, B. A. Benson, L. E. Bleem, J. E. Carlstrom, C. L. Chang, H. M. Cho, A. T. Crites, T. de Haan, M. A. Dobbs, E. M. George, N. W. Halverson, G. P. Holder, W. L. Holzapfel, S. Hoover, J. D. Hrubes, M. Joy, R. Keisler, L. Knox, A. T. Lee, E. M. Leitch, M. Lueker, D. Luong-Van, J. J. McMahon, J. Mehl, S. S. Meyer, J. J. Mohr, T. E. Montroy, S. Padin, T. Plagge, C. Pryke, C. L. Reichardt, J. E. Ruhl, E. Shirokoff, H. G. Spieler, B. Stalder, Z. Staniszewski, A. A. Stark, K. Story, K. Vanderlinde, J. D. Vieira, and R. Williamson. The First Public Release of South Pole Telescope Data: Maps of a 95 deg$^2$ Field from 2008 Observations. *The Astrophysical Journal*, 743:90, December 2011.

[290] M. M. Schmittfull, A. Challinor, D. Hanson, and A. Lewis. Joint analysis of CMB temperature and lensing-reconstruction power spectra. *Phys. Rev.* **D** , 88(6):063012, September 2013.

[291] Uros Seljak and Anze Slosar. B polarization of cosmic microwave background as a tracer of strings. *Phys. Rev.*, D74:063523, 2006.

[292] Leonardo Senatore, Eva Silverstein, and Matias Zaldarriaga. New Sources of Gravitational Waves during Inflation. *JCAP*, 1408:016, 2014.

[293] Pasquale Dario Serpico, S. Esposito, F. Iocco, G. Mangano, G. Miele, and O. Pisanti. Nuclear reaction network for primordial nucleosynthesis: A Detailed analysis of rates, uncertainties and light nuclei yields. *JCAP*, 0412:010, 2004.

[294] Paolo Serra, Federico Zalamea, Asantha Cooray, Gianpiero Mangano, and Alessandro Melchiorri. Constraints on neutrino – dark matter interactions from cosmic microwave background and large scale structure data. *Phys. Rev. D*, 81:043507, 2010.

[295] B. D. Sherwin and M. Schmittfull. Delensing the CMB with the cosmic infrared background. *Phys. Rev.* **D** , 92(4):043005, August 2015.

[296] Eva Silverstein and Alexander Westphal. Monodromy in the CMB: Gravity Waves and String Inflation. *Phys.Rev.*, D78:106003, 2008.

[297] G. Simard, D. Hanson, and G. Holder. Prospects for Delensing the Cosmic Microwave Background for Studying Inflation. *Ap. J.* , 807:166, July 2015.

[298] K. M. Smith. Pseudo-$C_\ell$ estimators which do not mix E and B modes. *Phys. Rev.* **D** , 74(8):083002–+, October 2006.

[299] K. M. Smith, D. Hanson, M. LoVerde, C. M. Hirata, and O. Zahn. Delensing CMB polarization with external datasets. *JCAP* , 6:014, June 2012.

[300] K. M. Smith, W. Hu, and M. Kaplinghat. Cosmological information from lensed CMB power spectra. *Phys. Rev.* **D** , 74(12):123002, December 2006.

[301] Lorenzo Sorbo. Parity violation in the Cosmic Microwave Background from a pseudoscalar inflaton. *JCAP*, 1106:003, 2011.

[302] Alexei A. Starobinsky. A New Type of Isotropic Cosmological Models Without Singularity. *Phys.Lett.*, B91:99–102, 1980.

[303] Gary Steigman. Equivalent Neutrinos, Light WIMPs, and the Chimera of Dark Radiation. *Phys. Rev.*, D87(10):103517, 2013.

[304] Andrew Stewart and Robert Brandenberger. Observational Constraints on Theories with a Blue Spectrum of Tensor Modes. *JCAP*, 0808:012, 2008.

[305] F. Stivoli, J. Grain, S. M. Leach, M. Tristram, C. Baccigalupi, and R. Stompor. Maximum likelihood, parametric component separation and CMB B-mode detection in suborbital experiments. *Mon. Not. Roy. Astron. Soc.*, 408:2319–2335, November 2010.

[306] Radek Stompor, Amedeo Balbi, Julian Borrill, Pedro Ferreira, Shaul Hanany, Andrew Jaffe, Adrian Lee, Sang Oh, Bahman Rabii, Paul Richards, George Smoot, Celeste Winant, and Jiun-Huei Wu. Making maps of the cosmic microwave background: The MAXIMA example. *Physical Review D*, 65(2):022003, December 2001.

[307] Alessandro Strumia and Francesco Vissani. Neutrino masses and mixings and... 2006.

[308] Tomohiro Takahashi and Jiro Soda. Chiral Primordial Gravitational Waves from a Lifshitz Point. *Phys. Rev. Lett.*, 102:231301, 2009.

[309] M. Tegmark. How to Make Maps from Cosmic Microwave Background Data without Losing Information. *The Astrophysical Journal Letters*, 480:L87–L90, May 1997.

[310] M. Tegmark et al. Cosmological parameters from sdss arecind wmap. *Phys. Rev.* **D** , page accepted, 2003. astro-ph/0310723.

[311] The Polarbear Collaboration, P. Ade, Y. Akiba, a. E. Anthony, K. Arnold, M. Atlas, D. Barron, D. Boettger, J. Borrill, S. Chapman, Y. Chinone, M. Dobbs, T. Elleflot, J. Errard, G. Fabbian, C. Feng, D. Flanigan, a. Gilbert, W. Grainger, N. W. Halverson, M. Hasegawa, K. Hattori, M. Hazumi, W. L. Holzapfel, Y. Hori, J. Howard, P. Hyland, Y. Inoue, G. C. Jaehnig, a. H. Jaffe, B. Keating, Z. Kermish, R. Keskitalo, T. Kisner, M. Le Jeune, a. T. Lee, E. M. Leitch, E. Linder, M. Lungu, F. Matsuda, T. Matsumura, X. Meng, N. J. Miller, H. Morii, S. Moyerman, M. J. Myers, M. Navaroli, H. Nishino, a. Orlando, H. Paar, J. Peloton, D. Poletti, E. Quealy, G. Rebeiz, C. L. Reichardt, P. L. Richards, C. Ross, I. Schanning, D. E. Schenck, B. D. Sherwin, a. Shimizu, C. Shimmin, M. Shimon, P. Siritanasak, G. Smecher, H. Spieler, N. Stebor, B. Steinbach, R. Stompor, a. Suzuki, S. Takakura, T. Tomaru, B. Wilson, a. Yadav, and O. Zahn. a Measurement of the Cosmic Microwave Background B -Mode Polarization Power Spectrum At Sub-Degree Scales With Polarbear. *The Astrophysical Journal*, 794(2):171, 2014.

[312] I. Tkachev, S. Khlebnikov, L. Kofman, and Andrei D. Linde. Cosmic strings from preheating. *Phys. Lett.*, B440:262–268, 1998.

[313] M. Tristram, C. Filliard, O. Perdereau, S. Plaszczynski, R. Stompor, and F. Touze. Iterative destriping and photometric calibration for Planck-HFI, polarized, multi-detector map-making. *Astronomy and Astrophysics*, 534:A88, October 2011.

[314] Jon Urrestilla, Neil Bevis, Mark Hindmarsh, Martin Kunz, and Andrew R. Liddle. Cosmic microwave anisotropies from BPS semilocal strings. *JCAP*, 0807:010, 2008.

[315] Jon Urrestilla, Pia Mukherjee, Andrew R. Liddle, Neil Bevis, Mark Hindmarsh, and Martin Kunz. Degeneracy between primordial tensor modes and cosmic strings in future CMB data from the Planck satellite. *Phys. Rev.*, D77:123005, 2008.

[316] Laura G. van den Aarssen, Torsten Bringmann, and Christoph Pfrommer. Is dark matter with long-range interactions a solution to all small-scale problems of $\Lambda$ CDM cosmology? *Phys. Rev. Lett.*, 109:231301, 2012.

[317] A. Vilenkin. Cosmological Density Fluctuations Produced by Vacuum Strings. *Phys. Rev. Lett.*, 46:1169–1172, 1981. [Erratum: Phys. Rev. Lett.46,1496(1981)].

[318] Robert V. Wagoner, William A. Fowler, and Fred Hoyle. On the Synthesis of elements at very high temperatures. *Astrophys. J.*, 148:3–49, 1967.

[319] Matthew G. Walker and Jorge Penarrubia. A Method for Measuring (Slopes of) the Mass Profiles of Dwarf Spheroidal Galaxies. *Astrophys. J.*, 742:20, 2011.

[320] Steven Weinberg. *Cosmology.* OUP Oxford, 2008.

[321] Steven Weinberg. Goldstone Bosons as Fractional Cosmic Neutrinos. *Phys.Rev.Lett.*, 110:241301, 2013.

[322] X. G. Wen and Edward Witten. World Sheet Instantons and the Peccei-Quinn Symmetry. *Phys. Lett.*, B166:397, 1986.

[323] Ryan J. Wilkinson, Celine Boehm, and Julien Lesgourgues. Constraining Dark Matter-Neutrino Interactions using the CMB and Large-Scale Structure. *JCAP*, 1405:011, 2014.

[324] Ryan J. Wilkinson, Julien Lesgourgues, and Celine Boehm. Using the CMB angular power spectrum to study Dark Matter-photon interactions. *jcap*, 1404:026, 2014.

[325] E. L. Wright. Scanning and Mapping Strategies for CMB Experiments. *ArXiv Astrophysics e-prints*, November 1996.

[326] W. L. K. Wu, J. Errard, C. Dvorkin, C. L. Kuo, A. T. Lee, P. McDonald, A. Slosar, and O. Zahn. A Guide to Designing Future Ground-based Cosmic Microwave Background Experiments. *Astrophys. J.*, 788:138, 2014.

[327] Mark Wyman, Douglas H. Rudd, R. Ali Vanderveld, and Wayne Hu. Neutrinos Help Reconcile Planck Measurements with the Local Universe. *Phys. Rev. Lett.*, 112(5):051302, 2014.

[328] Matias Zaldarriaga. Non-Gaussianities in models with a varying inflaton decay rate. *Phys. Rev.*, D69:043508, 2004.

[329] Matias Zaldarriaga and Diego D. Harari. Analytic approach to the polarization of the cosmic microwave background in flat and open universes. *Phys. Rev.*, D52:3276–3287, 1995.

[330] J. Zavala, Y. P. Jing, A. Faltenbacher, G. Yepes, Y. Hoffman, S. Gottlober, and B. Catinella. The velocity function in the local environment from LCDM and LWDM constrained simulations. *Astrophys. J.*, 700:1779–1793, 2009.

[331] Ogan zsoy, Kuver Sinha, and Scott Watson. How Well Can We Really Determine the Scale of Inflation? *Phys. Rev.*, D91(10):103509, 2015.